Towards a quantification of environmental and climatic factors between 60 and 20 ka in SE Europe using geochemistry and luminescence dating

Dissertation

der Mathematisch-Naturwissenschaftlichen Fakultät

der Eberhard Karls Universität Tübingen

zur Erlangung des Grades eines

Doktors der Naturwissenschaften

(Dr. rer. nat.)

vorgelegt von

Dipl.-Geogr. Ann-Kathrin Schatz

aus Tettnang

Tübingen

2014

Tag der mündlichen Qualifikation:	23.10.2014
Dekan:	Prof. Dr. Wolfgang Rosenstiel
1. Berichterstatter:	Prof. Dr. Thomas Scholten
2. Berichterstatter:	Prof. Dr. Dominik Faust

Table of contents

Part II - Cumulative Study

List of Tables

List of Figures

List of Abbreviations

^{14}C	radiocarbon dating
abs. e.	absolute error
AVL^{3}	average loess composition (Újvári et al., 2008)
BM	Bohemian Massif
BP / B.P.	before present
C Alps	Central Alps
CB	Carpathian Basin
CHUR	chondritic uniform reservoir (“bulk earth”)
D_e	equivalent dose
EC	East Carpathians
GAL	global average loess composition (Újvári et al., 2008)
GR	Grub/Austria
Gy	Gray
IRSL	infrared-stimulated luminescence (dating)
ka	kiloannum (10^3 years)
kW	Kilowatt
LGM	Last Glacial Maximum
LOI	loss on ignition
MAP	mean annual precipitation
MAT	mean annual temperature
MIS	Marine Isotope Stage
MJT	mean July temperature
MORB	mid-ocean ridge basalt
MS	magnetic susceptibility
NASC	North American Shale Composite
NU	Nussloch/Germany
OSL	optically stimulated luminescence (dating)
PAAS	Post-Archean American Shale
rel. e.	relative error
S.E.	standard error
SAR	single-aliquot regeneration (protocol)
TL	Thermoluminescence
TO	Tokaj/Hungary
UCC	upper continental crust
WC	West Carpathians
WI	weathering index
X	mass-specific magnetic susceptibility
XRF	X-ray fluorescence
$\delta^{13}C$	carbon stable isotopic composition
$\delta^{15}N$	nitrogen stable isotopic composition

Abstract

To further or understanding of past climate changes and their impact on the environment in the younger geological past, Quaternary terrestrial deposits such as loess-paleosol sequences (LPSS) potentially contain valuable information and have long been recognized as excellent archives of paleoclimate data. However, many loess paleosol studies lack truly interdisciplinary and multi-proxy approaches, as well as information about the origin, transport and sedimentation history of the material, or reliable quantitative climatic information that has been cross-validated with independent data from other sources. The aim of this cumulative study was to combine and apply a wide range of traditional and innovative methods to a loess-paleosol sequence at Tokaj in Northeast Hungary, one of the key locations of loess research in Southeast Europe.

In the first part, we provide the first complete chronostratigraphy for the section based on luminescence (OSL and IRSL) dating, which serves as a framework for all further analyses. Results show that previous age estimates were often too low, which may require a review of previous studies that rely on the now obsolete age model. Furthermore, this research also contributes to the introduction of $pIRIR_{290}$ as a new luminescence dating technique with a substantially extended age range. Sedimentation rates calculated from the updates ages more than double during Marine Isotope Stage (MIS) 2 (29-14 ka) compared to MIS 3 (57-29 ka), which is consistent with observations from other locations in the Carpathian Basin and confirms the pattern of decreasing dust sedimentation from North to South, probably with increasing distance from the dust source.

The second part deals with the weathering history of the section. We present a comparison of 14 weathering indices that may be used to quantify weathering intensity. The results show that most of them perform equally well, including the most widely-used CIA index, and that it is not necessary to restrict the choice of suitable indices. Suggestions for the selection of the most suitable index for a given LPSS are provided. The second half of this study attempts to quantify mean annual temperature and precipitation based on paleoclimate transfer functions and XRF, magnetic susceptibility and carbon isotopic data. Although the associated errors are large, we argue that robust results can be obtained by combining several independent approaches and literature data. All results are consistent with a general trend towards lower temperatures and a drier climate in MIS 2, and higher temperatures and a more humid climate in MIS 3.

In the third part, the results of the provenance study based on a combined Sr-Nd isotopic and elemental fingerprinting approach indicate that the source of dust in Tokaj has most likely been

stable over time, whereas those of dust in Austria and Germany have been more variable. Loess in Europe, and especially in the Carpathian Basin, is overall rather uniform. While a direct comparison of loess and rocks from potential source areas is difficult, the correlation with floodplain sediments is a highly promising approach. Results indicate that Tokaj loess may have been derived from the surrounding mountain chains and Danube sediments, while loess in Southwest Germany is probably a mixture of local and Rhine sediments. Our data also underlines the contribution of Alpine sediments to loess in both Southeast and West Europe.

Zusammenfassung

Für die Untersuchung von Klimaschwankungen in der jüngeren geologischen Vergangenheit und deren Auswirkungen auf die Umwelt haben sich quartäre terrestrische Sedimente wie beispielsweise Löss-Paläoboden-Sequenzen bewährt. Diese enthalten wichtige Informationen und sind schon lange als exzellente Paläoklima-Archive bekannt. Jedoch fehlt vielen Lössstudien ein tatsächlich interdisziplinärer Ansatz mit dem Einsatz verschiedenartiger Proxyverfahren, sowie grundlegende Informationen zu Herkunft, Transport und Sedimentationsgeschichte des Materials, oder verlässliche quantitative Klimainformationen, die anhand unabhängiger Daten aus anderen Quellen validiert wurden. Ziel dieser kumulativen Dissertation ist es, eine große Auswahl an traditionellen und innovativen Methoden an einem Lössprofil in Tokaj (Nordostungarn) zu kombinieren und anzuwenden.

Im ersten Teil dieser Arbeit wird die erste komplette Chronostratigraphie für das Lössprofil vorgestellt. Sie basiert auf Lumineszenzdatierung (OSL und IRSL) und ist für alle weiteren Studien von zentraler Bedeutung. Die Datierungen zeigen, dass frühere Altersschätzungen oft zu niedrig waren, weshalb eine Überprüfung und Neubewertung einiger früherer Studien notwendig wird, die sich auf die mittlerweile überholten Alter beziehen. Die Untersuchungen tragen weiterhin dazu bei, $pIRIR_{290}$ als neue, alternative Datierungstechnik mit einer deutlich verlängerten Altersspanne zu etablieren. Die aus den neuen Altern berechneten Sedimentationsraten sind in MIS 2 (29-14 ka) mehr als doppelt so hoch als in MIS 3 (57-29 ka) und vergleichbar mit denen an anderen Standorten im Pannonischen Becken. Diese Ergebnisse bestätigen die Beobachtung eines von Nord nach Süd abnehmenden Trends der Sedimentationsraten, was möglichweise auf die zunehmende Distanz zur Sedimentursprung zu erklären ist.

Der zweite Teil dieser Arbeit beschäftigt sich mit der Verwitterungsgeschichte des Lössprofils. Es werden 14 Verwitterungsindizes vorgestellt, die zur Quantifizierung der Verwitterungsintensität verwendet werden können. Die Ergebnisse zeigen, dass alle von ihnen, einschließlich des oft verwendeten CIA-Indexes, ähnlich gut funktionieren und es daher nicht notwendig ist, sich auf spezielle Indizes zu beschränken. Es werden jedoch auch Empfehlungen zur Auswahl eines geeigneten Indexes für ein spezifisches Lössprofil gegeben. Im zweiten Teil dieser Studie werden Jahresdurchschnittstemperaturen und -niederschläge anhand von Transferfunktionen und geochemischen und mineralmagnetischen Daten und Kohlenstoffisotopen berechnet. Obwohl die damit verbundenen Unsicherheiten und Fehler hoch sind, zeigen die Ergebnisse, dass robuste Resultate durch die Kombination mehrerer unabhängiger Ansätze und Literaturdaten erzielt werden können. Alle Ergebnisse weisen auf einen Trend zu niedrigeren Temperaturen und einem trockeneren Klima in MIS 2 und höheren Temperaturen und einem feuchteren Klima in MIS 3 hin.

Im dritten Teil zeigen die Ergebnisse eines kombinierten Elementar- und Sr-Nd-Isotopenansatzes, dass die Sedimentquelle für den Löss in Tokaj über die Zeit weitgehend konstant blieb, was für Löss in Österreich und Südwestdeutschland nur in geringerem Maße zutrifft. Löss in Europa, vor allem im Pannonischen Becken, ist generell relativ einheitlich. Ein direkter Vergleich von Löss und potentiellen Ursprungsgesteinen ist schwierig, aber der Vergleich mit fluvialen Sedimenten ist vielversrechend. Die Ergebnisse daraus zeigen, dass Löss in Tokaj wahrscheinlich aus Gesteinen der umgebenden Gebirge und aus Sedimenten der Donau entstanden ist, Löss in Südwestdeutschland ist hingegen eher eine Mischung aus örtlichen Gesteinen und Sedimenten des Rheins. Einen weiteren wichtigen Beitrag zu Löss in Südost- und Westeuropa stellen außerdem Sedimente der Alpen dar.

1. Introduction

The fact that human activity affects Earth's climate has been emphasized ever since the first IPCC Scientific Assessment (IPCC, 1990). The latest reports from 2007 (Jansen et al., 2007) and 2013 (Masson-Delmotte et al., 2013) both underline the role of paleoclimatology to gain relevant insights and further our understanding of past climate changes and their impact on the environment, as well as to validate and improve predictive climate models. Yet even for the younger geological past – the Quaternary – our knowledge is still fragmentary with regard to both space and time. While marine sediments and ice cores may provide continuous and highly resolved paleoclimatic data, terrestrial archives often lack continuity and tend to cover shorter time spans. On the other hand, however, terrestrial archives provide valuable local and regional information that cannot easily be derived from distal archives, such as marine and ice cores. Among a range of important terrestrial archives – e.g. peat bogs, river terraces, lake sediments, moraines – one of the most promising are loess-paleosol sequences (LPSS). LPSS are thick deposits of aeolian dust and intercalated paleosols representing cool and dry glacial or stadials when dust was deposited, and warm and humid interglacials and interstadials when soil formation occurred. These sedimentary sequences have a vast potential for reconstructions of the Pleistocene environmental and climatic history. Most attention is currently focused on LPSS in China and Southeast Europe, mainly Hungary and Serbia, where these archives are abundant. Other key regions are e.g. Southwest Germany (Antoine et al., 2009; Hatté et al., 1999; Rousseau et al., 2002), East Germany (Baumgart et al., 2013; Meszner et al., 2013; Zech et al., 2013a), France (Antoine et al., 1999; Rousseau and Puisségur, 1990; Rousseau et al., 1998), Belgium (Frechen et al., 2001; Vandenberghe et al., 1998), the Czech Republic (Frechen et al., 1999; Fuchs et al., 2013; Horáčková et al., in press), the US including Alaska (Arthur Bettis III et al., 2003; Muhs and Budahn, 2006; Muhs et al., 2013b; Roberts et al., 2003) and Central Asia (Bronger et al., 1998; Dodonov and Baiguzina, 1995; Forster and Heller, 1994). LPSS, especially at the most prominent locations, have undoubtedly received a lot of attention recently, leading to a multitude of results from established and new methods such as e.g. micromorphology (Kühn et al., 2013; Terhorst et al., in press), pollen (Wu et al., 2007; Zech et al., 2010) and grain-size analysis (Novothny et al., 2011; Varga et al., 2012), mineralogy (Mikulčić Pavlaković et al., 2011; Thamó-Bozsó et al., 2014), mineral magnetics (Forster and Heller, 1997; Lukić et al., 2014; Maher et al., 1994), paleontological studies based on molluscs, charcoal and macrofossils (Kovács et al., 2012; Marković et al., 2007; Sümegi and Rudner, 2001) and a wide range of geochemical methods (Sheldon and Tabor, 2009), including isotopic (Hatté et al., 2013; Tuthorn et al., 2014; Zech et al., 2013b) and biomarker analyses (Bai et al., 2009; Gocke et al., 2013; Zech et al., 2012). Despite

the combination of methods, studies often lack truly interdisciplinary and multi-proxy approaches, as well as basic information on the chronostratigraphy of a section and the origin and transport history of the sediments, or reliable quantitative results that have been validated with independent data from other sources. Moreover, each method or proxy has a different sensitivity for changes of climate and environment and an individual susceptibility for sediment alteration, e.g. by weathering (Buggle, 2011). Therefore, only the combination of multiple proxy approaches and subsequent cross-validation of the results allows for reliable insights into past environments and for accurate reconstructions of paleoclimate and climate changes.

The aim of this cumulative study is to combine and apply a wide range of traditional and innovative methods to a loess-paleosol sequence at Tokaj in Northeast Hungary, one of the key locations of loess research in Southeast Europe. The section comprises both Marine Isotope Stage 2 and 3 and potentially MIS 4 (14-29-57-71 ka; Lisiecki and Raymo, 2005) and has been subject to detailed (micro-)paleontological, sedimentological and geochemical investigations using e.g. mollusc and charcoal studies, grain size analysis, magnetic susceptibility, stable C and N isotopes, elemental analyses and radiocarbon dating (Pinczés, 1954, 1987; Rudner and Sümegi, 2001; Schatz et al., 2011; Sümegi, 2005; Sümegi and Hertelendi, 1998; Sümegi and Krolopp, 2002; Sümegi and Rudner, 2001). Topics that have not, or only partly, been addressed include the sedimentological, chronological and geochemical history of the section, i.e. formation and weathering processes and the chronostratigraphy, as well as the origin and transport pathways of the sediment. Hence, Study 1 provides a valid and comprehensive luminescence-based chronostratigraphy as a framework for all subsequent analyses. With this new data, sedimentation rates are calculated for Tokaj using an age-depth model. Sedimentation rates are then compared with rates from sections located to the West and South to gain insights into the spatial patterns of wind speed in the Carpathian Basin. Study 2 focuses on the weathering history of the section and the choice of a suitable measure of weathering intensity. A wide variety of weathering indices has been proposed in the literature, but there are very few recommendations about the most suitable one for loess-paleosol studies. The second part of Study 2 is devoted to (semi-)quantitative reconstructions of paleoclimate data such as mean annual precipitation and temperature using different independent proxy data – elemental data, magnetic susceptibility and stable carbon isotopic composition. The results are also cross-validated with regional proxy data from the literature and modelling results. Study 3 addresses the fact that there is only few quantitative evidence to support some widely acknowledged hypotheses about the origin of loess in the Carpathian Basin. Here, we use established techniques such as Sr-Nd isotopic analyses from sedimentary geology and compare the results with literature data of potential source areas, i.e. mountain ranges and floodplain sediments of major rivers. Study 3 is

complemented by a European perspective of sediment dynamics that shifts the regional focus from SE Europe to two additional study areas in Austria (Grub, East Austria) and Germany (Nussloch, Southwest Germany).

To predict and adapt to our future climate we need to understand the past – which we can only do if we leverage all available data in a truly multidisciplinary approach. It is to this overriding belief and ambition that this piece of work tries to contribute.

2. Study area

2.1 Loess in the Carpathian Basin

The Hungarian Quaternary paleoenvironment is one of the missing links to understand Quaternary climate in Europe (Rudner and Sümegi, 2001; Sümegi and Hertelendi, 1998; Sümegi and Rudner, 2001; Willis et al., 2000; Willis et al., 1995). The Carpathian Basin (Fig. 1), also called Pannonian Basin, is a large region of low relief surrounded by major mountain ranges that has remained unglaciated during the last ice age (Denton and Hughes, 1981) and therefore might have been an important refuge for temperate flora and fauna, or at least one of the first regions into which this flora and fauna expanded in the early postglacial (Sümegi and Hertelendi, 1998; Willis et al., 1995). The Carpathian Basin is largely part of Hungary and covers an area of 300.000 km^2. It is surrounded by the Carpathians in the North, East and Southeast, the Alps in the West and the Dinaric Alps in the Southwest (Rudner and Sümegi, 2001). The basin itself consists mainly of alluvial plains and basins. Generally, geology, topography, climate and vegetation are complex and heterogeneous. This is partly due to the highly complex geologic history of the area (Matenco and Radivojević, 2012), but also to Hungary being the meeting point of four distinct climatic regions: oceanic climate in the West, submediterranean conditions in the South, continental climate towards the East and sub-montane climate towards the North and in the mountainous regions (Rudner and Sümegi, 2001; Sümegi and Krolopp, 2002).

The Carpathian Basin is not part of the European Loess Belt stretching from Paris to Krakow, as it was cut off from the dust supply of the North European glaciations by the surrounding mountain belts. Consequently, other contributing source areas have to be taken into account. Smalley and Leach (1978) have proposed three different possible sources for Pleistocene dust: (a) sediments from the Alpine glaciers transported by the Danube and deposited on its floodplains in Hungary, (b) North European meltwater carrying debris through the Moravian depression (c) silt from the weathering of rocks in the Carpathians, carried by the Tisza. They also suggest that, in the

Carpathian Basin, aeolian loess is mainly a product of short-distance transport from adjacent river floodplains and that long-distance transport is usually fluvial in this region. Smalley and Leach conclude that the most important constituent of loess deposits in East and North East Hungary is the sedimentary input from Carpathian Tertiary flysch carried by the Tisza and Alpine glacial material carried by the Danube. The Carpathians are a 1500 km long Mesozoic-Tertiary mountain range stretching as a semicircle from Southeast to Northwest. They are part of the Alpine-Himalayan belt and consist mainly of folded and thrusted crystalline rocks, sedimentary basins, volcanic rocks and flysch-molasse belts (Rudner and Sümegi, 2001). The Tisza is one of the major rivers draining the Carpathian Mountains and the Great Hungarian Plain, flowing from NE to the South of Hungary before discharging into the Danube close to Novi Sad, Serbia. Smalley and Leach's hypotheses are, however, theoretical considerations and not backed up by actual data. First (semi-)quantitative evidence for the origin of loess in the Carpathian Basin has been provided by Thamó-Bozsó et al. (2014) using heavy mineral analyses and by a combined Sr-Nd and U-Pb isotopic approach of Újvári et al. (2012). The results largely confirm Smalley and Leach's hypothesis regarding Danube sediments as the main source of loess in the Carpathian Basin, but also show that the data base is still too small and the choice of methods too limited to allow for definite conclusions.

2.2 Physiogeographic setting of the Tokaj region

Tokaj forms the meeting point of the northern edge of the Great Hungarian Plain and the Southern edge of the (West) Carpathians, a low mountain region (Fig. 1). At Tokaj, the river Bodrog discharges into the Tisza, forming extensive floodplains. Today, Northeast Hungary is part of the continental climate zone (*Dfb* after Köppen's classification: cold climate type, no dry season, warm summer subtype), with a large seasonal temperature variance (mean January temperature: -3°C; mean July: 20°C) and a mean annual precipitation of ~ 600 mm with a summer maximum (Peel et al., 2007). However, the meso- and microclimates on the slopes of the hill differ from the regional climate. The conditions on the slopes facing north have been described as sub-montane (summer 19-20 °C, winter -3 °C), while sub-mediterranean conditions prevail on the southern slopes (summer 23-24 °C, winter 0 °C) (Sümegi and Hertelendi, 1998). The recent natural vegetation of Northeast Hungary consists of large grassland areas, but also of broad-leaved, needle-leaved and mixed forests (Hartley, 2003). While grassland and herbaceous vegetation cover is rather confined to the Great Hungarian Plain and its border areas, forests tend to occur in hilly, sub-montane regions. However, the vast majority of the land surface in this region is cultivated cropland that has replaced the natural vegetation.

The area around Tokaj is considered of highest paleoenvironmental significance, as it may have been an important refuge for deciduous and coniferous trees during the last ice age due to a favourable microclimate on the hill slopes (Sümegi and Hertelendi, 1998). The same authors even suggest a double forest refuge for both cold-loving and warm-loving species.

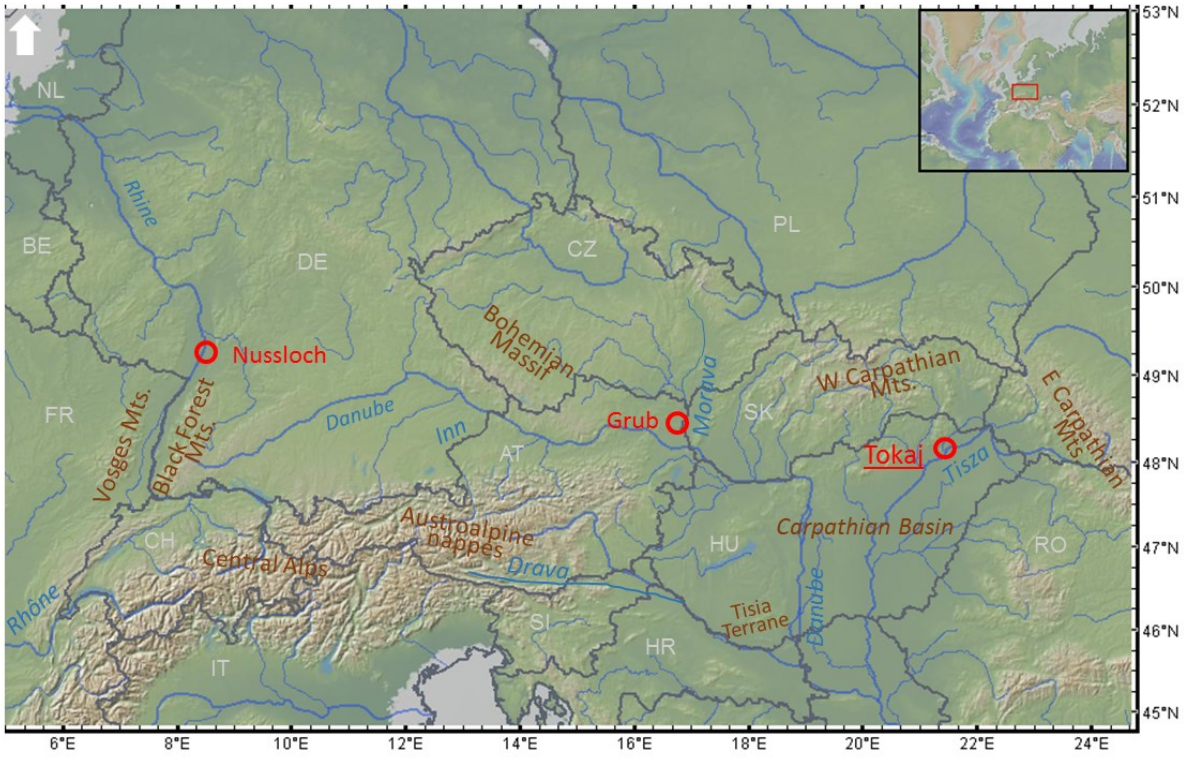

Fig. 1: Map of the study area, major rivers and mountain ranges and geological units. Tokaj is situated in NE Hungary on the banks of the Tisza river. Additional samples from Grub (Austria) and Nussloch (Germany) were only used in Study 3.

2.3 The Patkó quarry section

The study site is situated on the eastern slopes of Kopasz Hill (also called Nagy-hegy; 515 m a.s.l., 48°13'N, 20°27'E) on the southernmost part of the Tokaj Mountains. Kopasz Hill is an extinct stratovolcano Mid-Miocene age and built up of pyroxene andesite and dacite lava tongues (16.4 km^2) that have partly been eroded and subsequently covered by 15-20 m of Pleistocene loess (Kerényi, 1994; Sümegi and Hertelendi, 1998). The loess on top of the hill has been eroded over time, yet the flanks are still entirely covered. The thickest layers are typically found on the Eastern slopes. However, erosion rates are as high as 0.5-0.7 m per decade (Kerényi, 1994). There are about 11 well-described loess outcrops around Kopasz Hill (Sümegi, 2005). Several paleontological and sedimentological studies have been carried out at the Patkó quarry section

on the eastern slope of the mountain (Rudner and Sümegi, 2001; Sümegi and Hertelendi, 1998; Sümegi and Krolopp, 2002; Willis et al., 2000), where two well-developed paleosols and three loess layers are exposed on top of an approximately 40 m high dacite wall. The loess walls on top have been partly removed and cut backwards due to the mining activities, but the remaining loess has essentially stayed unaltered. Because of the artificial steps in the profile and security issues, the profile had to be split into two sections for sampling (Fig. 2a, b).

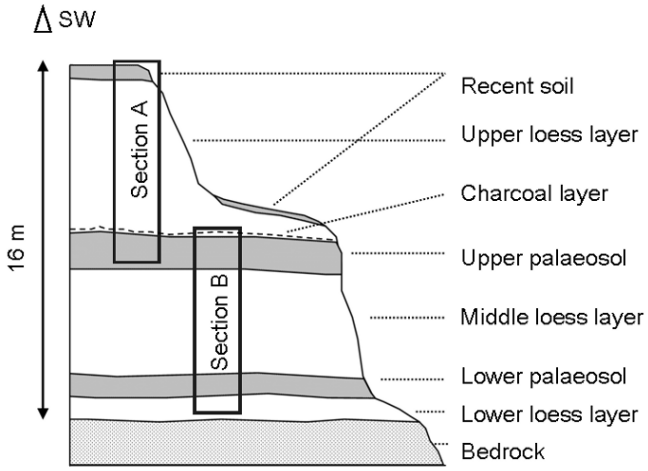

Fig. 2: a) Photo of the Patkó quarry section, facing W. The investigated loess section is situated on top of a 40 m high rock wall. The positions of the upper and lower palaeosols are indicated with arrows.

b) Profile sketch of the paleosol-loess section at Patkó quarry. Due to logistic reasons the profile had to be split into two overlapping sections for sampling (Section A and B).

The Patkó quarry outcrop and the results of first sedimentological and geochemical investigations have been described in detail by Sümegi and Rudner (2001) and Sümegi and Hertelendi (1998). However, a valid chronostratigraphy is still missing. Very basically, the lowermost yellow-brown, unstratified loess layer has been dated to 70-50 ka BP based on vertebrate remains found in similar stratigraphic positions elsewhere in the area (Pinczés, 1954, 1987). It is assumed that this layer accumulated during the first cold and dry phase of the last glacial. This is further supported by cryophilous molluscs found in this layer, indicating an open steppe or tundra environment with mean July temperatures of 12-13 °C. The Lower Paleosol lies on top of the lowermost loess layer. It is a dark brown soil with a high clay content that was formed under humid, warm conditions. Very low concentrations of soluble elements indicate strong weathering and pedogenesis. Similar to the Lower Paleosol, the Middle Loess layer contains no molluscs or charcoal. Therefore, no paleoenvironmental information has been reported. On top of this intermediate loess layer, the

Upper Paleosol developed, a reddish-brown, charcoal-rich horizon with low carbonate content. Mollusc data indicate a mild and wet climate similar to today. This reddish-brown paleosol rich in Al, Fe, and Mn is overlain by a bleached, whitish layer with high silica content, which has been interpreted as remnants of a Podsol. On top of this white layer, a thin charcoal layer of burned *Picea* and *Pinus* pieces can be found. This charcoal layer has been dated to 28-26 ka BP and interpreted as the result of extensive natural wildfires occurring after pedogenesis ceased and the climate became extremely dry, which is also supported by the sudden occurrence of xerophilous molluscs. Needle-leaved forests, dominated by *Picea*, are also in line with a possible Podsol development since Podsols are typical soils of coniferous boreal forests. Further evidence for forests at Kopasz Hill comes from the presence of fossil branches and trunks of the same age that have been found at another outcrop on the hill in the same stratigraphic position. In the Upper Loess layer, cryo-xerophilous and tundra-dwelling molluscs are abundant, indicating a cold continental steppe environment. Willis et al. (1995) report that from 12 ka BP onwards the climate became gradually warmer in Northeast Hungary and around 6-7 ka BP the first human communities developed in the area. However, at Tokaj, the sedimentary and archaeological record from this time has been eroded. The recent topsoil is only weakly developed which might be due to intensified natural and anthropogenically induced erosion (Kerényi, 1994) caused by the agricultural activities on the slopes and the mining in the quarry.

A recent study based on a combined mineral-magnetic, sedimentological and geochemical approach using C and N stable isotopes and biomarkers (Schatz et al., 2011) largely confirms the results from previous mollusc studies and provides more detailed insights into the paleoenvironmental history of the Tokaj region. The authors propose cyclic climatic and environmental changes during the entire time span that the profile covers (Fig. 3). The data suggest two cool, treeless-steppe periods during the time when the Upper Loess layer accumulated, but also intervals of more favorable climate in which trees and shrubs expanded, forming “open parkland” environments. Based on alkane and stable N isotopic data, pedogenesis most likely occurred under fertile steppe-grasslands, probably in an intensified, warm seasonal climate.

3. Methods and their use in paleosol-loess studies

3.1 Sample material and nomenclature

Due to the topology and to safety concerns, the Tokaj profile had to be sampled in two sections. After removing at least the first 30 cm of the front in order to avoid sampling weathered sediment

and recent biological material, the sections were prepared and fully described with regard to color, density, texture and occurrence of fossil and modern roots, carbonate mycelia and charcoal remains. For laboratory analyses, mixed samples were taken in 25 cm intervals, stored in plastic bags and dried at 40 °C for several days. Luminescence samples were taken by hammering steel cylinders horizontally into the loess wall, which were then sealed with light-tight lids. The samples from Nussloch and Grub (Study 3) were kindly provided by L. Zöller and taken according to standard sampling procedures, but in irregular intervals. The basic stratigraphies are explained in Study 3.

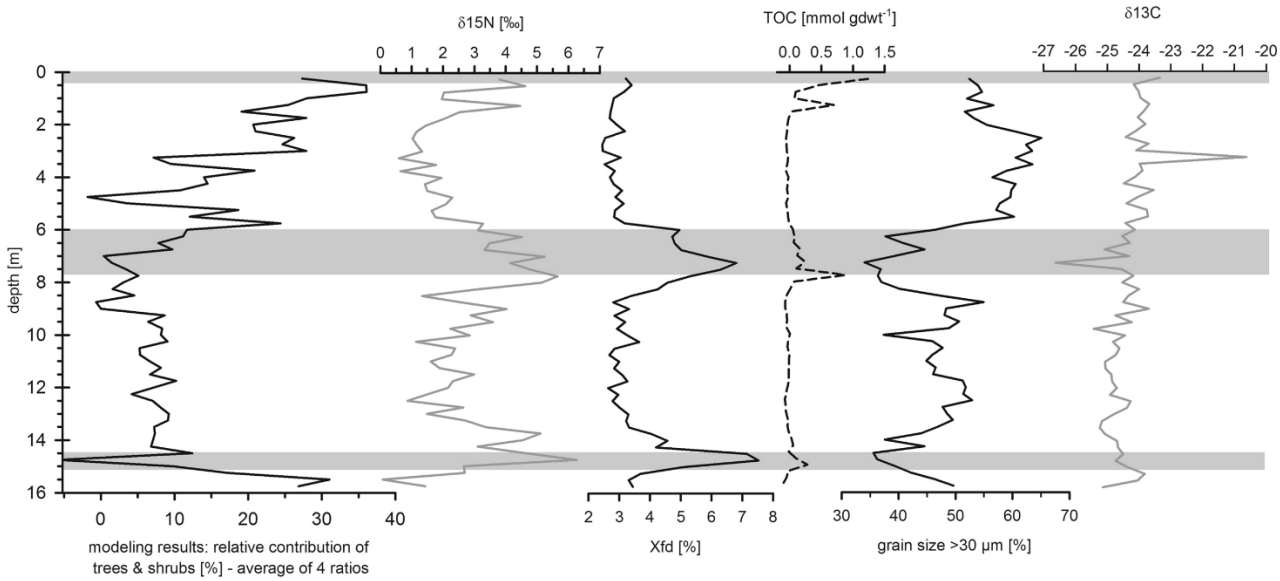

Fig. 3: Overview of previous research at the Tokaj paleosol loess section (Schatz et al., 2011), including (left to right) n-alkanes as a proxy of vegetation (shrubs and trees vs. grassland), stable N isotopes, frequency-dependent magnetic susceptibility, total organic carbon, grain size distribution (>30 µm) and stable carbon isotopes. Stable N isotopic ratios have been interpreted to increase with an increase in MAT and a decrease in MAP. Stable C isotopic ratios do not provide evidence for a shift from C3 to C4 vegetation or vice versa. Single peaks are considered outliers; the same applies for TOC. Paleosols are indicated by a grey shade.

3.2 Luminescence dating

Luminescence dating - usually referred to as “OSL” (optically-stimulated luminescence) for quartz samples and “IRSL” (infrared-stimulated luminescence) for feldspar samples - is the preferred dating method for Quaternary aeolian samples. It has three main advantages over other methods that are commonly used to determine sedimentation ages. First, luminescence dating can be applied to the constituent minerals of the sediment itself (quartz, feldspar) and is not constrained

to associated particles, as e.g. charcoal. Second, the derived ages do not need additional calibration, as e.g. ^{14}C dating. Third, it is one of the few methods that are able to date the time of sediment deposition or, more precisely, the last exposure of the mineral grains to daylight.

Luminescence dating is based on the fact that minerals in sediment are exposed to low-level ionizing radiation from the decay of radioactive isotopes in the surrounding sediment, mainly U, Th and K. The flux of ionizing radiation creates free charge within the crystal structure. Some of this charge, usually electrons, is trapped in meta-stable states within the crystal lattice. By exposing the crystal to daylight, the trapped electrons receive sufficient energy to leave the traps and return to their normal state. This release of trapped energy, usually called “bleaching”, “resetting” or “zeroing”, is the moment when the “clock” is set back (Fig. 4). Being shielded from daylight after sediment deposition and burial, trapped charge starts to build up in the crystals.

If samples are exposed to a light source under laboratory conditions, this causes the release of electrons and the emission of photons. The release of light is the luminescence signal. The light intensity is a measure of the amount of radiation-induced electrons, which is dependent upon (i) the rate of ionizing radiation per unit of time (“dose rate”) and (ii) the duration of burial, i.e. age. The longer a mineral is exposed to the flux of radiation the greater the radiation damage. The intensity of the radiation damage is consequently a measure for the total amount of energy absorbed from the ionizing radiation the mineral has received over a certain period of time (Aitken, 1998) and can be measured in the laboratory using a photomultiplier tube. The emitted luminescence signal is then compared with luminescence signals induced by different radiation doses. This is necessary to derive the laboratory dose required to give the same luminescence signal as was absorbed to give the 'natural' signal, usually termed “equivalent dose” (D_e). In addition to the equivalent dose, the rate of energy absorption from ionizing radiation has to be measured, taking into account the small contribution from cosmic rays and the effect of water in the sediment as well. Once both equivalent dose and dose rate have been determined, the luminescence age can be calculated cf. Eq. 1 (Aitken, 1985, 1998):

$$age\ [ka] = \frac{equivalent\ dose\ D_e\ [Gy]}{dose\ rate\ [Gy/ka]}$$

Despite being widely accepted as the main dating technique in loess studies, luminescence has two main shortcomings. On the one hand, the age range of quartz-based luminescence is rather short (ca. 50-70 ka; Murray et al., 2014). Quartz saturates at much lower doses as feldspar. In combination with a high dose rate, this may constrain the potential age range to the younger half

of the last glacial only. On the other hand, feldspar-based luminescence ages usually need to be corrected for “anomalous fading” (Wintle, 1973), a phenomenon that causes leakage of electrons from their traps and loss of the age signal. Although there are methods to detect and correct for anomalous fading (Huntley and Lamothe, 2001; Lamothe et al., 2003), an additional source of uncertainty is introduced.

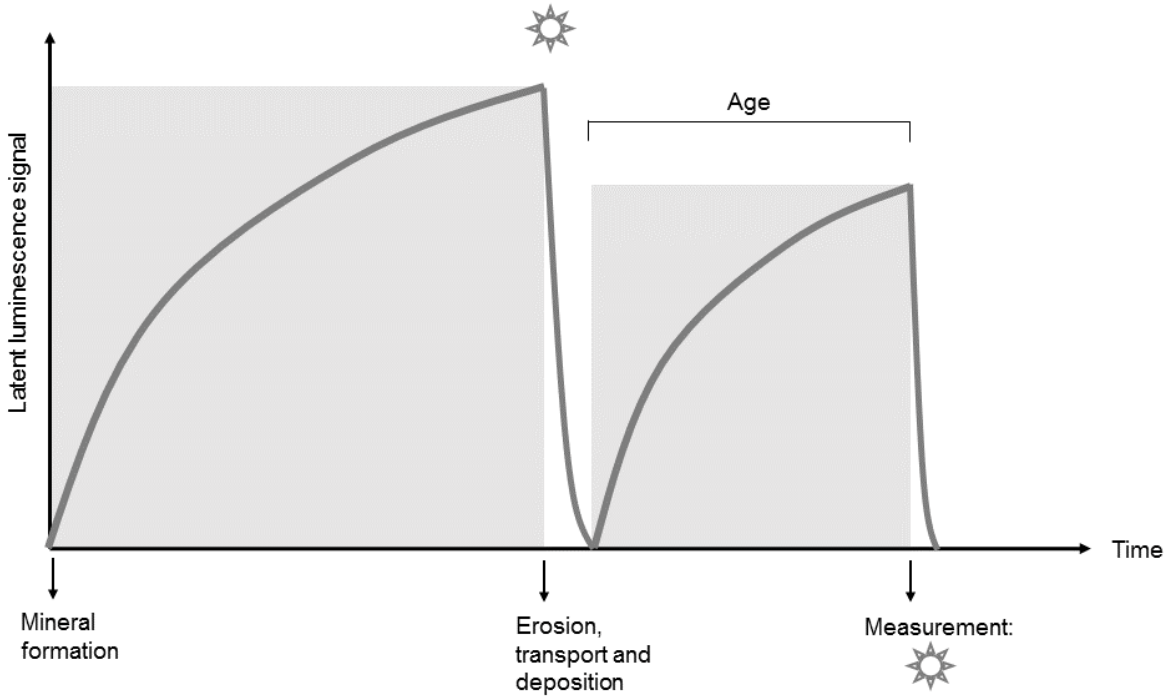

Fig. 4: Schematic representation of luminescence dating. Minerals are continuously exposed to natural radioactivity, through which they acquire a latent luminescence signal. During erosion, transport and deposition, the minerals are exposed to sunlight and all the previously accumulated luminescence is removed (“bleaching”). After burial, the signal starts to build up again, until the moment of measurement in the laboratory when the sample is exposed to a light source. The age obtained is the time that has elapsed between these two zeroing events (Vandenberghe, 2004).

Since there is no universally applicable measurement procedure, every sediment type and specific measurement approach have to be carefully matched and tested for suitability before the actual dating procedure can be carried out. For fine-grained quartz, the SAR protocol (Murray and Wintle, 2000) is a common and reliable approach that has been used in many different luminescence dating studies (Murray and Olley, 2002; Roberts, 2008). For feldspar, several measurement protocols have been proposed. Earlier studies have focused on the standard, low-temperature IRSL approach (IR_{50}), which requires fading correction (see Roberts, 2008 for a review). The elevated-temperature post-IR IRSL ($pIRIR_{290}$) protocol has recently gained a lot of attention since

it yields reliable results and requires no fading correction (Buylaert et al., 2012; Murray et al., 2014; Schmidt et al., 2014; Thiel et al., 2014; Thomsen et al., 2008).

3.3 Whole-rock geochemistry

3.3.1 Weathering Indices

Loess and paleosol samples can be analyzed as “whole rock” bulk samples just as any other rock sample, e.g. for X-ray fluorescence (XRF) analyses to study major, trace and rare earth composition. Under weathering conditions, the elemental composition of a rock, sediment or soil changes. Soluble and mobile elements are depleted, while less soluble and immobile elements are enriched and retained. Furthermore, mineral transformation and formation of secondary minerals such as clay, iron oxides or salts may occur. Weathering proxies, i.e. proxies of mineral alteration, contain one or more mobile and immobile elements, respectively, often alkali and earth alkali elements with a small ionic radius (e.g. Na, Ca, Mg, Sr) as mobile and elements with intermediate ionic potential (e.g. Al, Si, Ti, Rb, Ba) as immobile refractory elements (Buggle et al., 2011). Elemental ratios, e.g. Al/Si, a measure of “clayeyness”, are superior to single-element abundances since chemical heterogeneity and variation in absolute abundance are eliminated and additional process information may be gained. Yet simple element ratios only quantify single weathering processes such as clay formation, gleyization, leaching or salinization (Sheldon and Tabor, 2009; their table 3). In order to quantify weathering more thoroughly and measure weathering intensity more accurately, more complex weathering indices (WI) have been developed which are calculated using two or more major elements.

Common multi-element WIs based on a wide variety of elements are the Σbases/Al ratio (Retallack, 2001) and the Paleosol Weathering Index (PWI; Gallagher and Sheldon, 2013). Other WIs are based on a more limited selection of elements (Al, K, Na, Ca) to focus on the weathering behavior of feldspar minerals only. An advantage of these feldspar indices is the fact that all index elements are hosted in the same mineral group, which helps minimizing the effects of variations in mineralogy. Common feldspar indices are the widely used Chemical Index of Alteration (CIA; Nesbitt and Young, 1982) and Indices A and B (Kronberg and Nesbitt, 1981).

In order to exclude potential effects arising from the inconsistency in K weathering (Buggle et al., 2011), several indices without K were developed, most prominently the Chemical Index of Weathering (CIW, also called CIA-K; Harnois, 1988), which is the K-free equivalent of the CIA,

and the Plagioclase Index of Alteration (PIA, Fedo et al., 1995), a further modification of CIA and CIW that adjusts for Al contained in K-feldspar and results in an account of pure plagioclase weathering. The Yang et al. (2006) index uses Ti instead of Al as a refractory element and has been developed specifically for loess-paleosol studies, whereas WI-1 and WI-2 (Darmody et al., 2005) are still to gain more attention. Due to problems associated with determining the correct amount of silicate-bound Ca, indices that do not rely on Ca might be preferable, such as the index of Feng (1997) or the Chemical Proxy of Alteration (CPA, also known as CIW'; Cullers, 2000, Buggle et al., 2011), which excludes both Ca and K, thus attempting to avoid all potential biases.

Trace element indices are another sub-group of weathering indices. Both Ba/Sr and Rb/Sr represent leaching behavior during weathering with Ba and Rb being less soluble than Sr. Potential weakness in these indices are the poorly understood behavior of Rb and Ba in the sediment (Gallet et al., 1996; Sheldon and Tabor, 2009), grain-size dependence and the fact that variable and low initial concentrations may result in erroneously high weathering intensities. In addition to that, Sr substitutes for Ca and is therefore controlled by calcite and dolomite behavior.

Despite an ongoing debate about the reliability of weathering indices (Buggle et al., 2011; Li and Yang, 2010; Xiao et al., 2010), many successful applications have been published to date, mainly, but not limited to, Quaternary loess and paleosols in Europe (Buggle et al., 2011; Kovács, 2007; Kühn et al., 2013; Újvári et al., 2008; Újvári et al., 2014; Vancampenhout et al., 2013), North and South America (Goldberg and Humayun, 2010; Hall and Penner, 2013; Meier et al., 2014), China (Baumann et al., 2014; Chen et al., 1999; Xiong et al., 2010), Southern Arabia (Pietsch and Kühn, 2012) and Siberia (Zech et al., 2008). A compilation of how frequently these indices are employed in loess paleosol studies is given in Table 1.

3.3.2 Paleoclimate reconstructions

Weathering indices may not only be used to quantify weathering intensity, but also to estimate paleoclimate parameters, i.e. mean annual temperature (MAT) and mean annual precipitation (MAP) via specifically calibrated empirical transfer functions (Sheldon et al., 2002; Sheldon and Tabor, 2009). This is due to the fact that the degree of chemical weathering increases with available precipitation and temperature, which both serve to accelerate the depletion of soluble elements in sediments and soils. All other factors equal, more clay should be formed in a wetter climate than in an arid climate during the same period of time. To quantify these relationships, several transfer or climofunctions have been developed based on empirical relationships of MAT

and MAP and the geochemical compositions of modern soils from a large North American dataset (Marbut, 1935). Ideally, a dataset used as a basis for transfer functions specifically for (Southeast) Europe would contain local soil data but such a dataset is not available. The North American soils used to derive the transfer functions have a very large variety in formation times, formation processes and parent materials. Therefore, it can be assumed that they are representative for European paleosols as well and, consequentially, the transfer functions can be applied to those, too.

Table 1: Compilation of weathering indices from Study 3 calculated with elemental data (XRF). For an overview of how often these indices have been used in previous loess studies, they were classified into two groups based on a rough review (Google Scholar) of Quaternary loess studies in Europe, N America or China. Infrequent ("X) is defined as none or very few publications (<5), frequent ("F") as 5 or more citations.

Weathering index		**Elements**	**Reference**	**Use**
Multi-element	CIA	Al, Na, Ca, K	Nesbitt and Young (1982)	F
	Index A	Si, Ca, K, Na, Al	Kronberg and Nesbitt (1981)	X
	Index B	Ca, Na, K, Al	Kronberg and Nesbitt (1981)	X
	PWI	Na, Mg, K, Ca	Gallagher and Sheldon (2013)	X
	Σbases/Al	Ca, Mg, Na, K, Al	Retallack (2001)	X
K-free	CIW (CIA-K)	Al, Na, Ca	Harnois (1988); Maynard (1993)	F
	PIA	Al-K, Al, Ca, Na-K	Fedo et al. (1995)	X
	YANG	Ca, Na, Mg, Ti	Yang et al. (2006)	F
	WI-1	Si, Ca, Fe, Ti	Darmody et al. (2005)	X
	WI-2	Si, Ca, Fe, Ti, Al	Darmody et al. (2005)	X
Ca-free	CPA (CIW')	Al, Na	Buggle et al. (2011); Cullers (2000)	F
	FENG	Al, Fe, Na, K, Mg, P	Feng (1997)	X
Trace element	Ba/Sr	Ba, Sr		F
	Rb/Sr	Rb, Sr		F

Positive evidence encouraging the use of the transfer functions for paleosols has e.g. been reported by Sheldon et al. (2002), Sheldon (2004) and Sheldon (2009) who found their paleoclimate estimates consistent with results obtained from independent paleobotanical proxies, or accurate over a wide age range (Hamer et al., 2007; Retallack, 2005; Sheldon, 2005). Furthermore, the transfer functions successfully predict modern MAP even for soil types that are not represented in the original Marbut (1935) database (Driese et al., 2005; Nordt, 2006). With regard to the application of the transfer functions not only to paleosols, but also to loess, Kühn et al. (2013) have argued that they can indeed be used for both materials. Since loess is the parent material of the paleosol, it should include a genuine climate signal as well. In their study, Kühn et

al. (2013) used two different equations and received similar MAP and MAT results for loess. Their results show a clear trend towards lower temperatures for loess than for the paleosol and MAT/MAP estimates that are comparable to those obtained from other proxies. These observations encourage the application of the transfer functions to loess.

On the other hand, several issues arise with the use of transfer functions and need to be addressed when interpreting the results. First, other processes than weathering may change the chemical composition of sediments and soils as well and may therefore lead to a bias. Second, large uncertainties are usually associated with the MAPs and MATs, which tend to be underestimated and are sometimes not reported in a statistically sound way (Újvári, 2014). An error range of up to several degrees Celsius for MAT or hundred mm/a for MAP needs to be taken into account. Both factors require a careful evaluation of the results and a verification with independent estimates from the literature or from transfer functions based on other proxies such as magnetic susceptibility or stable isotopes. Despite the lack of precision, the geochemistry-based reconstructions are able to demonstrate significant trends and provide valuable and, at least semi-quantitative, paleoclimate information.

Although published for several years, the transfer functions are still to gain more attention in loess-paleosol studies, especially for SE Europe since most successful studies have been conducted elsewhere, with recent studies in Germany (Kühn et al., 2013), North America (Meier et al., 2014) and Southern Arabia (Pietsch and Kühn, 2012). A compilation of how frequently these equations are employed in loess paleosol studies is given in Table 2.

Climate parameter	Equation	Reference	Use
MAP-1	-259.3*Ln[Σ(bases/Al)]+759	Sheldon et al., 2009	F
MAP-2	-130.9*Ln(Ca/Al)+467	Sheldon et al., 2009	X
MAP-3	$221.9*e^{0.0179*(CIA-K)}$	Sheldon et al., 2009	X
MAT-1	46.9*(Al/Si)+4	Sheldon, 2006	X
MAT-2	-18.5*[(K+Na)/Al]+17.3	Sheldon et al., 2002	X
MAT-3	-2.74*Ln(PWI)+21.39	Gallagher & Sheldon, 2013	X

Table 2: Paleoclimate transfer functions for mean annual temperature (MAT) and mean annual precipitation (MAP) calculated from elemental data (XRF). Some of the functions are based on weathering indices (Σbases/Al, CIA-K, PWI) listed in Table 1. For an overview of how often these transfer functions have been used in previous loess studies, they were classified into two groups based on a rough review (Google Scholar) of Quaternary loess studies in Europe, N America or China. Infrequent (“X) is defined as none or very few publications (<5), frequent (“F”) as 5 or more citations.

3.3.3 Geochemical characterization

In provenance studies, the abundances of major, trace and rare earth elements, displayed as elemental ratios or normalized diagrams of elemental variations ("spider diagrams"), may serve as characteristic sediment "fingerprints" and be subsequently compared with those of potential source rocks. Element ratios for provenance analyses are conceptually similarly to those used for weathering analyses (3.3.1) and usually consist of one element with variable abundances over a wide range of different rock types, such as e.g. Ti, and another element with relatively constant abundance, e.g. Al (Sheldon and Tabor, 2009). Both elements should be of low mobility and not prone to removal or enrichment by weathering in order to avoid bias. Common ratios are SiO_2/Al_2O_3, TiO_2/Al_2O_3, TiO_2/SiO_2, K_2O/Al_2O_3, Na_2O/Al_2O_3 or combinations thereof, e.g. Na_2O/Al_2O_3 vs. K_2O/Al_2O_3. Spider diagrams are a widely used method to display enrichment and depletion patterns of a wide range of major and trace elements compared to a reference composition such as the average composition of the upper continental crust (UCC).

Both element ratios and spider diagrams help to characterize a sample based on characteristic abundances of its elemental composition. These characteristic patterns will then be used for comparison with patterns of potential source rocks, average rock or sediments compositions (e.g. GAL, global average loess composition; Újvári et al., 2008) or other sediments to explore similarities and differences and to identify e.g. common transport pathways. This was successfully done by Muhs and Budahn (2006) for Alaskan loess and fluvial samples or Buggle et al. (2008), who compared loess from Serbia, Romania and Ukraine with floodplain sediments from Central and Southeast Europe. Other studies based on the geochemical characterization of loess deposits and potential source areas have been carried out e.g. in China, South Korea, the US, Croatia and Hungary (Hwang et al., in press; Jahn et al., 2001; Mikulčić Pavlaković et al., 2011; Muhs et al., 2008; Muhs et al., 2013a; Újvári et al., 2008; Újvári et al., 2014).

Potential limitations and constraints may arise from any alteration of the original geochemical and mineralogical composition of a sample e.g. by pedogenesis and weathering, secondary mineral formation or sorting during transport. To minimize this bias, paleosol samples are usually excluded in loess provenance studies. Mixing may also obscure the characteristic chemical signatures of multiple sediment sources. Therefore, sediment sources can only be ruled out, but not confirmed based on elemental fingerprinting alone (Buggle et al., 2008; Újvári et al., 2012). While limiting the informative power of the results, fingerprinting methods still provide valuable information by excluding potential source areas and uncovering similarities and differences of sediments and potential sources.

3.4 Sr-Nd isotopic characterization

The use of strontium and neodymium isotopic ratios is based on the fact that rocks of different geologic origin have distinct Sr and Nd isotopic signatures. Mantle rocks, such as Mid Ocean Ridge Basalts (MORBs) have high $^{143}Nd/^{144}Nd$ ratios, resulting in positive ε_{Nd} values, and low $^{87}Sr/^{86}Sr$ ratios and therefore plot in the upper left quadrant of the Sr-Nd diagram (Fig. 5). Crustal rocks and sediments derived from them, in contrast, have high $^{87}Sr/^{86}Sr$ and low $^{143}Nd/^{144}Nd$ ratios, i.e. negative ε_{Nd} values, and plot in the lower right quadrant of the Sr-Nd diagram. The bulk earth composition (Chondritic uniform reservoir, CHUR) delineates the four quadrants in the Sr-Nd diagram and serves as a reference. Instead of the $^{143}Nd/^{144}Nd$ ratio, the ε_{Nd} value is usually reported, which is calculated by normalizing the Nd ratio of a sample to the CHUR ratio (0.512638, Jacobsen and Wasserburg, 1980) cf. Eq. 2:

$$\varepsilon_{Nd} = \left[\frac{\left(\frac{^{143}Nd}{^{144}Nd}\right)_{sample} - \left(\frac{^{143}Nd}{^{144}Nd}\right)_{CHUR}}{\left(\frac{^{143}Nd}{^{144}Nd}\right)_{CHUR}} \right] * 10.000$$

The different isotopic compositions of Sr and Nd in a sample are due to fundamental differences in their geochemical behavior. The radiogenic isotope ^{87}Sr is a daughter atom produced by the radioactive decay of ^{87}Rb, a trace element which substitutes for K in clay minerals. Rubidium is a highly incompatible element that, during fractional crystallization of the mantle, stays in the magmatic melt rather than becoming part of mantle minerals and is therefore enriched in crustal rocks. By comparing the abundance of ^{87}Sr with that of the non-radiogenic and stable ^{86}Sr, the isotopic ratio $^{87}Sr/^{86}Sr$ may serve as a characteristic isotopic fingerprint of a sample. While closely related, the geochemical behavior of Nd is directly opposed to that of Sr. ^{143}Nd is a decay product of ^{147}Sm. Samarium, however, is highly mantle-compatible and therefore depleted in crustal rocks. Nd-enriched mantle rocks have higher $^{143}Nd/^{144}Nd$ ratios and positive ε_{Nd} values. Together with non-radiogenic and stable ^{144}Nd, the $^{143}Nd/^{144}Nd$ ratio complements the $^{87}Sr/^{86}Sr$ fingerprinting method.

The combination of both systems allows for distinguishing rocks based on their geologic origin and chemical composition and may ultimately help identifying the parent rocks of sediments in provenance studies. Sr-Nd analyses have served as a valuable tool for loess provenance studies in China and South America, where they were used to identify and delineate major contributing dust source areas and examine source stability over time (Chen et al., 2007; Gallet et al., 1998; Smith et al., 2003; Sun, 2002, 2005; Zhang et al., 2012). First results for Southeast European

loess have been reported by Újvári et al. (2012), who used a combination of Sr-Nd and U-Pb isotopic provenance indicators to characterize loess samples in the Carpathian Basin and compare them with a large variety of potential source areas.

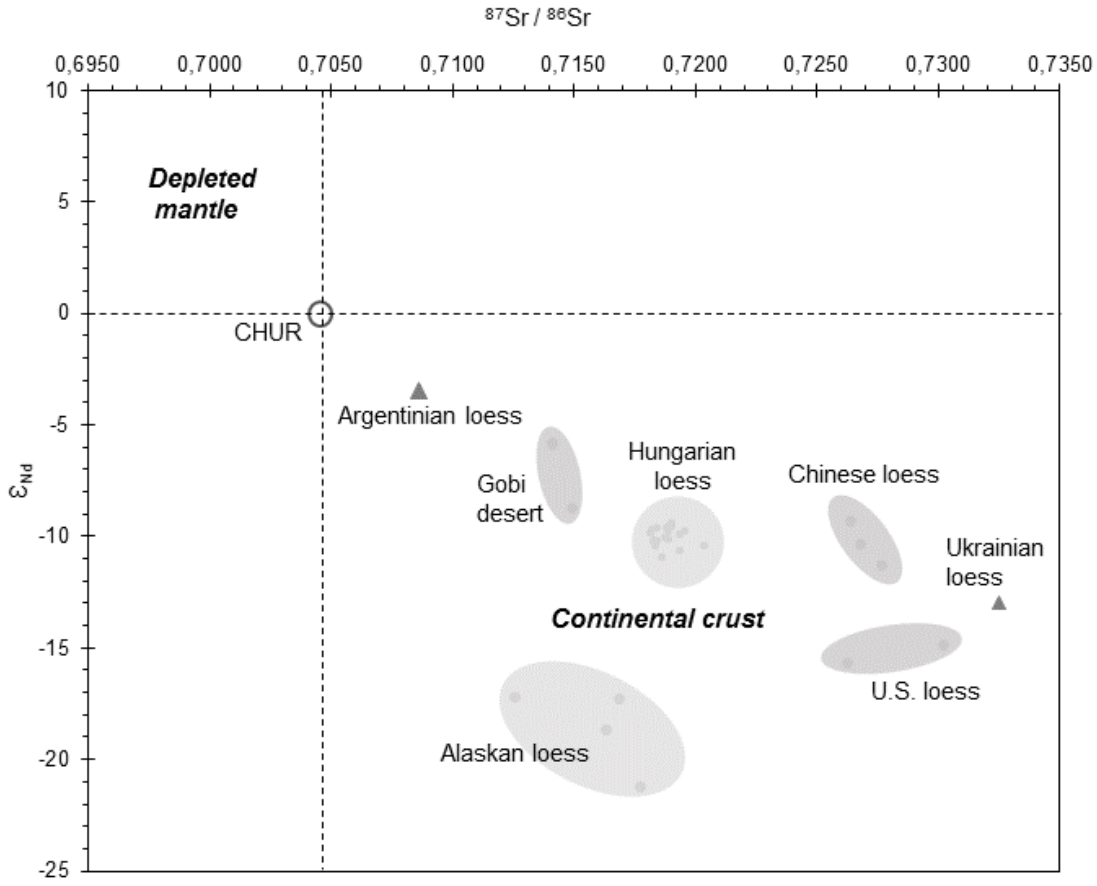

Fig. 5: $^{87}Sr/^{86}Sr$ vs. ε_{Nd} diagram showing the positions of the depleted mantle, the continental crust, the chondritic uniform reservoir (CHUR, "bulk earth") and selected loess samples from N and S America, Europe and Asia.

4. Results and discussion

4.1 Application of established and novel luminescence techniques (Study 1)

4.1.1 Method development

One aim of study 1 was to compare standard quartz OSL with standard feldspar (polymineral) IR_{50} luminescence ages and ages obtained using a novel feldspar (polymineral) dating protocol at elevated temperatures ($pIRIR_{290}$), which is expected to have an extended age range and be less prone to fading. For quartz OSL, using the standard SAR protocol (Murray and Wintle, 2003) on

9 samples spread roughly evenly over the entire profile, all luminescence characteristics were satisfactory and the ages obtained range from roughly 60 ka to 20 ka. While the youngest 5 samples are considered reliable, the oldest three have natural signals at 70% of saturation and may therefore underestimate. A comparison of IR_{50} and OSL ages shows that IR_{50} underestimates substantially if not appropriately corrected for fading. However, the results show that even fading-corrected IR_{50} ages still underestimate in the younger section of the age range of the profile and were therefore entirely not considered any further.

The luminescence characteristics of the results obtained using the novel $pIRIR_{290}$ protocol (Thiel et al., 2011) are all satisfactory. In contrast to OSL, the natural signal is well below saturation level; the samples pass the dose recovery, recycling and recuperation tests. As previously pointed out (Buylaert et al., 2012; Buylaert et al., 2011; Sohbati et al., 2012), a significant residual dose, i.e. a non-bleachable component of the signal, may be present, which will lead to erroneous ages if unaccounted for. The magnitude of this residual was measured in a bleaching experiment under natural and controlled laboratory light conditions. Three aliquots of each sample were bleached for 1 week in a Hönle SOL2 solar simulator simulating daylight/night; the same number of aliquots were exposed to daylight for the same period of time (Denmark, February). A mean residual dose of ca. 10 Gy was measured, which is consistent with the $pIRIR_{290}$ doses reported for polymineral fine-grains extracted from modern dust (Buylaert et al., 2011), and subsequently subtracted from all $pIRIR_{290}$ equivalent doses.

Fading tests showed that while the $pIRIR_{290}$ signal is more stable than the IR_{50} signal, fading is still measurable on laboratory time scales (ca. 1 % / decade) despite the considerable evidence that accurate ages are obtained without fading correction (Buylaert et al., 2012) and that the $pIRIR_{290}$ signal in “infinitely” old samples is very close to saturation (Buylaert et al., 2011; Thiel et al., 2011; Thomsen et al., 2011). Both fading-corrected and uncorrected $pIRIR_{290}$ ages are in good agreement with OSL ages but correction may tend to cause overestimation for young samples. Moreover, comparison with an independent ^{14}C age obtained from a charcoal layer found directly on top of the Upper Paleosol at an adjacent section shows better agreement with the uncorrected $pIRIR_{290}$ age. The comparison of OSL, IR_{50} and $pIRIR_{290}$ shows that both OSL and (uncorrected) $pIRIR_{290}$ are most reliable, but $pIRIR_{290}$ is applicable over a wider age range and therefore more suitable for the older samples of the Tokaj profile, which are already rather close to saturation of the signal.

4.1.2 Chronostratigraphy

The second aim of Study 1 was to establish a reliable chronostratigraphy using reliable numerical age control for the Tokaj paleosol loess profile. The previous chronology is fragmentary and based on uncalibrated radiocarbon ages from an adjacent section, as well as on stratigraphic correlations with other Hungarian profiles and archaeological findings (Sümegi and Hertelendi, 1998). The new chronology is shown in Table 3. Ages range from 62-21 ka (OSL) and 57-25 ka ($pIRIR_{290}$) from the most recent soil to the top of the lower paleosol.

According to the results, the lower paleosol, previously dated to ca. 50-40 ka uncal. BP (52-42 ka cal. BP; all uncalibrated ^{14}C ages were converted using the Cal-Pal tool: Danzeglocke, 2007), has most likely developed before the onset of Marine Isotope Stage (MIS) 3 (>57 ka), but may be potentially older in case of a hiatus. It is similar in age to the 56 ka age in the lowest Last Glacial loess unit at Crvenka, North Serbia, but here the underlying soil has been interpreted to be part of the S1 complex (MIS 5, 130-71 ka; Marković et al., 2008; Stevens et al., 2011). The middle loess layer at Tokaj, previously estimated to 42-34 ka cal. BP, accumulated between c. 50 and 60 ka, in the colder periods of MIS 3. This layer might correspond to the 'VL1L2' loess in North Serbia (Marković et al., 2008; Marković et al., 2011) although here it usually extends into MIS 4 (60-71 ka) without any intercalated soils. Two samples from the upper paleosol indicate that it probably formed during the later stages of MIS 3, which is consistent with previous estimates of 35-30 ka cal. BP. However, the results of 27-39 ka (OSL) and 30-39 ka ($pIRIR_{290}$) do not necessarily indicate the time of soil formation, but rather the time of deposition of the sediment in which the soil subsequently developed. Furthermore, the results for the lower sample are only minimum ages as it is located 25 cm above the transition from the middle loess layer to the paleosol. Bracketing the upper paleosol with ages from the over- and underlying loess layers, an age range for the time of soil formation of 45-25 ka can be derived. Similar soils of corresponding age ranges have been reported at Crvenka (38 ka; Stevens et al., 2011), Stari Slankamen (34 ka; Schmidt et al., 2010) and Surduk (32 ka; Fuchs et al., 2008) in Northern Serbia. The samples from the upper loess layer suggest that it was deposited between 21-30 ka (OSL) and 25-28 ka ($pIRIR_{290}$) during MIS 2 (24-11 ka) in the Upper Pleniglacial. This is partly consistent with a previous estimate of 29-13 ka cal. BP. Similar MIS 2 loess layers have been reported from Northern Serbia ('V L1L1' loess; Fuchs et al., 2008; Schmidt et al., 2010; Stevens et al., 2011), as well as from other locations in Hungary (Novothny et al., 2011). The youngest OSL ages indicate that loess deposition either ended around 20 ka or that younger loess layers have been eroded or overprinted by Holocene pedogenesis.

Previous studies in Tokaj are all based on the old, fragmentary chronostratigraphy. The differences between this old chronology and the luminescence chronostratigraphy (Table 3) clearly demonstrate that a thorough review and re-assessment of previous studies and published proxy data is necessary.

	New chronology		**Old chronology**
	OSL	**pIRIR$_{290}$**	**^{14}C**
Upper loess layer	27-21 ka	28-25 ka	29-13 ka cal. BP
Upper paleosol	39-27 ka	39-30 ka	35-30 ka cal. BP
Middle loess layer	62-50 ka	60-45 ka	42-34 ka cal. BP
Lower paleosol	>62 ka	>60 ka	52-42 ka cal. BP
Lower loess layer	-	-	(70-60 ka BP)

Table 3: Comparison of the old and new chronology of the Tokaj profile. New OSL and pIRIR$_{290}$ ages are from Study 1, old ages are from Sümegi and Hertelendi (1998), reported originally as uncalibrated radiocarbon ages and converted using the *Calpal online* tool (Danzeglocke, 2007). The age of the lower loess layer is an estimate (unconfirmed) based on paleontological findings.

4.2 Weathering intensity and the suitability of weathering indices (Study 2)

One aim of Study 2 was to examine weathering intensity and conditions in order to contribute to the general understanding of paleoclimate. Weathering intensity can be quantified via a wide selection of geochemical weathering indices (WIs) and elemental ratios (Chapter 3.3.1; Buggle et al., 2011; Sheldon and Tabor, 2009). 14 WIs from loess and paleosol samples from the upper part of the Tokaj profile were calculated and evaluated with respect to sensitivity. The results confirm that paleosol samples are more weathered than loess samples. All samples are less weathered than standard reference materials for weathered continental material (Post-Archean Australian Shale - PAAS, North American Shale Composite - NASC) and plot parallel to the A-CN line in the A-CN-K diagram, which shows that weathering follows the plagioclase weathering trend with a constant K-feldspar/plagioclase ratio. The degree of weathering is variable; paleosol samples are located closer to the CN corner and PAAS, which indicates progressive enrichment of Al and depletion of Ca and Na (plagioclase weathering) with increasing weathering intensity, while the K content (K-feldspar, micas) remains constant. A comparison of WI results from Tokaj with those from other loess and dust deposits in the Carpathian Basin shows similarities with most loess deposits, while Red Clay samples are more intensely weathered. The average weathering

intensity of loess from this region (AVL3, Újvári et al., 2008) is slightly lower or similar, depending on the WI.

The shapes of the WI depth plots for Tokaj are overall rather similar and well-correlated, indicating that there are equally suited to track changes in weathering intensity. Anomalies associated with the use of K in these equations, resulting in differences between K-free and K-based indices, cannot be observed in our dataset. The two trace element WIs, Ba/Sr and Rb/Sr, are highly correlated with the majority of the main element WIs. Yet due to a lack of understanding of their weathering behavior, coupling to $CaCO_3$ dynamics and grain-size dependence, the use of these indices is discouraged. There are two subgroups of WIs which, although moderately to well correlated with the other WIs, show slightly different depth plots. WI-1, WI-2 and Index A include Si as an additional element in their calculations, which might explain this minor deviation and decrease in correlation coefficients. PWI and, to a lesser extent, CPA are particularly weakly correlated with all other indices, which might be due to the relative overemphasis of Na in the equations.

The sensitivity of the weathering indices was evaluated by comparing and correlating them with mass-specific magnetic susceptibility (X) values. X is the only direct weathering proxy available. Such a validation step has not been included in previous studies, which discussed various WI data without examining correlations with other weathering proxies (Buggle et al., 2011; Varga et al., 2011). The results show that all WIs are moderately to well correlated with X (r = 0.68-0.87), with FENG ranking highest, followed by the trace element indices. PWI is least correlated with X, but still acceptable. The performance of the FENG index is surprising because multi-element indices have come under suspicion due to their reliance on Na and Ca, which may bias results if secondary carbonates or Na salts are present (Baumann et al., 2014; Buggle et al., 2011). Yet for the Tokaj loess paleosol section it yields the best result, probably because the samples are not affected by secondary Na salt formation. For future loess paleosol studies at other locations, we recommend an individual evaluation of WI sensitivity to identify the best-performing index since weathering conditions vary through time and space.

4.3 Paleoenvironment and -climate (Study 2)

Besides the quantification of weathering intensity, another aim of Study 2 was the application of several transfer functions derived from different proxy records - elemental data, mass-specific magnetic susceptibility (X), stable carbon isotopes ($\delta^{13}C$) – to estimate mean annual precipitation

and temperature (MAP, MAT) and to compare the results with literature data of local and regional paleoclimate. The study focuses exclusively on the upper part of the sequence because the only paleotemperature data for the Northeastern part of Hungary and Tokaj are malacothermometer paleotemperatures (Sümegi and Hertelendi, 1998) from the upper half of the profile. Furthermore, the chronostratigraphy (Schatz et al., 2012) for the upper half of the sequence is more detailed. The results show that absolute MAP and MAT values vary depending on the methods and proxy data used but paleosol values have always higher MAP and MAT (Δ = 100-200 mm/a and 0.1-2.0 °C). All results indicate that the climate was warmer and wetter during paleosol formation in MIS 3 and cooler and drier during dust deposition in MIS 2.

The MAT results for the paleosol (45-27 ka) are in a range of 8.8 ±0.6 °C to 9.9 ±4.4 °C and 8.4 ±0.9 °C (*X*-based). The $\delta^{13}C$-based mean summer temperature of 18.0 ±1.4 °C was converted to a MAT of 8.8 °C via an empirical conversion formula (Hall and Penner, 2013). These temperatures agree within the error limits and are similar to the current MAT of 9.8 °C (World Data Center for Meteorology, 2011). It has been proposed by various researchers that the climate of the Carpathian Basin during MIS 3 was warmer and drier than elsewhere in Europe (Fitzsimmons and Hambach, 2014; Willis et al., 2000; Willis and van Andel, 2004). A MAT range of 10-17 °C was suggested for parts of Slovakia and the Czech Republic (Kovács et al., 2012). Based on the malacothermometer method, Sümegi and Hertelendi (1998) found mean July paleotemperatures equivalent to MATs of 7.4-8.8 °C for Tokaj. While local proxy data in the literature agree well with each other, these temperature estimates are usually not consistent with results from large-scale paleoclimatic reconstructions, as e.g. the Paleoclimatic Atlas of the Northern Hemisphere (MAT 2-4 °C; Frenzel et al., 1992). This might be due large uncertainty ranges in proxy data, a higher climatic variability during the Last Glacial Maximum (LGM), complex terrain, a too coarse spatial resolution of model data, the sensitivity of regional climate to vegetation cover or a combination thereof and have been observed and discussed before (Kageyama et al., 2006; Mairesse et al., 2013; Strandberg et al., 2011).

The MAT results for the upper loess layer (27-21 ka) are in a range of 8.5 ±0.6 °C to 8.9 ±4.4 °C (XRF-based) and 6.6 ±0.7 °C (*X*-based). Literature temperatures of the LGM from climate models and local proxies are considerably lower (-5 to 8 °C) but it is not sure if the Tokaj section even includes the LGM since OSL and IRSL ages differ for this period of time. The results from this study were therefore not considered to be LGM temperatures. Non-LGM temperatures from MIS 2 derived from isotopic analyses of bones, shells and groundwater (Corcho Alvarado et al., 2011;

Kovács et al., 2012) are in a range of 4-11 °C for Hungary and 6-8 °C for Tokaj, specifically (Sümegi and Hertelendi, 1998).

X-based MAP results for the paleosol vary from 258 mm/a to 390 mm/a, XRF-based MAP from 685 ±156 mm/a to 785 ±235 mm/a, while current MAP is 546 mm/a. Literature data is scarce and rather vague and suggest values between 240 and 850 mm/a. For the loess layer, XRF-based methods yield a range of 572 ±156 mm/a to 687 ±235 mm/a, while the *X*-MAP is again lower (222 ±24 mm/a). Literature MAP values are lower and between 50 and 450 mm/a. *X*-based MAP reconstructions are generally more consistent with the literature, whereas most XRF-based results are probably too high.

Overall, our results are consistent with regional proxy evidence from the literature and indicate that the region sustained milder climatic conditions than elsewhere in Europe during MIS 2 and 3 and might have been a possible location for the hypothesized cold stage refugia of temperate flora and fauna. The paleoclimate of the region was probably spatially highly diverse and different from the surroundings. Large-scale models may not be able to express these heterogeneous conditions, a fact that is also reflected in the wide range of predicted model MATs and MAPs in the literature. Local proxy data may serve to refine these models.

4.4 Dust dynamics

4.4.1 Wind speed and sediment pathways (Study 1 & Study 3)

Recent results based on highly resolved luminescence chronologies indicate that loess deposition is often episodic and sedimentation rates can be highly variable by up to 1-2 orders of magnitude. These variations cannot be reliably obtained from grain size or magnetic susceptibility data and are only revealed by independent dating (Buylaert et al., 2008; Stevens et al., 2006; Stevens and Lu, 2009; Stevens et al., 2008; Stevens et al., 2007). In Study 1, a comparison between implicitly assumed linear sedimentation rates and a new age-depth model shows that sedimentation rates at Tokaj are variable, indeed, and differ significantly over time. While uniform sedimentation is 0.42 mm/a on average, the luminescence-based age-depth model yields a considerably lower rate of 0.3 mm/a for the middle loess layer, and a substantially higher rate of 0.86 mm/a for the upper loess layer. This suggests more active source regions, higher transport rates, or more effective trapping, or a combination of these processes during this period.

The sedimentation peak in MIS 2, during the accumulation of the upper loess, has also been observed at other locations in the Carpathian Basin, e.g. at Surduk, Serbia (Fuchs et al., 2008), Süttő, Hungary (Novothny et al., 2011) and Crvenka, Serbia (Stevens et al., 2011). Absolute sedimentation rates between these sites and Tokaj are comparable and match the general pattern of a North-South trend of decreasing sediment magnitudes in the Carpathian Basin, which might be due to a closer proximity to dust source areas (Stevens et al., 2011; Újvári et al., 2010). The implications of these more detailed insights into sediment dynamics are potentially substantial. Many published proxy studies, such as earlier studies at Tokaj (Schatz et al., 2011; Sümegi and Hertelendi, 1998), are based on assumed uniform sedimentation rates. In the light of the new data, a thorough review and re-assessment of proxy data and interpretations is necessary.

The results from the Sr-Nd isotopic analyses in Study 3 show that despite the higher sedimentation rate in MIS 2 and potential reasons - changing source, transport and/or trapping parameters - the sediment source of loess at Tokaj has remained stable over time. This is not only true for the MIS 2 peak but in fact for the entire time span the profile covers (60-20 ka). Careful analysis of 20 samples from the profile shows low internal variability and an absence of shifts, peaks or trends for both $^{87}Sr/^{86}Sr$ and $^{143}Nd/^{144}Nd$ values. Furthermore, Sr and Nd ratios have a very low correlation coefficient (r^2=0.01). A change of source would be characterized by a synchronous, inversely correlated shift in both isotopic systems.

Tokaj loess is geochemically very similar to other European loess, especially to loess from Southeast Europe (e.g. Southwest and Central Hungary). Both Sr-Nd isotopic signatures and major and trace elemental data of several loess samples from this region are indistinguishable or near-identical. A genetic link between major Southeast European loess deposits in Hungary, Croatia, Slovakia and Austria has been observed before (Újvári et al., 2012), defined as a common loess region, “D4”, (Smalley and Leach, 1978) and interpreted as a common, distal sediment source or a mixture of sources with roughly identical proportions, and a common transport pathway. No evidence was found for a significant contribution of local material, such as e.g. from Tokaj volcanic rocks.

The direct comparison of loess and potential source rocks from major geological units surrounding the Carpathian Basin (Fig. 1) is only of limited validity. This is due to two reasons: (i) a significant share of detrital (i.e. non-secondary) carbonates is present in SE European loess samples, which 'dilutes' both the isotopic signatures and the elemental contents. (ii) the source signal may be modified by weathering, sorting and transport, especially elemental fingerprints. A tentative comparison of rocks and loess shows that most rocks have very different Sr-Nd and elemental

distribution patterns. However, some similarities can be found, e.g. for East Carpathian flysch, Bohemian Massif sediments, West Carpathian granites, Central Alpine granitoids, Alpine molasse and granites from the Tisia terrane in the Carpathian Basin. These results are consistent with Smalley and Leach's (1978) hypotheses but need to be examined in more detail.

It has often been argued that fluvial rather than aeolian processes acted as the main transport mechanism for material that later accumulated as loess. Smalley and Leach (1978) assume that glacial sediments from the Alps were transported to the North and Southeast by the Rhine and Danube Rivers, deposited in floodplains and river banks and subsequently transported by the wind to build proximal loess deposits. Several provenance studies have therefore focused on studying floodplain deposits as potential source materials of loess (Buggle et al., 2008; Muhs and Budahn, 2006; Újvári et al., 2012). A comparison of Holocene, Pleistocene and Miocene floodplain and suspended samples from the Austroalpine cover nappes area, the Bohemian Massif, the Drava catchment, the Western Carpathians, the Rhine and Rhône, Morava and Danube and their tributaries, and from Central and Eastern Hungary reveals similarities between the elemental signatures of Tokaj loess and sediments from East and Central Hungary, the Bohemian Massif, the Western Carpathians and the Drava and Morava Rivers (Fig. 1). Sr-Nd analyses show similarities with recent suspended and Pleistocene fluvial sediment from the Danube and Miocene Pannonian sands, a local sediment of the North Carpathian Basin. The results are in line with the rock data and previous findings from the Northwest and Central Carpathian Basin (Buggle et al., 2008; Thamó-Bozsó et al., 2014; Újvári et al., 2012) and confirm the fundamental theoretical hypotheses of loess origin (Smalley et al., 2009; Smalley and Leach, 1978).

4.4.2 Dust dynamics – a European perspective (Study 3)

Study 3 compares elemental data and the Sr-Nd fingerprints of three loess sections spanning MIS 2 and 3 in Europe - Tokaj in Northeast Hungary, Grub in East Austria and Nussloch in Southwest Germany (Fig. 1). Previous hypotheses about the origin of the sediments suggest a mixture of glacial material from the Alps, carried by the Danube, and from northern Europe, transported by the Morava River, for Grub and material from the Central Alps in Switzerland, transported by the Rhine and deposited in the Upper Rhine Graben, for Nussloch (Antoine et al., 2009; Antoine et al., 2001; Hill, 2005; Smalley et al., 2009; Smalley and Leach, 1978; Zech et al., 2012).

The results of the combined elemental and isotopic approach indicate that while the source of Tokaj loess has remained stable, the sources of the loess at Grub and Nussloch may have shifted. At Grub, there is a weak trend between 50-30 ka. At Nussloch, a more pronounced shift of 1 ε_{Nd}

unit between 30-20 ka was observed. The weak trend at Grub is not consistent in both the Sr and Nd systems (r^2=0.11), but can be confirmed for Nussloch (r^2=0.74).

However, despite possible shifts, the data of all three locations are very similar to each other and to other loess deposits in Europe. This is especially true for Southeast European loess, but also for loess from France, Germany and distal deposits (North Africa, Mediterranean Sea, Spitsbergen). Loess from Grub is particularly similar to loess from Tokaj, Croatia, Germany and Hungary, which confirms the overall uniformity of loess in the Northern Carpathian Basin and adjacent areas. For loess at Nussloch, similarities can be found with e.g. German loess, but variance regarding elemental and isotopic composition is much higher in Central and Western European loess.

A comparison of loess and rocks from potential source areas reveals similar results for Grub as for Tokaj, i.e. some similarities with rocks from the Bohemian Massif, the Alps and the Western Carpathians, but also with rocks from locations of which a contribution is less likely (Eastern Carpathians, Tisia terrane). Nussloch has similar results and Alpine sediments have been suggested as the main source of sediments previously (Hill, 2005; Smalley and Leach, 1978) but a contribution of southeast European material to the Nussloch site is highly unlikely since neither rivers nor dominant wind systems exist and have existed throughout the Quaternary to constantly transport material from the Carpathian Basin to Southwest Germany. These results demonstrate the main shortcoming of the isotopic and elemental fingerprinting methods. By using these methods, sediment sources can only be ruled out, but not confirmed. However, the results indicate that Tokaj, Grub and Nussloch loess and Alpine molasses samples have several geochemical similarities and should be included in further analyses, since these sediments have probably been derived from the same initial source, i.e. the Alps, and may have supplied material for both Southeast and Central European loess via the Rhine and the Danube.

Floodplain data confirms that both Tokaj and Grub loess is related to fluvial sediments from the Western Carpathians, the Bohemian Massif and the Danube. For Nussloch, little data is available but samples show strong similarities with Rhine and Rhône sediments, suggesting transport from the Swiss Central Alps via the Rhine to the Upper Rhine Graben, as suggested by Hill (2005). A further contribution of a mixture of sediments from the Black Forest Mountains and the Vosges Mountains bordering the Upper Rhine Graben is possible as well and requires further examination.

5. Conclusions

Loess-paleosol sequences in the Carpathian Basin represent valuable archives of Mid- and Late Pleistocene paleoclimate and -environment. The multi-proxy approach of this cumulative study contributed to increase and deepen our understanding of regional climatic and environmental factors in the Northeastern part of the basin. With the OSL and IRSL ages of Study 1, we were able to establish the first complete chronostratigraphy for the Tokaj section, which serves as a framework for all further analyses. Results show that previous age estimates were too low for both the upper part of the section (MIS 2 loess, ca. 26-20 ka) and the lower part (MIS 3 loess, ca. 60-40 ka). The age of the upper paleosol is now estimated to ca. 45-25 ka, while the lower paleosol must have developed before ca. 60 ka. Sedimentation rates calculated from the updates ages more than double during MIS 2 compared to MIS 3, which is consistent with observations from other locations in the Carpathian Basin and confirms the pattern of decreasing dust sedimentation from North to South. In addition to the chronostratigraphy, Study 1 also contributed to the introduction of $pIRIR_{290}$ as a new luminescence dating technique with a substantially extended age range.

Study 2 provides a comparison of 14 weathering indices that may be used to quantify weathering intensity. The results show that most of them perform equally well, including the most widely-used CIA index, and that, therefore, it is not necessary to restrict the choice of suitable indices to those containing only very few elements. Rather, we recommended to calculate several indices and evaluate their sensitivity towards weathering, e.g. by correlating them with magnetic susceptibility. The second part of Study 2 attempts to quantify MAT and MAP based on paleoclimate transfer functions and XRF, magnetic susceptibility and carbon isotopic data. Although the associated errors are large we argue that robust results can be obtained by combining several independent approaches and literature data. The results suggest a MAT similar to today of 8-10 °C for the time of soil formation in MIS 3 and a MAT of 6-9 °C for the time of dust deposition in MIS 2. For MAP, variance is higher depending on the input proxy data. X-based MAP is generally more consistent with literature data, while XRF-based MAP is probably too high. All results are consistent with a general trend towards lower temperatures and a drier climate in MIS 2, and higher temperatures and a more humid climate in MIS 3.

The results of the provenance study (Study 3) based on a combined Sr-Nd isotopic and elemental fingerprinting approach show that the source of dust in Tokaj has most likely been stable over time, whereas those of dust in Austria and Southwest Germany have been more variable. Loess in Europe, and especially in the Carpathian Basin, is overall rather uniform. While a direct

comparison of loess and rocks from potential source areas is difficult, the correlation with floodplain sediments is a highly promising approach. Results indicate that Tokaj loess may have been derived from the surrounding mountain chains, but also from Danube and local Miocene sediments, while loess in Southwest Germany is probably a mixture of local and Rhine sediments. Our data also underlines the contribution of Alpine sediments, deposited and lithified as Alpine molasse in the forelands and transported by major rivers such as the Rhine and the Danube, to loess in both Southeast and West Europe.

References

Aitken, M.J., 1985. Thermoluminescence Dating. Academic Press, London.

Aitken, M.J., 1998. An introduction to optical dating : the dating of Quaternary sediments by the use of photon-stimulated luminescence. Oxford University Press, Oxford.

Antoine, P., Rousseau, D.-D., Lautridou, J.-P., Hatté, C., 1999. Last interglacial-glacial climatic cycle in loess-palaeosol successions of north-western France. Boreas 28, 551-563.

Antoine, P., Rousseau, D.-D., Moine, O., Kunesch, S., Hatté, C., Lang, A., Tissoux, H., Zöller, L., 2009. Rapid and cyclic aeolian deposition during the Last Glacial in European loess: a high-resolution record from Nussloch, Germany. Quaternary Science Reviews 28, 2955-2973.

Antoine, P., Rousseau, D.-D., Zöller, L., Lang, A., Munaut, A.-V., Hatté, C., Fontugne, M., 2001. High-resolution record of the last Interglacial–glacial cycle in the Nussloch loess–palaeosol sequences, Upper Rhine Area, Germany. Quaternary International 76–77, 211-229.

Arthur Bettis III, E., Muhs, D.R., Roberts, H.M., Wintle, A.G., 2003. Last Glacial loess in the conterminous USA. Quaternary Science Reviews 22, 1907-1946.

Bai, Y., Fang, X., Nie, J., Wang, Y., Wu, F., 2009. A preliminary reconstruction of the paleoecological and paleoclimatic history of the Chinese Loess Plateau from the application of biomarkers. Palaeogeography, Palaeoclimatology, Palaeoecology 271, 161-169.

Baumann, F., Kühn, P., Dörfer, C., Schmidt, K., He, J.-S., Scholten, T., 2014. Pedogenesis, permafrost, substrate and topography: Plot and landscape scale interrelations of weathering processes on the central-eastern Qinghai-Tibet Plateau. Geoderma 226-227, 300-316.

Baumgart, P., Hambach, U., Meszner, S., Faust, D., 2013. An environmental magnetic fingerprint of periglacial loess: Records of Late Pleistocene loess–palaeosol sequences from Eastern Germany. Quaternary International 296, 82-93.

Bronger, A., Winter, R., Heinkele, T., 1998. Pleistocene climatic history of East and Central Asia based on paleopedological indicators in loess–paleosol sequences. CATENA 34, 1-17.

Buggle, B., 2011. Reconstruction of the Late and Mid-Pleistocene climate and landscape history in SE-Central Europe - A paleopedological and geochemical multi-proxy approach in loess-paleosol studies, Faculty of Biology, Chemistry and Earth Sciences. University of Bayreuth, Bayreuth, Germany.

Buggle, B., Glaser, B., Hambach, U., Gerasimenko, N., Marković, S., 2011. An evaluation of geochemical weathering indices in loess–paleosol studies. Quaternary International 240, 12-21.

Buggle, B., Glaser, B., Zöller, L., Hambach, U., Marković, S., Glaser, I., Gerasimenko, N., 2008. Geochemical characterization and origin of Southeastern and Eastern European loesses (Serbia, Romania, Ukraine). Quaternary Science Reviews 27, 1058-1075.

Buylaert, J.-P., Jain, M., Murray, A.S., Thomsen, K.J., Thiel, C., Sohbati, R., 2012. A robust feldspar luminescence dating method for Middle and Late Pleistocene sediments. Boreas 41, 435-451.

Buylaert, J.-P., Thiel, C., Murray, A., Vandenberghe, D.G., Yi, S., Lu, H., 2011. IRSL and post-IR IRSL residual doses recorded in modern dust samples from the Chinese Loess Plateau. Geochron 38, 432-440.

Buylaert, J.P., Murray, A.S., Vandenberghe, D., Vriend, M., De Corte, F., Van den haute, P., 2008. Optical dating of Chinese loess using sand-sized quartz: Establishing a time frame for Late Pleistocene climate changes in the western part of the Chinese Loess Plateau. Quaternary Geochronology 3, 99-113.

Chen, J., An, Z., Head, J., 1999. Variation of Rb/Sr Ratios in the Loess-Paleosol Sequences of Central China during the Last 130,000 Years and Their Implications for Monsoon Paleoclimatology. Quaternary Research 51, 215-219.

Chen, J., Li, G., Yang, J., Rao, W., Lu, H., Balsam, W., Sun, Y., Ji, J., 2007. Nd and Sr isotopic characteristics of Chinese deserts: Implications for the provenances of Asian dust. Geochimica et Cosmochimica Acta 71, 3904-3914.

Corcho Alvarado, J.A., Leuenberger, M., Kipfer, R., Paces, T., Purtschert, R., 2011. Reconstruction of past climate conditions over central Europe from groundwater data. Quaternary Science Reviews 30, 3423-3429.

Cullers, R.L., 2000. The geochemistry of shales, siltstones and sandstones of Pennsylvanian–Permian age, Colorado, USA: implications for provenance and metamorphic studies. Lithos 51, 181-203.

Danzeglocke, U., 2007. CalPal Online - The CalPal Online Radiocarbon Calibration.

Darmody, R.G., Thorn, C.E., Allen, C.E., 2005. Chemical weathering and boulder mantles, Kärkevagge, Swedish Lapland. Geomorphology 67, 159-170.

Denton, G.H., Hughes, T.J., 1981. The last great ice sheets. Wiley, New York.

Dodonov, A.E., Baiguzina, L.L., 1995. Loess stratigraphy of Central Asia: Palaeoclimatic and palaeoenvironmental aspects. Quaternary Science Reviews 14, 707-720.

Driese, S.G., Nordt, L.C., Lynn, W.C., Stiles, C.A., Mora, C.I., Wilding, L.P., 2005. Distinguishing Climate in the Soil Record Using Chemical Trends in a Vertisol Climosequence from the Texas Coast Prairie, and Application to Interpreting Paleozoic Paleosols in the Appalachian Basin, U.S.A. Journal of Sedimentary Research 75, 339-349.

Fedo, C.M., Nesbitt, H.W., Young, G.M., 1995. Unraveling the effects of potassium metasomatism in sedimentary rocks and paleosols, with implications for paleoweathering conditions and provenance. Geology 23, 921-924.

Feng, Z.-D., 1997. Geochemical Characteristics of a Loess-Soil Sequence in Central Kansas. Soil Sci Soc Am J 61, 534-541.

Fitzsimmons, K.E., Hambach, U., 2014. Loess accumulation during the last glacial maximum: Evidence from Urluia, southeastern Romania. Quaternary International 334-335, 74-85.

Forster, T., Heller, F., 1994. Loess deposits from the Tajik depression (Central Asia): Magnetic properties and paleoclimate. Earth and Planetary Science Letters 128, 501-512.

Forster, T., Heller, F., 1997. Magnetic enhancement paths in Loess sediments from Tajikistan, China and Hungary. Geophysical Research Letters 24, 17-20.

Frechen, M., van Vliet-Lanoë, B., van den Haute, P., 2001. The Upper Pleistocene loess record at Harmignies/Belgium - high resolution terrestrial archive of climate forcing. Palaeogeography, Palaeoclimatology, Palaeoecology 173, 175-195.

Frechen, M., Zander, A., Cílek, V., Ložek, V., 1999. Loess chronology of the Last Interglacial/Glacial cycle in Bohemia and Moravia, Czech Republic. Quaternary Science Reviews 18, 1467-1493.

Frenzel, B., Pécsi, M., Velichko, A.A., 1992. Atlas of Paleoclimates and Paleoenvironments of the Northern Hemisphere, Late Pleistocene - Holocene. Geographical Institute, Hungarian Academy of Sciences and Gustav Fischer Verlag, Budapest, Stuttgart.

Fuchs, M., Kreutzer, S., Rousseau, D.-D., Antoine, P., Hatté, C., Lagroix, F., Moine, O., Gauthier, C., Svoboda, J., Lisá, L., 2013. The loess sequence of Dolní Věstonice, Czech Republic: A new OSL-based chronology of the Last Climatic Cycle. Boreas 42, 664-677.

Fuchs, M., Rousseau, D.-D., Antoine, P., HattÉ, C., Gauthier, C., MarkoviĆ, S., Zoeller, L., 2008. Chronology of the Last Climatic Cycle (Upper Pleistocene) of the Surduk loess sequence, Vojvodina, Serbia. Boreas 37, 66-73.

Gallagher, T.M., Sheldon, N.D., 2013. A new paleothermometer for forest paleosols and its implications for Cenozoic climate. Geology 41, 647-650.

Gallet, S., Jahn, B.-m., Torii, M., 1996. Geochemical characterization of the Luochuan loess-paleosol sequence, China, and paleoclimatic implications. Chemical Geology 133, 67-88.

Gallet, S., Jahn, B.-M., Van Vliet Lanoë, B., Dia, A., Rossello, E., 1998. Loess geochemistry and its implications for particle origin and composition of the upper continental crust. Earth and Planetary Science Letters 156, 157-172.

Gocke, M., Kuzyakov, Y., Wiesenberg, G.B., 2013. Differentiation of plant derived organic matter in soil, loess and rhizoliths based on n-alkane molecular proxies. Biogeochemistry 112, 23-40.

Goldberg, K., Humayun, M., 2010. The applicability of the Chemical Index of Alteration as a paleoclimatic indicator: An example from the Permian of the Paraná Basin, Brazil. Palaeogeography, Palaeoclimatology, Palaeoecology 293, 175-183.

Hall, S.A., Penner, W.L., 2013. Stable carbon isotopes, C3–C4 vegetation, and 12,800 years of climate change in central New Mexico, USA. Palaeogeography, Palaeoclimatology, Palaeoecology 369, 272-281.

Hamer, J.M.M., Sheldon, N.D., Nichols, G.J., Collinson, M.E., 2007. Late Oligocene–Early Miocene paleosols of distal fluvial systems, Ebro Basin, Spain. Palaeogeography, Palaeoclimatology, Palaeoecology 247, 220-235.

Harnois, L., 1988. The CIW index: A new chemical index of weathering. Sedimentary Geology 55, 319-322.

Hartley, A.P., J.-F.; Ledwith, M.; Champeaux, J.-L.; De Badts, E.; Bartalev, S.A., 2003. Global Land Cover 2000 database: Vegetation Map of Europe. European Commission, Joint Research Centre, Land Resource Management Unit.

Hatté, C., Antoine, P., Fontugne, M., Rousseau, D.-D., Tisnérat-Laborde, N., Zöller, L., 1999. New chronology and organic matter δ13C paleoclimatic significance of Nußloch loess sequence (Rhine Valley, Germany). Quaternary International 62, 85-91.

Hatté, C., Gauthier, C., Rousseau, D.D., Antoine, P., Fuchs, M., Lagroix, F., Markovic, S.B., Moine, O., Sima, A., 2013. Excursions to C4 vegetation recorded in the Upper Pleistocene loess of Surduk (Northern Serbia): an organic isotope geochemistry study. Clim Past 9, 1001-1014.

Hill, T.C., 2005. Geochemical evidence for weathering in NW European loess on a sub-millennial scale during the last Ice Age. University of Gloucestershire, Gloucestershire, p. 238.

Horáčková, J., Ložek, V., Juřičková, L., in press. List of malacologically treated Holocene sites with brief review of palaeomalacological research in the Czech and Slovak Republics. Quaternary International.

Huntley, D.J., Lamothe, M., 2001. Ubiquity of anomalous fading in K-feldspars and the measurement and correction for it in optical dating. Canadian Journal of Earth Sciences 38, 1093-1106.

Hwang, S., Park, C.-S., Yoon, S.-O., Choi, J., in press. Origin and weathering properties of loess-paleosol sequence in the Goseong area on the east coast of South Korea. Quaternary International.

IPCC, 1990. Climate Change: The IPCC Scientific Assessment. Cambridge University Press, Cambridge, UK, New York, USA and Melbourne, Australia.

Jacobsen, S.B., Wasserburg, G.J., 1980. Sm-Nd isotopic evolution of chondrites. Earth and Planetary Science Letters 50, 139-155.

Jahn, B.-M., Gallet, S., Han, J., 2001. Geochemistry of the Xining, Xifeng and Jixian sections, Loess Plateau of China: eolian dust provenance and paleosol evolution during the last 140 ka. Chemical Geology 178, 71-94.

Jansen, E., JOverpeck, J., Briffa, K.R., Duplessy, J.-C., Joos, F., Masson-Delmotte, V., Olago, D., Otto-Bliesner, B., Peltier, W.R., Rahmstorf, S., Ramesh, R., Raynaud, D., Rind, D., Solomina, O., Villalba , R., Zhang, D., 2007. Chapter 6: Paleoclimate, In: Solomon, S., Qin, D., Manning, M., Chen, Z., Marquis, M., Averyt, K.B., Tignor, M., Miller, H.L. (Eds.), Climate Change 2007: The Physical Science Basis. Contribution of Working Group I to the Fourth Assessment Report of the Intergovernmental Panel on Climate Change. Cambridge University Press, Cambridge, UK and New York, USA.

Kageyama, M., Laîné, A., Abe-Ouchi, A., Braconnot, P., Cortijo, E., Crucifix, M., de Vernal, A., Guiot, J., Hewitt, C.D., Kitoh, A., Kucera, M., Marti, O., Ohgaito, R., Otto-Bliesner, B., Peltier, W.R., Rosell-Melé, A., Vettoretti, G., Weber, S.L., Yu, Y., 2006. Last Glacial Maximum temperatures over the North Atlantic, Europe and western Siberia: a comparison

between PMIP models, MARGO sea–surface temperatures and pollen-based reconstructions. Quaternary Science Reviews 25, 2082-2102.

Kerényi, A., 1994. Loess erosion on the Tokaj Big-Hill. Quaternary International 24, 47-52.

Kovács, J., 2007. Chemical weathering intensity of the Late Cenozoic “Red Clay” deposits in the Carpathian Basin. Geochem. Int. 45, 1056-1063.

Kovács, J., Moravcová, M., Újvári, G., Pintér, A.G., 2012. Reconstructing the paleoenvironment of East Central Europe in the Late Pleistocene using the oxygen and carbon isotopic signal of tooth in large mammal remains. Quaternary International 276–277, 145-154.

Kronberg, B.I., Nesbitt, H.W., 1981. Quantification of weathering, soil geochemistry and soil fertility. Journal of Soil Science 32, 453-459.

Kühn, P., Techmer, A., Weidenfeller, M., 2013. Lower to middle Weichselian pedogenesis and palaeoclimate in Central Europe using combined micromorphology and geochemistry: the loess-paleosol sequence of Alsheim (Mainz Basin, Germany). Quaternary Science Reviews 75, 43-58.

Lamothe, M., Auclair, M., Hamzaoui, C., Huot, S., 2003. Towards a prediction of long-term anomalous fading of feldspar IRSL. Radiation Measurements 37, 493-498.

Li, C., Yang, S., 2010. Is chemical index of alteration (CIA) a reliable proxy for chemical weathering in global drainage basins? American Journal of Science 310, 111-127.

Lisiecki, L.E., Raymo, M.E., 2005. A Pliocene-Pleistocene stack of 57 globally distributed benthic δ18O records. Paleoceanography 20, PA1003.

Lukić, T., Basarin, B., Buggle, B., Marković, S.B., Tomović, V.M., Raljić, J.P., Hrnjak, I., Timar-Gabor, A., Hambach, U., Gavrilov, M.B., 2014. A joined rock magnetic and colorimetric perspective on the Late Pleistocene climate of Orlovat loess site (Northern Serbia). Quaternary International 334-335, 179-188.

Maher, B.A., Thompson, R., Zhou, L.P., 1994. Spatial and temporal reconstructions of changes in the Asian palaeomonsoon: A new mineral magnetic approach. Earth and Planetary Science Letters 125, 461-471.

Mairesse, A., Goosse, H., Mathiot, P., Wanner, H., Dubinkina, S., 2013. Investigating the consistency between proxy-based reconstructions and climate models using data assimilation: a mid-Holocene case study. Clim Past 9, 2741-2757.

Marbut, C.F., 1935. Atlas of American Agriculture, Part III, Soils of the United States, In: Agriculture, U.S.D.o. (Ed.), 8 ed. US Government Printing Office, Washington (D.C.).

Marković, S.B., Bokhorst, M.P., Vandenberghe, J., McCoy, W.D., Oches, E.A., Hambach, U., Gaudenyi, T., Jovanović, M., Zöller, L., Stevens, T., Machalett, B., 2008. Late Pleistocene loess-palaeosol sequences in the Vojvodina region, north Serbia. Journal of Quaternary Science 23, 73-84.

Marković, S.B., Hambach, U., Stevens, T., Kukla, G.J., Heller, F., McCoy, W.D., Oches, E.A., Buggle, B., Zöller, L., 2011. The last million years recorded at the Stari Slankamen (Northern Serbia) loess-palaeosol sequence: revised chronostratigraphy and long-term environmental trends. Quaternary Science Reviews 30, 1142-1154.

Marković, S.B., Oches, E.A., McCoy, W.D., Frechen, M., Gaudenyi, T., 2007. Malacological and sedimentological evidence for “warm” glacial climate from the Irig loess sequence, Vojvodina, Serbia. Geochemistry, Geophysics, Geosystems 8, Q09008.

Masson-Delmotte, V., Schulz, M., Abe-Ouchi, A., Beer, J., Ganopolski, A., González Rouco, J.F., Jansen, E., Lambeck, K., Luterbacher, J., Naish, T., Osborn, T., Otto-Bliesner, B., Quinn, T., Ramesh, R., Rojas, M., Shao, X., Timmermann, A., 2013. Information from Paleoclimate Archives, In: Stocker, T.F., Qin, D., Plattner, G.-K., Tignor, M., Allen, S.K., Boschung, J., Nauels, A., Xia, Y., Bex, V., Midgley, P.M. (Eds.), Climate Change 2013: The Physical Science Basis. Contribution of Working Group I to the Fifth Assessment Report of the Intergovernmental Panel on Climate Change. Cambridge University Press, Cambridge, UK and New York, USA.

Matenco, L., Radivojević, D., 2012. On the formation and evolution of the Pannonian Basin: Constraints derived from the structure of the junction area between the Carpathians and Dinarides. Tectonics 31, TC6007.

Maynard, J.B., 1993. Chemistry of Modern Soils as a Guide to Interpreting Precambrian Paleosols. The Journal of Geology 100, 279-289.

Meier, H.A., Driese, S.G., Nordt, L.C., Forman, S.L., Dworkin, S.I., 2014. Interpretation of Late Quaternary climate and landscape variability based upon buried soil macro- and micromorphology, geochemistry, and stable isotopes of soil organic matter, Owl Creek, central Texas, USA. Catena 114, 157-168.

Meszner, S., Kreutzer, S., Fuchs, M., Faust, D., 2013. Late Pleistocene landscape dynamics in Saxony, Germany: Paleoenvironmental reconstruction using loess-paleosol sequences. Quaternary International 296, 94-107.

Mikulčić Pavlaković, S., Crnjaković, M., Tibljaš, D., Šoufek, M., Wacha, L., Frechen, M., Lacković, D., 2011. Mineralogical and geochemical characteristics of Quaternary sediments from the Island of Susak (Northern Adriatic, Croatia). Quaternary International 234, 32-49.

Muhs, D.R., Bettis, E.A., Aleinikoff, J.N., McGeehin, J.P., Beann, J., Skipp, G., Marshall, B.D., Roberts, H.M., Johnson, W.C., Benton, R., 2008. Origin and paleoclimatic significance of late Quaternary loess in Nebraska: Evidence from stratigraphy, chronology, sedimentology, and geochemistry. Geological Society of America Bulletin 120, 1378-1407.

Muhs, D.R., Bettis Iii, E.A., Roberts, H.M., Harlan, S.S., Paces, J.B., Reynolds, R.L., 2013a. Chronology and provenance of last-glacial (Peoria) loess in western Iowa and paleoclimatic implications. Quaternary Research 80, 468-481.

Muhs, D.R., Budahn, J.R., 2006. Geochemical evidence for the origin of late Quaternary loess in central Alaska. Canadian Journal of Earth Sciences 43, 323-337.

Muhs, D.R., Budahn, J.R., McGeehin, J.P., Bettis III, E.A., Skipp, G., Paces, J.B., Wheeler, E.A., 2013b. Loess origin, transport, and deposition over the past 10,000 years, Wrangell-St. Elias National Park, Alaska. Aeolian Research 11, 85-99.

Murray, A.S., Olley, J.M., 2002. Precision and accuracy in the optically stimulated luminescence dating of sedimentary quartz: a status review. Geochronometria 21, 1-16.

Murray, A.S., Schmidt, E.D., Stevens, T., Buylaert, J.P., Marković, S.B., Tsukamoto, S., Frechen, M., 2014. Dating Middle Pleistocene loess from Stari Slankamen (Vojvodina, Serbia) - Limitations imposed by the saturation behaviour of an elevated temperature IRSL signal. Catena 117, 34-42.

Murray, A.S., Wintle, A.G., 2000. Luminescence dating of quartz using an improved single-aliquot regenerative-dose protocol. Radiation Measurements 32, 57-73.

Murray, A.S., Wintle, A.G., 2003. The single aliquot regenerative dose protocol: potential for improvements in reliability. Radiation Measurements 37, 377-381.

Nesbitt, H.W., Young, G.M., 1982. Early Proterozoic climates and plate motions inferred from major element chemistry of lutites. Nature 299, 715-717.

Nordt, L., Orosz, M., Driese, S., Tubbs, J., 2006. Vertisol Carbonate Properties in Relation to Mean Annual Precipitation: Implications for Paleoprecipitation Estimates. The Journal of Geology 114, 501-510.

Novothny, Á., Frechen, M., Horváth, E., Wacha, L., Rolf, C., 2011. Investigating the penultimate and last glacial cycles of the Süttő loess section (Hungary) using luminescence dating, high-resolution grain size, and magnetic susceptibility data. Quaternary International 234, 75-85.

Peel, M.C., Finlayson, B.L., McMahon, T.A., 2007. Updated world map of the Köppen-Geiger climate classification. Hydrol Earth Syst Sc 11, 1633-1644.

Pietsch, D., Kühn, P., 2012. Early Holocene paleosols at the southwestern Ramlat As-Sab'atayn desert margin: New climate proxies for southern Arabia. Palaeogeography, Palaeoclimatology, Palaeoecology 365–366, 154-165.

Pinczés, Z., 1954. The loess blanket of Nagy-hegy at Tokaj. Földrajzi Értesítö 3, 575-584.

Pinczés, Z., 1987. Guide Book of Excursions. Carpatho-Balcan Geomorphological Commission, Debrecen.

Retallack, G.J., 2001. Soils of the past. Blackwell, Oxford.

Retallack, G.J., 2005. Earliest Triassic Claystone Breccias and Soil-Erosion Crisis. Journal of Sedimentary Research 75, 679-695.

Roberts, H.M., 2008. The development and application of luminescence dating to loess deposits: a perspective on the past, present and future. Boreas 37, 483-507.

Roberts, H.M., Muhs, D.R., Wintle, A.G., Duller, G.A.T., Bettis Iii, E.A., 2003. Unprecedented last-glacial mass accumulation rates determined by luminescence dating of loess from western Nebraska. Quaternary Research 59, 411-419.

Rousseau, D.-D., Puisségur, J.-J., 1990. A 350,000-year climatic record from the loess sequence of Achenheim, Alsace, France. Boreas 19, 203-216.

Rousseau, D.-D., Zöller, L., Valet, J.-P., 1998. Late Pleistocene Climatic Variations at Achenheim, France, Based on a Magnetic Susceptibility and TL Chronology of Loess. Quaternary Research 49, 255-263.

Rousseau, D.D., Antoine, P., Hatté, C., Lang, A., Zöller, L., Fontugne, M., Othman, D.B., Luck, J.M., Moine, O., Labonne, M., Bentaleb, I., Jolly, D., 2002. Abrupt millennial climatic changes from Nussloch (Germany) Upper Weichselian eolian records during the Last Glaciation. Quaternary Science Reviews 21, 1577-1582.

Rudner, Z.E., Sümegi, P., 2001. Recurring Taiga forest-steppe habitats in the Carpathian Basin in the Upper Weichselian. Quaternary International 76–77, 177-189.

Schatz, A.-K., Buylaert, J.-P., Murray, A., Stevens, T., Scholten, T., 2012. Establishing a luminescence chronology for a palaeosol-loess profile at Tokaj (Hungary): A comparison of quartz OSL and polymineral IRSL signals. Quaternary Geochronology 10, 68-74.

Schatz, A.-K., Zech, M., Buggle, B., Gulyás, S., Hambach, U., Marković, S.B., Sümegi, P., Scholten, T., 2011. The late Quaternary loess record of Tokaj, Hungary: Reconstructing palaeoenvironment, vegetation and climate using stable C and N isotopes and biomarkers. Quaternary International 240, 52-61.

Schmidt, E.D., Machalett, B., Marković, S.B., Tsukamoto, S., Frechen, M., 2010. Luminescence chronology of the upper part of the Stari Slankamen loess sequence (Vojvodina, Serbia). Quaternary Geochronology 5, 137-142.

Schmidt, E.D., Tsukamoto, S., Frechen, M., Murray, A.S., 2014. Elevated temperature IRSL dating of loess sections in the East Eifel region of Germany. Quaternary International 334–335, 141-154.

Sheldon, N.D., 2005. Do red beds indicate paleoclimatic conditions?: A Permian case study. Palaeogeography, Palaeoclimatology, Palaeoecology 228, 305-319.

Sheldon, N.D., 2009. Nonmarine records of climatic change across the Eocene-Oligocene transition. Geological Society of America Special Papers 452, 241-248.

Sheldon, N.D., Retallack, G.J., Tanaka, S., 2002. Geochemical Climofunctions from North American Soils and Application to Paleosols across the Eocene-Oligocene Boundary in Oregon. The Journal of Geology 110, 687-696.

Sheldon, N.D., Retallack, Gregory J., 2004. Regional Paleoprecipitation Records from the Late Eocene and Oligocene of North America. The Journal of Geology 112, 487-494.

Sheldon, N.D., Tabor, N.J., 2009. Quantitative paleoenvironmental and paleoclimatic reconstruction using paleosols. Earth-Science Reviews 95, 1-52.

Smalley, I., O'Hara-Dhand, K., Wint, J., Machalett, B., Jary, Z., Jefferson, I., 2009. Rivers and loess: The significance of long river transportation in the complex event-sequence approach to loess deposit formation. Quaternary International 198, 7-18.

Smalley, I.J., Leach, J.A., 1978. The origin and distribution of the loess in the Danube basin and associated regions of East-Central Europe - A review. Sedimentary Geology 21, 1-26.

Smith, J., Vance, D., Kemp, R.A., Archer, C., Toms, P., King, M., Zárate, M., 2003. Isotopic constraints on the source of Argentinian loess – with implications for atmospheric circulation and the provenance of Antarctic dust during recent glacial maxima. Earth and Planetary Science Letters 212, 181-196.

Sohbati, R., Murray, A.S., Buylaert, J.-P., Ortuño, M., Cunha, P.P., Masana, E., 2012. Luminescence dating of Pleistocene alluvial sediments affected by the Alhama de Murcia fault (eastern Betics, Spain) – a comparison between OSL, IRSL and post-IRIRSL ages. Boreas 41, 250-262.

Stevens, T., Armitage, S.J., Lu, H., Thomas, D.S.G., 2006. Sedimentation and diagenesis of Chinese loess: Implications for the preservation of continuous, high-resolution climate records. Geology 34, 849-852.

Stevens, T., Lu, H., 2009. Optically stimulated luminescence dating as a tool for calculating sedimentation rates in Chinese loess: comparisons with grain-size records. Sedimentology 56, 911-934.

Stevens, T., Lu, H., Thomas, D.S.G., Armitage, S.J., 2008. Optical dating of abrupt shifts in the late Pleistocene East Asian monsoon. Geology 36, 415-418.

Stevens, T., Marković, S.B., Zech, M., Hambach, U., Sümegi, P., 2011. Dust deposition and climate in the Carpathian Basin over an independently dated last glacial–interglacial cycle. Quaternary Science Reviews 30, 662-681.

Stevens, T., Thomas, D.S.G., Armitage, S.J., Lunn, H.R., Lu, H., 2007. Reinterpreting climate proxy records from late Quaternary Chinese loess: A detailed OSL investigation. Earth-Science Reviews 80, 111-136.

Strandberg, G., Brandefelt, J., Kjellström, E., Smith, B., 2011. High-resolution regional simulation of last glacial maximum climate in Europe. Tellus Series A - Dynamic Meteorology and Oceanography 63, 107-125.

Sümegi, P., 2005. Loess and Upper Paleolithic environment in Hungary. An Introduction to the Environmental History of Hungary. Aurea, Nagykovácsi.

Sümegi, P., Hertelendi, E., 1998. Reconstruction of microenvironmental changes in the Kopasz Hill loess area at Tokaj (Hungary) between 15 and 70 ka BP. Radiocarbon 40, 855-863.

Sümegi, P., Krolopp, E., 2002. Quatermalacological analyses for modeling of the Upper Weichselian palaeoenvironmental changes in the Carpathian Basin. Quaternary International 91, 53-63.

Sümegi, P., Rudner, Z.E., 2001. In situ charcoal fragments as remains of natural wild fires in the upper Würm of the Carpathian Basin. Quaternary International 76–77, 165-176.

Sun, J., 2002. Provenance of loess material and formation of loess deposits on the Chinese Loess Plateau. Earth and Planetary Science Letters 203, 845-859.

Sun, J., 2005. Nd and Sr isotopic variations in Chinese eolian deposits during the past 8 Ma: Implications for provenance change. Earth and Planetary Science Letters 240, 454-466.

Terhorst, B., Kühn, P., Damm, B., Hambach, U., Meyer-Heintze, S., Sedov, S., in press. Paleoenvironmental fluctuations as recorded in the loess-paleosol sequence of the Upper Paleolithic site Krems-Wachtberg. Quaternary International.

Thamó-Bozsó, E., Kovács, L.Ó., Magyari, Á., Marsi, I., 2014. Tracing the origin of loess in Hungary with the help of heavy mineral composition data. Quaternary International 319, 11-21.

Thiel, C., Buylaert, J.-P., Murray, A., Terhorst, B., Hofer, I., Tsukamoto, S., Frechen, M., 2011. Luminescence dating of the Stratzing loess profile (Austria) – Testing the potential of an elevated temperature post-IR IRSL protocol. Quaternary International 234, 23-31.

Thiel, C., Horváth, E., Frechen, M., 2014. Revisiting the loess/palaeosol sequence in Paks, Hungary: A post-IR IRSL based chronology for the 'Young Loess Series'. Quaternary International 319, 88-98.

Thomsen, K., Murray, A., Jain, M., 2011. Stability of IRSL signals from sedimentary K-feldspar samples. Geochron 38, 1-13.

Thomsen, K.J., Murray, A.S., Jain, M., Bøtter-Jensen, L., 2008. Laboratory fading rates of various luminescence signals from feldspar-rich sediment extracts. Radiation Measurements 43, 1474-1486.

Tuthorn, M., Zech, M., Ruppenthal, M., Oelmann, Y., Kahmen, A., Valle, H.F.d., Wilcke, W., Glaser, B., 2014. Oxygen isotope ratios (18O/16O) of hemicellulose-derived sugar biomarkers in plants, soils and sediments as paleoclimate proxy II: Insight from a climate transect study. Geochimica et Cosmochimica Acta 126, 624-634.

Újvári, G., 2014. Interactive comment on "Paleoclimate and weathering of the Tokaj (NE Hungary) loess-paleosol sequence: a comparison of geochemical weathering indices and paleoclimate parameters" by A.-K. Schatz et al. Climate of the Past Discussions 10, C19-C26.

Újvári, G., Kovács, J., Varga, G., Raucsik, B., Marković, S.B., 2010. Dust flux estimates for the Last Glacial Period in East Central Europe based on terrestrial records of loess deposits: a review. Quaternary Science Reviews 29, 3157-3166.

Újvári, G., Varga, A., Balogh-Brunstad, Z., 2008. Origin, weathering, and geochemical composition of loess in southwestern Hungary. Quaternary Research 69, 421-437.

Újvári, G., Varga, A., Ramos, F.C., Kovács, J., Németh, T., Stevens, T., 2012. Evaluating the use of clay mineralogy, Sr–Nd isotopes and zircon U–Pb ages in tracking dust provenance: An example from loess of the Carpathian Basin. Chemical Geology 304–305, 83-96.

Újvári, G., Varga, A., Raucsik, B., Kovács, J., 2014. The Paks loess-paleosol sequence: A record of chemical weathering and provenance for the last 800 ka in the mid-Carpathian Basin. Quaternary International 319, 22-37.

Vancampenhout, K., Langohr, R., Slaets, J., Buurman, P., Swennen, R., Deckers, J., 2013. Paleo-pedological record of the Rocourt Pedosequence at Veldwezelt–Hezerwater (Belgian Pleistocene loess belt): Part 1 — Evolution of the parent material. Catena 107, 118-129.

Vandenberghe, D., 2004. Investigation of the optically stimulated luminescence dating method for application to young geological samples. Ghent University, Ghent, Belgium, p. 358.

Vandenberghe, J., Huijzer, B.S., Mücher, H., Laan, W., 1998. Short climatic oscillations in a western European loess sequence (Kesselt, Belgium). Journal of Quaternary Science 13, 471-485.

Varga, A., Újvári, G., Raucsik, B., 2011. Tectonic versus climatic control on the evolution of a loess–paleosol sequence at Beremend, Hungary: an integrated approach based on paleoecological, clay mineralogical, and geochemical data. Quaternary International 240, 71-86.

Varga, G., Kovács, J., Újvári, G., 2012. Late Pleistocene variations of the background aeolian dust concentration in the Carpathian Basin: an estimate using decomposition of grain-size distribution curves of loess deposits. Netherlands Journal of Geosciences 91, 159-171.

Willis, K.J., Rudner, E., Sümegi, P., 2000. The Full-Glacial Forests of Central and Southeastern Europe. Quaternary Research 53, 203-213.

Willis, K.J., Sümegi, P., Braun, M., Tóth, A., 1995. The late Quaternary environmental history of Bátorliget, N.E. Hungary. Palaeogeography, Palaeoclimatology, Palaeoecology 118, 25-47.

Willis, K.J., van Andel, T.H., 2004. Trees or no trees? The environments of central and eastern Europe during the Last Glaciation. Quaternary Science Reviews 23, 2369-2387.

Wintle, A.G., 1973. Anomalous Fading of Thermo-luminescence in Mineral Samples. Nature 245, 143-144.

World Data Center for Meteorology, W., 2011. 9th Series World Weather Records (WWR) 1991-2000, Asheville.

Wu, F., Fang, X., Ma, Y., Herrmann, M., Mosbrugger, V., An, Z., Miao, Y., 2007. Plio–Quaternary stepwise drying of Asia: Evidence from a 3-Ma pollen record from the Chinese Loess Plateau. Earth and Planetary Science Letters 257, 160-169.

Xiao, S., Liu, W., Li, A., Yang, S., Lai, Z., 2010. Pervasive autocorrelation of the chemical index of alteration in sedimentary profiles and its palaeoenvironmental implications. Sedimentology 57, 670-676.

Xiong, S., Ding, Z., Zhu, Y., Zhou, R., Lu, H., 2010. A ~6 Ma chemical weathering history, the grain size dependence of chemical weathering intensity, and its implications for provenance change of the Chinese loess–red clay deposit. Quaternary Science Reviews 29, 1911-1922.

Yang, S., Ding, F., Ding, Z., 2006. Pleistocene chemical weathering history of Asian arid and semi-arid regions recorded in loess deposits of China and Tajikistan. Geochimica et Cosmochimica Acta 70, 1695-1709.

Zech, M., Andreev, A., Zech, R., Müller, S., Hambach, U., Frechen, M., Zech, W., 2010. Quaternary vegetation changes derived from a loess-like permafrost palaeosol sequence in northeast Siberia using alkane biomarker and pollen analyses. Boreas 39, 540-550.

Zech, M., Krause, T., Meszner, S., Faust, D., 2013a. Incorrect when uncorrected: Reconstructing vegetation history using n-alkane biomarkers in loess-paleosol sequences – A case study from the Saxonian loess region, Germany. Quaternary International 296, 108-116.

Zech, M., Rass, S., Buggle, B., Löscher, M., Zöller, L., 2012. Reconstruction of the late Quaternary paleoenvironments of the Nussloch loess paleosol sequence, Germany, using n-alkane biomarkers. Quaternary Research 78, 226-235.

Zech, M., Tuthorn, M., Detsch, F., Rozanski, K., Zech, R., Zöller, L., Zech, W., Glaser, B., 2013b. A 220 ka terrestrial δ18O and deuterium excess biomarker record from an eolian permafrost paleosol sequence, NE-Siberia. Chemical Geology 360–361, 220-230.

Zech, M., Zech, R., Zech, W., Glaser, B., Brodowski, S., Amelung, W., 2008. Characterisation and palaeoclimate of a loess-like permafrost palaeosol sequence in NE Siberia. Geoderma 143, 281-295.

Zhang, H., Lu, H., Jiang, S.-Y., Vandenberghe, J., Wang, S., Cosgrove, R., 2012. Provenance of loess deposits in the Eastern Qinling Mountains (central China) and their implications for the paleoenvironment. Quaternary Science Reviews 43, 94-102.

Acknowledgements

This thesis would not have been possible without the personal, academic and financial support and understanding of my principal supervisor, Prof. Dr. Thomas Scholten. I am more that grateful to him for managing to balance the level of independence that allowed for my research to thrive – but also the right amount of supervision and support. I appreciate his vast knowledge and skill in many areas and learned a lot from his assistance in writing proposals, applications and research papers.

I would also like to thank Prof. Dr. Dominik Faust from the Technical University of Dresden for taking time out from his busy schedule to serve as second examiner of this thesis.

Study 2 vastly benefited from the ideas, advice and support of my departmental colleague Dr. Peter Kühn, for which I am extremely grateful. I would like to thank the entire Soil Science and Geomorphology group at the University of Tübingen for the stimulating and pleasant academic and social environment.

I probably learned much of my writing and research skills during my stay at the Risø lab in Denmark, where I worked together with Jan-Pieter Buylaert and Andrew Murray. Many thanks for having such a welcoming and stimulating work atmosphere!

At the University of Science and Technology of China in Hefei, I would like to thank Prof. Dr. Fukun Chen for inviting me to his work group, providing access to the lab and support by his staff and graduate students. Special thanks to Jiade Wu and Yue Qi for sample preparation and mass spectrometer measurements. Wolfgang Siebel at Tübingen University was involved in the design and coordination of Study 3 and initiated my stay at USTC, which turned out to be a wonderful experience – many thanks!

Several other colleagues and friends have contributed minor and major parts to my research projects. My initial scholarship proposal improved a lot from the support and feedback of Thomas Stevens at Royal Holloway, University of London, who also put me in contact with the Risø lab in Denmark and contributed lab work and expertise to Study 1. Ludwig Zöller at the University of Bayreuth contributed samples and expertise to Study 3. Fieldwork in Tokaj would not have been possible without the joint efforts of Michael Zech, Björn Buggle, Markus Fuchs, and Pál Sümegi, Sándor Gulyás and their team at Szeged University.

Furthermore, I would like to acknowledge the financial, academic and technical support of the University of Tübingen and the State of Baden-Württemberg, particularly in the award of a PhD scholarship that provided the necessary financial support for this research.

Finally, but above all, I would like to thank my parents, my sister, my friends and especially Curdin for their personal support, encouragement and great patience at all times.

Contributions

This cumulative dissertation includes three studies. My own contribution comprises the preparation of the three manuscripts as first author, including study design, field work, data analysis, interpretation and all figures. Approximate contributions to each manuscript:

Sampling

- Tokaj: equal contributions of Ann-Kathrin Schatz (AS), Michael Zech, Björn Buggle, Markus Fuchs (University of Bayreuth, Germany), Pál Sümegi, Sándor Gulyás & team (Szeged University, Hungary)
- Nussloch & Grub samples (Study 3): Ludwig Zöller (100%)

Study 1: Luminescence, published in Quaternary Geochronology

- Luminescence
    - Sample prep: AS (100%)
    - Measurements: AS (50%), Jan-Pieter Buylaert (50%)
- Study design, data analysis and interpretation: AS (60%), Jan-Pieter Buylaert (35%), Andrew Murray (5%)
- Manuscript preparation: AS (80%), Jan-Pieter Buylaert (20%)
- Comment to improve manuscript: Jan-Pieter Buylaert (70%), Andrew Murray (25%), Thomas Stevens (5%)

Study 2: Weathering and paleoclimate, published in Climates of the Past Discussions

- XRF analyses
    - Sample prep: AS (100%)
    - Measurement: H. Taubald & team (100%)
- Study design: AS (90%), Peter Kühn (10%)
- Data analysis and interpretation: AS (95%), Gábor Újvári (5%)
- Manuscript preparation: AS (100%)
- Comment to improve manuscript: Peter Kühn (70%), Gábor Újvári (20%), Thomas Scholten (10%)

Study 3: Sediment provenance, submitted to Central European Journal of Geosciences

- XRF analyses (see study 2)
- Sr-Nd analyses
    - Sample prep: AS (50%), Jiade Wu (50%)
    - Measurement: AS (50%), Jiade Wu (25%), Yue Qi (25%)
- Study design: AS (100%)
- Data analysis and interpretation: AS (100%)
- Manuscript preparation: AS (100%)
- Comments to improve manuscript: Wolfgang Siebel (50%), Ludwig Zöller (45%), Yue Qi (3%), Jiade Wu (2%)

Part II – Cumulative Study

Study 1: Establishing a luminescence chronology for a paleosol-loess profile at Tokaj (Hungary): A comparison of quartz OSL and polymineral IRSL signals

Ann-Kathrin Schatz [a,b], Jan-Pieter Buylaert [b,c], Andrew Murray [b], Thomas Stevens [d,e], Thomas Scholten [a]

a) Soil Science and Geomorphology Work Group, Department of Geosciences, University of Tübingen, Rümelinstr. 19-23, D-72070 Tübingen, Germany

b) Nordic Laboratory for Luminescence Dating, Department of Earth Sciences, University of Aarhus, Risø DTU, 4000 Roskilde, Denmark

c) Radiation Research Division, Risø National Laboratory for Sustainable Energy, Risø DTU, 4000 Roskilde, Denmark

d) Centre for Quaternary Research, Department of Geography, Royal Holloway, University of London, Egham, Surrey TW20 0EX, UK

e) Faculty of Sciences, University of Novi Sad, Trg Dositeja Obradovića 3, 21000 Novi Sad, Serbia

Published in: Quaternary Geochronology 10 (2012), p.68-74, doi: 10.1016/j.quageo.2012.02.018

The original publication is available at:
http://www.sciencedirect.com/science/article/pii/S187110141200043X

Abstract

We present a comparative study of quartz OSL, polymineral IRSL at low temperature (50°C, IR_{50}) and post-IR elevated temperature (290°C) IRSL ($pIRIR_{290}$) feldspar dating on nine samples from the Tokaj loess section in NE Hungary (SE Europe). Preheat plateau tests show a drop in quartz OSL D_e between 160 and 240°C but above 240°C a clear D_e plateau is present. Quartz OSL SAR is shown to be generally appropriate to these samples (recycling, recuperation) but a satisfactory dose recovery result was only obtained when a dose was added to a sample without any prior optical or thermal pre-treatment; this gave a dose recovery ratio of 1.04±0.05 after subtracting the natural dose from the measured dose. The $pIRIR_{290}$ SAR protocol also results in acceptable dose recovery results for the $pIRIR_{290}$ signal (1.08±0.01) when a large dose is added to the natural dose. Bleaching experiments suggest a detectable non-bleachable residual $pIRIR_{290}$ dose of 10±4 Gy. Agreement with quartz OSL ages is best achieved by correcting the IR_{50} ages for fading; however this is not necessary when using the $pIRIR_{290}$ signal. With respect to Hungarian Late Quaternary geology our results indicate that the major part of the Tokaj loess has been deposited during MIS 3 (60-24 ka), with periods of soil formation occurring during the onset of MIS 3 (≥58 ka) and between about 35 to 25 ka. Our results also indicate episodic deposition of loess and varying, non-linear sedimentation rates during MIS 3. Proxy analyses in the literature are based on the traditional concept of continuous deposition; in the light of our new data the use of such simple assumptions must be reconsidered.

Keywords: loess; Hungary; OSL; SAR; post-IR IRSL; bleaching

1. Introduction

Loess-paleosol sequences are an important terrestrial archive of Quaternary climate fluctuations and an essential tool for deciphering the impact of climate change on local and regional landscapes and ecosystems. Several recent studies have focused on the Carpathian Basin in SE Europe because of its favourable geomorphological setting and multiple loess paleosol sequences; it preserves well-resolved spatial and temporal records of the European late Quaternary history (Marković et al., 2008; Sümegi and Krolopp, 2002; Újvári et al., 2010; Willis et al., 2000). Besides providing information about local and regional paleoclimate and paleoenvironment, these records can also be compared with other extensive loess deposits such as in the Chinese Loess Plateau and other regions in the Eurasian loess belt (Frechen and Dodonov, 1998; Frechen et al., 2009; Machalett et al., 2008; Stevens et al., 2007), or correlated with marine and ice core records (Stevens et al., 2008, 2011).

The Tokaj section in NE Hungary (see supplementary section; Fig. S1) is one of the key Hungarian loess sections for paleoclimatic reconstructions. Detailed paleontological (molluscs, charcoal), sedimentological and geochemical studies (biomarkers, stable isotopes) have been carried out at this site (Rudner and Sümegi, 2001; Schatz et al., 2011; Sümegi and Hertelendi, 1998; Sümegi and Rudner, 2001). However, the current chronostratigraphy of the profile is fragmentary and based on uncalibrated radiocarbon ages obtained from mollusc shells and charcoal recovered from an adjacent section, as well as on stratigraphic correlations with other Hungarian profiles (Sümegi and Hertelendi, 1998). Detailed and reliable numerical age control is lacking, limiting the interpretation of paleoclimatic and paleoenvironmental information and restricting the correlation of this record with other loess-paleosol profiles of the Carpathian Basin and with marine archives.

The post-IR IRSL signal of feldspar (Thomsen et al., 2008) has been shown to be more stable than the conventional IRSL signal usually measured at ~50°C (Buylaert et al., 2009). In the post-IR IRSL method the samples are, after a preheat, first stimulated with IR at low temperature (typically 50°C, IR_{50}) and subsequently IR stimulated at an elevated temperature to record a more stable post-IR IRSL signal ($pIRIR_{elevT}$) In this paper we establish the first luminescence chronology for the Tokaj profile by comparing fine-grained quartz OSL ages with polymineral fine-grain IR_{50} and $pIRIR_{290}$ ages obtained following Thiel et al. (2011a) and Buylaert et al. (2012). The resulting ages and calculated sedimentation rates are presented in the context of other Hungarian sections and implications for previously published paleoenvironmental proxy information are discussed.

2. Geological setting

Tokaj is situated in the northeast of the Carpathian Basin, a region of approximately 300,000 km^2 surrounded by major mountain ranges (Fig. S1). The area around Tokaj has been suggested as one of the rare refuges for deciduous and coniferous trees during the last glacial and has, as a result, received considerable attention (Rudner and Sümegi, 2001; Schatz et al., 2011; Sümegi and Hertelendi, 1998; Sümegi and Krolopp, 2002; Sümegi and Rudner, 2001; Willis et al., 2000). The study site itself is situated on the eastern slopes of Kopasz Hill (Patkó quarry; 100 m a.s.l., 48,07' N, 21,24' E; Fig. S1), in the southernmost part of the Tokaj Mountains where the river Bodrog discharges into the Tisza.

This Late Pleistocene 15 m high section consists of three loess layers and two intercalated paleosols (Fig. 1). Independent age control is only available for the upper paleosol. A charcoal layer was observed on top of a paleosol at a similar profile in the immediate vicinity and dated to 28-26 ^{14}C ka BP (uncalibrated) (Sümegi and Hertelendi, 1998). For the upper loess layer the same authors suggest an age range of 26-12 ^{14}C ka BP (uncalibrated) based on radiocarbon ages obtained from mollusc shells. We converted the published uncalibrated radiocarbon ages using the CalPal online tool (Danzeglocke et al., 2011) and suggest an age of ~35-30 ka for the upper reddish-brown paleosol, and 29-13 ka for the upper loess layer. (All subsequent ^{14}C ages cited in this paper were calibrated in the same manner.)

3. Sample preparation, measurement facilities and dosimetry

Nine samples were taken during a field campaign in 2009 (lab codes: 103001-103009; Fig. 1). All samples for equivalent dose (D_e) determination were treated under subdued red laboratory light. Polymineral fine-grains (4-11µm) were separated from bulk sediment using conventional sample preparation techniques (10% HCl, 10% H_2O_2, Stokes' settling). A portion of this material was etched for 5-7 days with H_2SiF_6 to obtain fine-grained quartz. The purity of this quartz extract was confirmed by the absence of a significant IRSL signal (<3% of the corresponding blue light stimulated luminescence) and OSL-IR depletion ratios (Duller, 2003) within 10% of unity. Both polymineral and quartz fine grains were settled on aluminium discs from an acetone suspension (2 mg/ml).

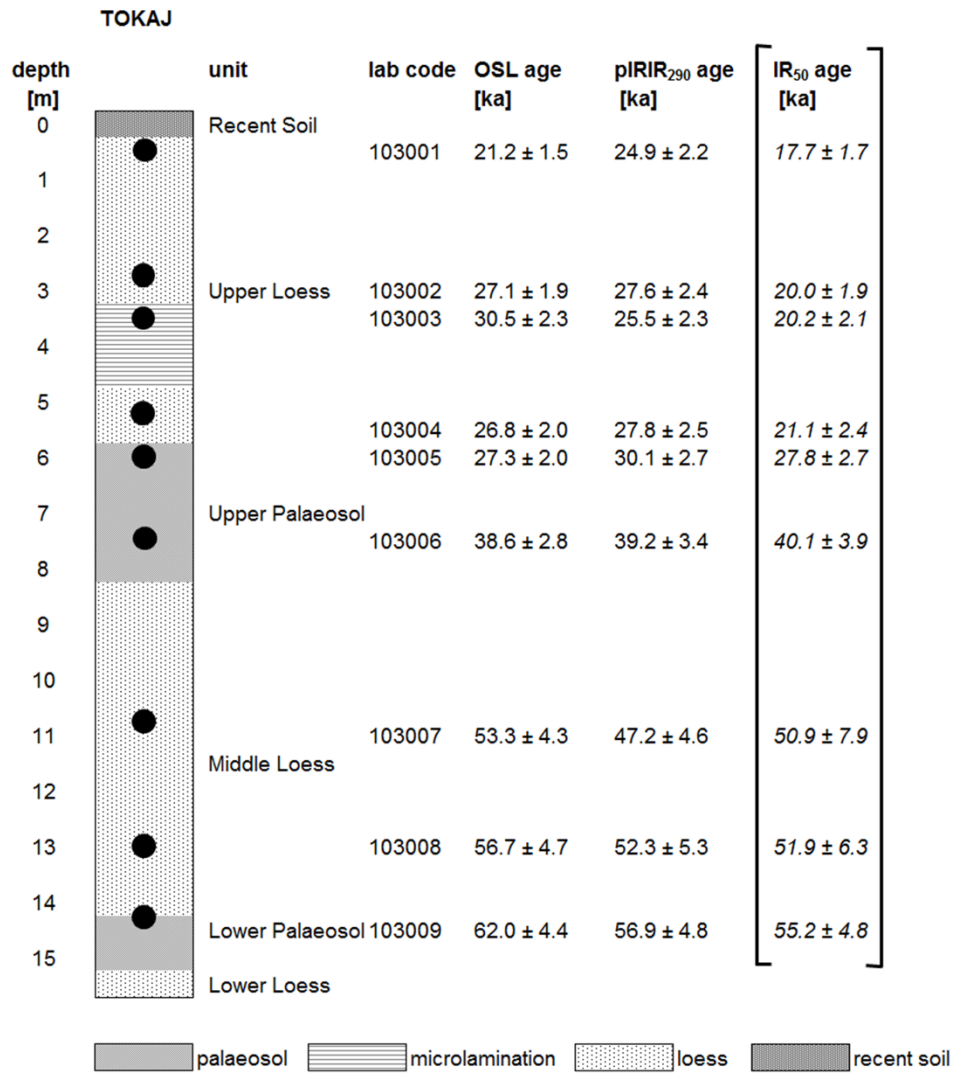

Fig. 1: Stratigraphic log and quartz OSL, polymineral $pIRIR_{290}$ (uncorrected, residual subtracted; see section 4.2 for details) and IR_{50} ages (corrected, residual subtracted) of the Tokaj paleosol-loess profile. The positions of the luminescence samples (lab codes 103001-09) are indicated by black circles. IR_{50} ages were included for completeness; however, quartz OSL and $pIRIR_{290}$ ages are considered the most reliable ages.

A Risø TL/OSL DA-20 reader equipped with blue LEDs (470nm, ~80 mW/cm^2) and IR diodes (875 nm, ~135 mW/cm^2) was used for all measurements. Quartz measurements were made with a U-340 filter and feldspar emission was detected through a blue filter pack (Schott BG39/ Corning 7/59).

High resolution laboratory gamma spectrometry (Murray et al., 1987) was used to determine the dose rates. Dose rates for fine-grained quartz (assuming a-value of 0.04±0.01, Rees-Jones, 1995) do not vary much down the section and range from 3.37 to 3.87 Gy/ka. For the polymineral

fine-grains an a-value of 0.08±0.02 was used (Rees-Jones, 1995). The concentrations of uranium, thorium and potassium were converted into dose rates using the dose rate conversion factors of (Olley et al., 1996) and water-content attenuation factors (Aitken, 1985). From an examination of the European loess literature (Frechen et al., 1997; Novothny et al., 2010; Stevens et al., 2011) and a consideration of the setting of our section, we have adopted a life-time average water content of 15±5% for all our samples. Radionuclide concentrations and the total dose rates are given in Table S2.

There is no unambiguous evidence for disequilibrium between ^{238}U and ^{226}Ra in any single sample (Table S2) and the mean ^{238}U to ^{226}Ra ratio is 0.97±0.06 (n=9). We assume secular equilibrium has persisted throughout the lifetime of the site with the possible exception of some ^{222}Rn loss which we assume to be 20±10%.

4. Luminescence measurements

4.1 Quartz OSL measurements

All quartz dose measurements were performed using a SAR protocol with a preheat of 260°C for 10 s, a cut-heat of 240°C and a blue-light cleanout for 40 s at 280°C (Murray and Wintle, 2003). Stimulation with blue LEDs was for 40 s at 125°C. All calculations were made using the first 0.32 s of the decay curve minus a background derived from the interval 0.8-1.6 s (early background subtraction, Ballarini et al., 2007).

A typical dose response curve and the results of a preheat plateau test for two samples are shown in Figs. S3 and S4 (supplementary section), respectively. The quartz OSL signal is clearly dominated by a fast component (inset Fig. S3) and the dose response curve is well-represented by a single saturating exponential. The mean D_0, estimated using the oldest sample (103009), is 173±9 Gy (n=12).

From Fig. S4a it can be seen that that the De is independent of temperature for preheats >240°C. Recycling ratios are all satisfactory, i.e. within 10% of unity, especially for higher preheat temperatures (Fig. S4a, Table S5). Recuperation is below 5% of the natural signal for all samples and over the entire temperature range (Table S5, Fig. S4b). A preheat/cut-heat combination of 260°C (10s) / 240°C was chosen, and dose recovery tests were then undertaken using sample 103005. Three natural aliquots were bleached twice with blue light for 100 s at room temperature (with a 10 ks pause in between) and another set of three aliquots received a 5 min Hönle SOL2 solar simulator bleach to remove the natural signal. A beta dose of ~90 Gy was then given in the

reader and measured as usual. These optical treatments gave rather poor measured to given dose values of 1.29±0.06 and 1.88±0.34 for blue LED and SOL2 bleach respectively. A further dose recovery test was then carried out using the same preheat settings but now by adding a large dose (~100 Gy) on top of the natural dose of the youngest sample (103001; De= 71±2 Gy); after subtraction of the natural De from the measured dose the dose recovery ratio was satisfactory (1.04±0.05, n=6), suggesting that the protocol can recover a known dose given before any optical or thermal pre-treatment.

4.2 Post-IR IRSL on polymineral fine-grains

4.2.1 Measurement of dose

All measurements on polymineral fine-grains were made using a recently proposed post-IR IRSL protocol (Thiel et al., 2011a; Buylaert et al., 2012) (Table S6). There is increasing evidence that the $pIRIR_{290}$ signal measured in steps 4 and 8 does not fade significantly (Buylaert et al., 2012; Thiel et al., 2011b; Thomsen et al., 2011). The initial ~2 s of signal less a background derived from the last ~40s of the decay curves was used for calculations.

Typical dose response curves (IR_{50} and $pIRIR_{290}$) for an aliquot of sample 103005 are shown in Fig. 2. While the shapes of the dose response curves are almost indistinguishable, the signal intensity of the $pIRIR_{290}$ signal is much higher than that of the IR_{50} signal (inset Fig. 2); similar observations were made by Thiel et al. (2011a) and Stevens et al. (2011) for Austrian and Serbian loess, respectively. It can also be seen that the natural signals are well below the saturation level of the dose response curves. For feldspar SAR dose response curves, 86% of signal saturation corresponds typically to ~1100 Gy (e.g. Buylaert et al., 2012); natural IR_{50} and $pIRIR_{290}$ doses in this study are well-below this value. Recycling ratios are close to unity for both IR_{50} and $pIRIR_{290}$ measurements and the 10% criterion is met by all samples (Table S5). Values range from 0.93±0.03 (103009, IR_{50}) to 1.07±0.05 (103007, IR_{50}). Recuperation is always well below 5% (Table S5); minimum and maximum values are 0.90±0.04% (103009, IR_{50}) and 2.7±0.3% (103002, IR_{50}), respectively.

As with quartz, a dose recovery test using laboratory bleached samples resulted in rather poor results (ratios >>1.2), and so a second dose recovery test without prior optical treatment was carried out. A large dose (~280 Gy) was added on top of the natural dose for three aliquots of the youngest sample 103001. After subtracting the natural D_e value from the measured dose, the dose

recovery ratios are 0.86±0.01 and 1.08±0.01 for IR_{50} and $pIRIR_{290}$, respectively (Table S5). At least for the $pIRIR_{290}$ signal this dose recovery test is considered acceptable.

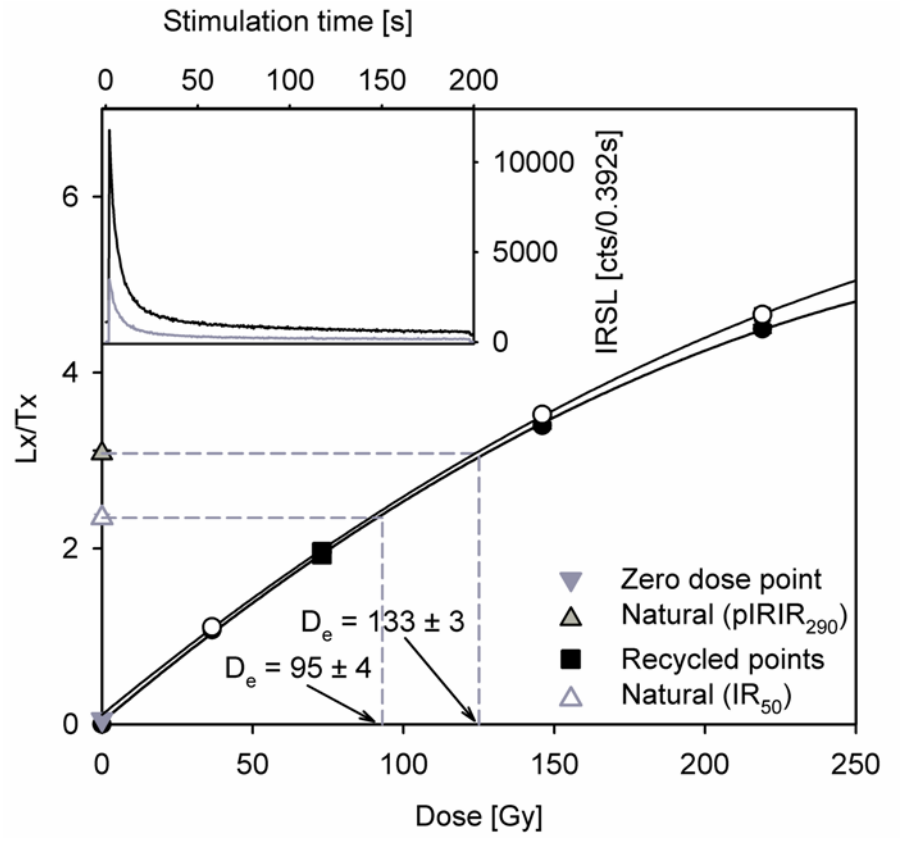

Fig. 2: IR_{50} (open circles) and $pIRIR_{290}$ (closed circles) dose response and natural decay curves (inset; grey: IR_{50}, black: $pIRIR_{290}$) for sample 103005. The values of the zero dose points and recycled points in the graph are almost identical; no individual symbols were used in order to improve the readability of the graph.

4.2.2 Bleaching experiment

Buylaert et al. (2011) have observed significant residual doses in modern Chinese dust (up to 20 Gy for the $pIRIR_{290}$ signal). Sohbati et al. (2011) and Buylaert et al. (2012) have suggested that there may in fact be an unbleachable component to these residuals. Unfortunately, a modern analogue is not available at or near this site. The best estimate of any residual is obtained by laboratory and sunlight bleaching experiments of the individual samples. Three aliquots of each sample were bleached for 1 week in a Hönle SOL2 solar simulator simulating daylight/night cycles

and at ~1m from the light source to minimize any heating; the same number of aliquots were exposed to daylight for the same period of time (Denmark, February).

Fig. 3 shows residual dose plotted against D_e for the IR_{50} and $pIRIR_{290}$ signals. As reported before by Sohbati et al. (2011) for $pIRIR_{225}$ and Buylaert et al. (2012) for $pIRIR_{290}$, there is a correlation between observed residual dose and D_e value. Sohbati et al. (2011) suggested that this trend implies that short-term laboratory bleaching is not as effective as bleaching under natural conditions; this may also explain why our dose recovery results obtained using laboratory bleached samples were unsatisfactory (see section 4.2.1). The youngest sample (D_e=104.6±1.3 Gy) still has a residual of 12 Gy (SOL2) and 16 Gy (natural daylight). Extrapolating the regression line in Fig. 3 to zero total dose gives intercepts of 8±2 and 12±2 Gy, respectively. These residual doses at D_e=0 presumably represent a signal unbleachable in nature, and so we have subtracted a mean residual dose of 10±4 Gy from the $pIRIR_{290}$ equivalent doses. This residual dose is consistent with the $pIRIR_{290}$ doses reported for polymineral fine-grains extracted from modern dust collected across the Chinese Loess Plateau (Buylaert et al., 2011). For IR_{50} there may also be a small unbleachable residual intercept (~4±2 Gy for both laboratory and daylight bleaching) corresponding to about 6.5% of the smallest values of D_e; this residual was subtracted from the IR_{50} equivalent doses in the same manner as for $pIRIR_{290}$.

4.2.3 Anomalous fading

Fading rate measurements (g_{2days}) were made using the same SAR protocol used for the equivalent dose, with a fixed regenerative dose of ~100 Gy and a test dose of ~30 Gy. The mean fading rates for the IR_{50} and $pIRIR_{290}$ signals are 2.3±0.2%/decade and 1.07±0.11% (n=31, 9 samples) confirming that the $pIRIR_{290}$ signal is more stable than the IR_{50} signal. Three aliquots were used per sample and sample-averaged fading rates for IR_{50} range from 1.9±0.2%/decade to 3.5±0.4%/decade and for $pIRIR_{290}$ from 0.3±0.3%/decade to 1.6±0.5%/decade (Table S5). It is interesting to note that the $pIRIR_{290}$ signal still shows measurable fading on laboratory timescales despite the considerable evidence that accurate ages are obtained without fading correction (Buylaert et al., 2012) and that the $pIRIR_{290}$ signal in “infinitely” old samples is very close to saturation (Buylaert et al., 2011; Thiel et al., 2011a; Thomsen et al., 2011). Sample-averaged fading rates were used to correct the IR_{50} and $pIRIR_{290}$ ages using the model of Huntley and Lamothe (2001). The individual fading rates (*g*-value) and uncorrected and corrected ages for both signals are presented in Table S5.

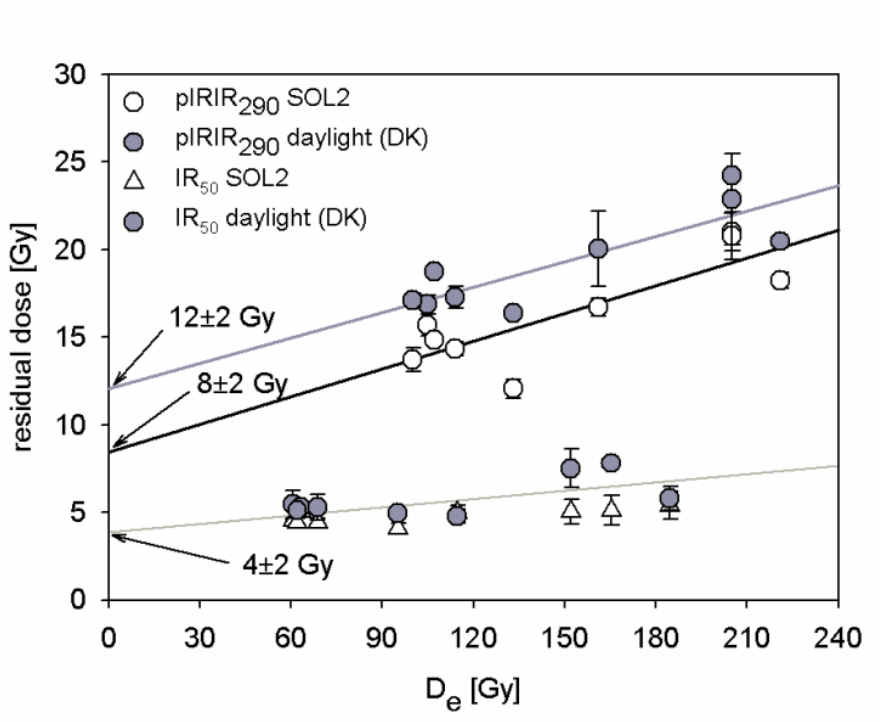

Fig. 3: Results of laboratory (Hönle SOL2 simulator) and daylight bleaching experiments for the IR_{50} (triangles) and $pIRIR_{290}$ (circles) signals. Three aliquots were measured per sample (error bars represent 1s.e.). Extrapolating the regression line to zero age gives 8±2 and 12±2 Gy for $pIRIR_{290}$ and 4±2 Gy for IR_{50}.

5. Results and discussion

5.1 Age comparison

When comparing a stratigraphic sequence of ages derived from the same signal one must of course only consider the independent sources of uncertainty on each age. Only at the top of the sequence (3 and 3.75 m) is there any suggestion of age inversion (Table S5). This inversion may be significant in the quartz OSL and feldspar $pIRIR_{290}$ data but is not apparent in the IR_{50} feldspar data. Removing the systematic errors on the ages from these two samples gives quartz ages of 27.1±0.9 ka (103002) and of 30.5 ±1.3 ka (103003) and uncorrected $pIRIR_{290}$ ages of 27.6 ±1.2 (103002) and of 25.5±1.2 (103003). In both quartz and feldspar these ages are probably significantly different from each other but it is difficult to ascribe a reason for this discrepancy

because the deviations are in opposite directions. Thus we cannot deduce, for example, that these discrepancies arise because of incomplete bleaching or inaccurate dose rate estimation.

Figure 4 shows the uncorrected and corrected IR_{50} and post-IR IR_{290} ages (including correction for residual doses) plotted against quartz OSL ages. For the five youngest samples (lab codes 103001-103005; dose range 70-130 Gy) we consider quartz OSL ages as reliable independent age control. The oldest three samples (lab codes 103007-103009) have quartz doses around 200 Gy with natural signals at ~70% of saturation, and we are less confident of the accuracy of these ages.

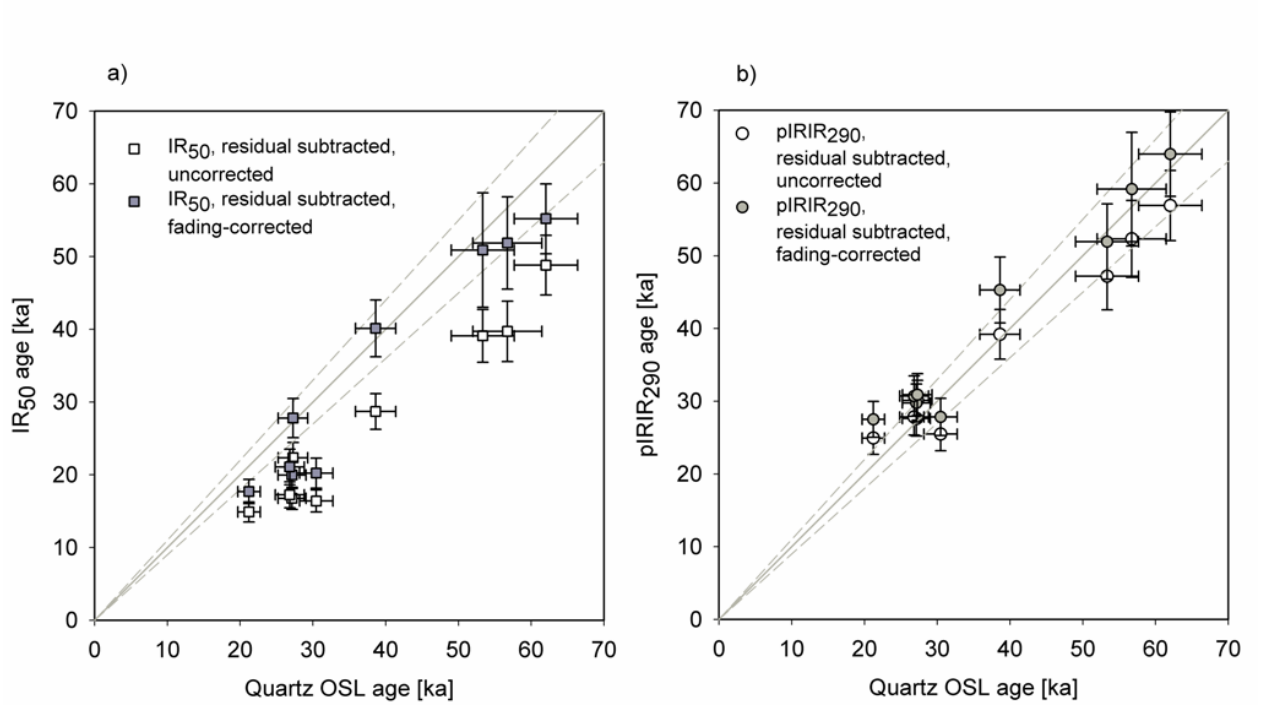

Fig. 4: a) Uncorrected and fading-corrected IR_{50} ages plotted against quartz OSL ages. An unbleachable residual of 4±2 Gy was subtracted from all IR_{50} data. The grey dashed lines show a deviation of 10% from the 1:1 grey solid line. b) Uncorrected and fading-corrected $pIRIR_{290}$ ages plotted against quartz OSL ages. An unbleachable residual of 10±4 Gy was subtracted from all $pIRIR_{290}$ data.

From Fig. 4a it can be seen that the uncorrected IR_{50} ages clearly underestimate compared to quartz OSL ages over the entire age range (20-60 ka). Fading correction appears to overcome most of the underestimation for the older samples but, surprisingly, at least for three young samples the correction is not sufficient. For $pIRIR_{290}$ both uncorrected and corrected ages are in good agreement with quartz although it is possible that correction may tend to cause

overestimation for the youngest five samples (Fig. 4b, ratio corrected $pIRIR_{290}$ to quartz OSL age = 1.12±0.06).

Both quartz OSL and feldspar IRSL ages are equally sensitive to the assumed water content of 15±5%. Using sensitivity analysis we deduce that all our ages would increase by ~1% for a 1% increase in water content at least over a range of ±10%.

As discussed above, the age of the upper paleosol is taken as 35-30 ka based on correlation with an adjacent profile from which a single ^{14}C age is available. This independent age control should be compared with the luminescence ages from sample 103005 for which quartz gave 27±2 ka, $pIRIR_{290}$ gave 30±3 ka (uncorrected) and 31±3 ka (corrected). This supports the earlier conclusions that the $pIRIR_{290}$ signal does not require a fading correction to give accurate ages.

Similarly, we use the ^{14}C ages reported by Sümegi and Hertelendi (1998) for an adjacent section to provide age control for the upper loess layer of between 26 and 18 ka. Overall, these ages are very consistent with our data, especially when we take into account that the exact transitions from loess to paleosols were not specifically dated. We conclude from the comparison of quartz OSL, polymineral IR_{50} and $pIRIR_{290}$ and from the good agreement with the independent age control that standard quartz OSL and polymineral $pIRIR_{290}$ seem to yield the most reliable ages. The results of the IR_{50} measurements are not considered any further as they clearly underestimate or, if corrected, still deviate from quartz OSL for younger samples. The chronology of the Tokaj profile will now be discussed based on quartz OSL and polymineral $pIRIR_{290}$.

5.2 Chronology of the Tokaj profile

Fig. 1 shows the luminescence ages together with the lithology of the Tokaj profile. Both the uncorrected $pIRIR_{290}$ ages and the quartz OSL ages increase with depth (except between 3 and 6 m) and are stratigraphically consistent with no significant inversions (with the possible exception of samples 103002 and 103003, as discussed above). Ages range from 21±2 ka (OSL) and 25±2 ka ($pIRIR_{290}$) below the most recent soil to 62±4 ka (OSL) and 57±5 ka ($pIRIR_{290}$) directly on top of the lower paleosol.

This lower paleosol appears to have developed before the onset of MIS 3 (>58 ka), assuming no stratigraphic gaps in the profile. In case of a hiatus, the lower paleosol can be considerably older than the overlying loess. The age is remarkably similar to the 56±4 ka age in the lowest last glacial

loess unit at Crvenka, but here the underlying soil has been interpreted to be part of the S1 complex (MIS 5, 71-130 ka; Marković et al., 2008, Stevens et al., 2011).

The middle loess layer in Tokaj is represented by three samples (103007-09) and accumulated between *c.* 50 and 60 ka, in the colder periods of MIS 3. This layer might correspond to the 'VL1L2' loess in the adjacent Vojvodina region in Serbia (after the Vojvodina chronostratigraphic system; Marković et al., 2008; 2011) although here it usually extends into MIS 4 (60-71 ka) without any intercalated soils. Further investigations are needed to better constrain the timing of soil and loess formation in the early last glacial across this region. The Upper Paleosol is represented by two samples taken from the top and the lower half of the soil (103005, 103006). Results of 27±2 and 39±3 ka (OSL) and 30±3 and 39±4 ka ($pIRIR_{290}$), respectively, indicate that this soil probably formed during the later stages of MIS 3.

However these ages do not necessarily indicate the time of soil formation, but rather the time of deposition of the sediment in which the soil subsequently developed. Furthermore, the results for sample 103006 are only minimum ages for these processes as this sample is located about 25 cm above the transition from the middle loess layer to the paleosol. Bracketing the upper paleosol with ages from the over- and underlying loess layers, an age range for the time of soil formation of between c. 45 ka and c. 25 ka can be derived. Similar soils of corresponding age ranges have been reported at Crvenka (38±4 ka; Stevens et al., 2011), Stari Slankamen (34.4±2.2 ka, Schmidt et al., 2010) and Surduk (31.8±3.7 ka, Fuchs et al., 2008) in Vojvodina, Serbia. Earlier studies of the Tokaj profile using biomarkers, stable C and N isotopes (Schatz et al, 2001), molluscs (Sümegi and Hertelendi, 1998) and charcoal (Sümegi and Rudner, 2001) have shown that the climate became warmer and drier during the time of soil formation, most likely resulting in a dry steppe environment. The Vojvodina MIS 3 soils and pedocomplexes ('VL1S1') are, however, often less well developed than at Tokaj, probably indicating different paleoclimatic conditions in the south of the Carpathian Basin.

Four samples (103001-04) taken from the uppermost loess layer have ages from 21.2±1.5 ka (OSL) and 25±2 ka ($pIRIR_{290}$) to 30±2 ka (OSL) and 28±2 ka ($pIRIR_{290}$). These ages all suggest that the upper loess layer was deposited during MIS 2 (11-24 ka) in the upper pleniglacial. Similar MIS 2 loess layers have been reported from the Vojvodina region ('V L1L1' loess) (Fuchs et al., 2008; Schmidt et al., 2010; Stevens et al., 2011), as well as from other locations in Hungary (Novothny et al., 2011). According to Sümegi and Hertelendi (1998) the upper loess layer was deposited from 29 ka BP, which is compatible with our data, but is also hypothesized to cover the period until ~13,000 yrs ago, although there is no radiocarbon age in their publication that confirms

this assumption. However, our youngest OSL age is 21.2±1.5 ka, which clearly indicates that loess deposition either ended around 20 ka or that younger loess layers have been eroded or overprinted by Holocene pedogenesis.

5.3 Sedimentation rates and implications for proxy records

Recent results based on highly resolved luminescence chronologies indicate that loess deposition is often episodic and sedimentation rates can be highly variable by up to 1-2 orders of magnitude. These variations cannot be reliably obtained from grain size or MS data and are only revealed by independent dating (Buylaert et al., 2008; Stevens et al., 2006; Stevens and Lu, 2009; Stevens et al., 2008, 2007). Fig. 5 shows a comparison of an assumed uniform sedimentation rate and sedimentation rates based on the new OSL/$pIRIR_{290}$ age depth model of the Tokaj profile. The luminescence derived sedimentation rates differ significantly and are considerably more variable throughout the profile compared to the uniform sedimentation rate. While sedimentation is considerably lower during the middle loess layer (0.30 mm/a compared to 0.42mm/a), values for the last glacial upper loess layer are almost twice as high as previously assumed (0.86 m/a compared to 0.42mm/a). This suggests more active source regions, higher transport rates, or more effective trapping, or a combination of these processes during this period. This MIS 2 centred peak in loess accumulation rates has also been observed elsewhere in the Carpathian Basin, most pronounced at Surduk (Fuchs et al., 2008), Süttő (Novothny et al., 2009; Novothny et al., 2011) and Crvenka (Stevens et al., 2011). In addition to the relative increases in dust deposition during this period, absolute sedimentation rate values between these sites are comparable and match the general pattern of decreasing magnitudes from the north to the south of the Carpathian Basin, potentially due to a closer proximity to likely dust source areas (Stevens et al., 2011; Újvári et al., 2010). Previous proxy studies in Tokaj are all based on an assumed uniform sedimentation rate; our luminescence chronology suggests that a thorough review and re-assessment of the proxy data and interpretations is necessary.

6. Conclusion

In this study we compare fine-grained SAR quartz OSL ages with IR_{50} and $pIRIR_{290}$ ages from polymineral fine-grains from the Tokaj loess-paleosol section, NE Hungary and present the first $pIRIR_{290}$ ages of Hungarian loess.

In general, the luminescence characteristics are satisfactory for all signals. An unbleachable residual of ~10 Gy ($pIRIR_{290}$) and ~4 Gy (IR_{50}) was estimated through a laboratory bleaching experiment and subtracted from the appropriate D_e estimates. As expected, the IR_{50} signal shows significant fading (g_{2days} ~2.3 %/decade) and uncorrected IR_{50} ages severely underestimate both for young and old samples compared to standard SAR quartz OSL ages. Fading correction improves the results substantially, but even after correction the younger samples still underestimate and are therefore not used to establish a numerical chronology. The $pIRIR_{290}$ laboratory fading rate is much smaller (~1%/decade) and we report uncorrected as well as fading-corrected $pIRIR_{290}$ ages. Uncorrected $pIRIR_{290}$ ages and quartz OSL ages agree well with each other and seem to confirm that $pIRIR_{290}$ ages do not require fading correction.

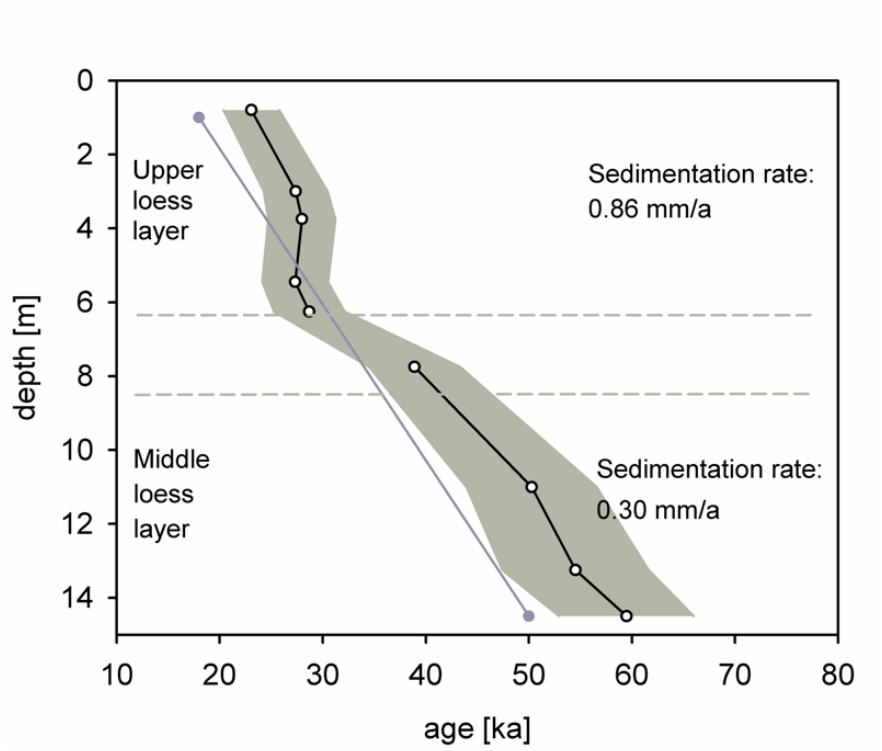

Fig. 5: Comparison of an assumed uniform sedimentation rate (grey solid line) and the rates derived from the luminescence age-depth model (black solid line). For the latter, ages are taken as the mean of the quartz OSL age and the polymineral $pIRIR_{290}$ age (uncorrected, residual subtracted). Sedimentation rates are calculated from the quotient of the difference between two ages and the difference in depth. Errors, propagated in quadrature, are shown as a grey shaded band. The uniform sedimentation rate (0.42 mm/a) is based on 2 rough tie points taken from the literature (Sümegi and Hertelendi, 1998); the upper tie point is the youngest reported loess age (18 ka BP, ^{14}C), the lower is an estimate of the minimum age of the lower paleosol (50 ka BP). Please note that this uniform rate is only intended for illustrative purposes.

Using the uncorrected $pIRIR_{290}$ and OSL ages we present the first complete chronology for the Tokaj loess profile. This luminescence chronostratigraphy is supported by previously published radiocarbon ages and is consistent with other loess-paleosol profiles in the Carpathian Basin. Following the terminology of the Vojvodina region, an L1L1 (~20-26 ka) and L1L2 loess layer (~40-60 ka) are present at Tokaj, as well as a strongly developed L1S1 paleosol (~25-45 ka) and a second paleosol that presumably developed before MIS 3 (>58 ka). Contrary to previous assumptions and interpretations we found that loess accumulation rates are highly variable and range from 0.30 mm/a to 0.86 mm/a. Peaks in these values are comparable in age and magnitude to sedimentation rates reported from other locations in Hungary and Serbia. Since previous studies at the Tokaj site all assume a uniform sedimentation rate, these proxy interpretations require a thorough review.

Acknowledgements

The authors would like to thank Pál Sümegi for his support during field trips to the site and for comments on the manuscript, Markus Fuchs and Michael Zech for their help with sampling the profile, Sébastien Huot for the Excel macros to calculate fading rates and corrected ages, Ágnes Novothny for kindly providing additional material and the anonymous reviewer for his suggestions that helped to improve the manuscript. A. Schatz is grateful to the Gender Equality Commission of the University of Tübingen for funding parts of this project.

Supplementary material

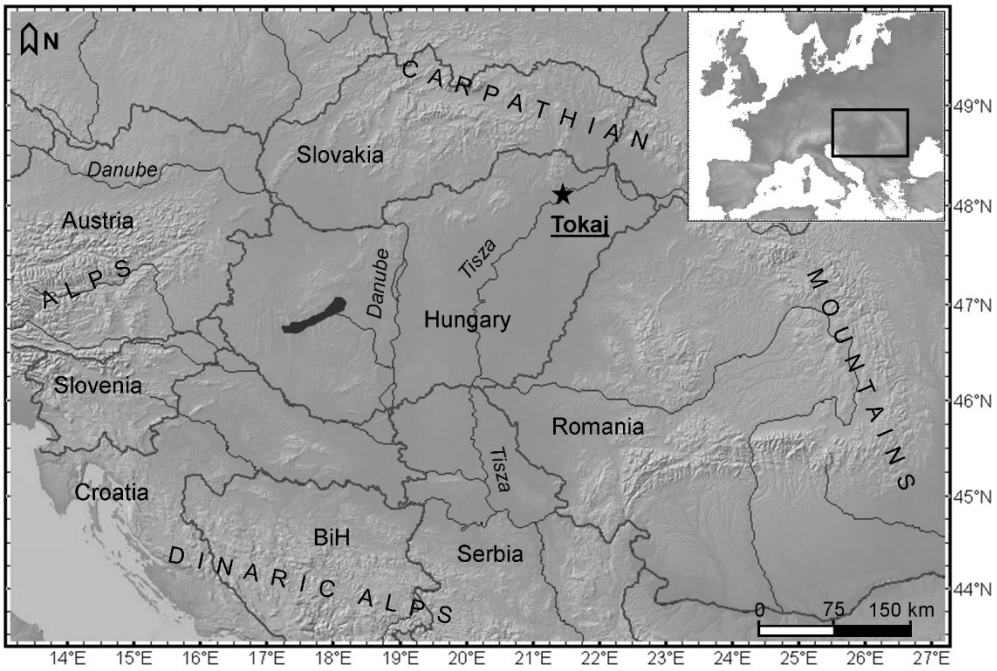

Fig. S1: Location of the studied paleosol-loess profile at Tokaj, NE Hungary.

sample lab code	depth [m]	U-238 [Bq/kg]	Ra-226 [Bq/kg]	Th-232 [Bq/kg]	K-40 [Bq/kg]	Quartz dose rate [Gy/ka]	PM dose rate [Gy/ka]	cosmic dose rate [Gy/ka]
103001	0.8	50.5 ± 7.3	38.1 ± 0.7	45.3 ± 0.8	493 ±12	3.4 ± 0.2	3.8 ± 0.3	0.207 ± 0.010
103002	3	28.0 ± 5.1	36.5 ± 0.5	43.2 ± 0.6	490 ± 9	3.1 ± 0.2	3.5 ± 0.3	0.161 ± 0.008
103003	3.75	34.5 ± 6.8	37.5 ± 0.6	43.6 ± 0.8	475 ± 10	3.1 ± 0.2	3.5 ± 0.3	0.151 ± 0.008
103004	5.45	33.4 ± 9.3	39.6 ± 0.8	46.9 ± 0.9	514 ± 13	3.3 ± 0.2	3.8 ± 0.3	0.131 ± 0.007
103005	6.25	47.1 ± 8.1	43.9 ± 0.8	52.6 ± 0.9	524 ± 12	3.6 ± 0.2	4.1 ± 0.3	0.123 ± 0.006
103006	7.75	41.6 ± 5.4	43.1 ± 0.6	52.4 ± 0.7	468 ± 10	3.4 ± 0.2	3.9 ± 0.3	0.109 ± 0.005
103007	11	52.6 ± 8.9	48.4 ± 0.8	57.1 ± 0.9	470 ± 12	3.6 ± 0.2	4.1 ± 0.4	0.086 ± 0.004
103008	13.25	31.2 ± 7.2	44.6 ± 0.7	53.0 ± 0.8	441 ± 10	3.2 ± 0.2	3.7 ± 0.3	0.074 ± 0.004
103009	14.5	42.0 ± 6.9	38.9 ± 0.7	49.6 ± 0.8	480 ± 12	3.3 ± 0.2	3.7 ± 0.3	0.068 ± 0.003

Table S2: Uranium, radium, thorium and potassium content as measured by gamma spectrometry, and calculated effective dose rates to fine-grained quartz and polymineral (PM) grains. See text for details. Uncertainties mentioned with the analytical data and resulting dose rates are both random (1 s.e.) and systematic (~1.5%); a systematic uncertainty of 5% is associated with the cosmic dose rates.

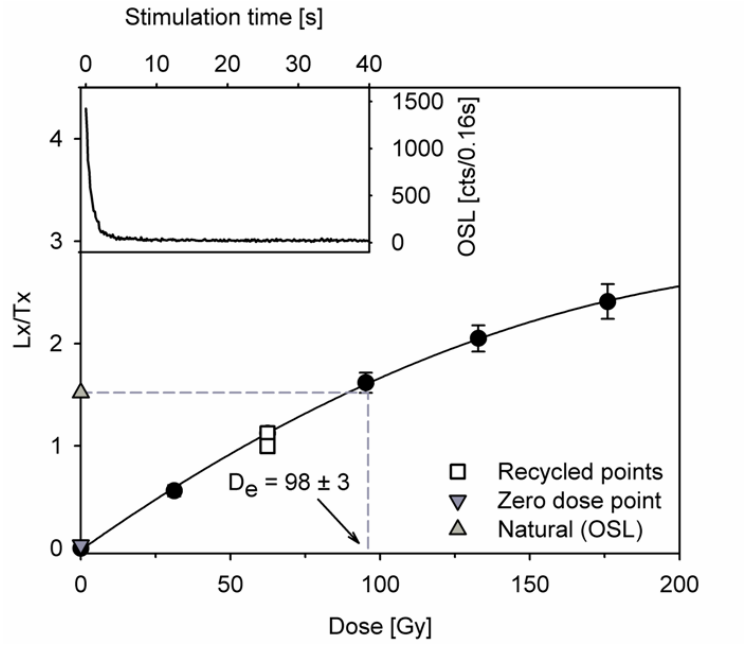

Fig. S3: Example of a quartz OSL dose response and natural decay curve (inset) for sample 103005.

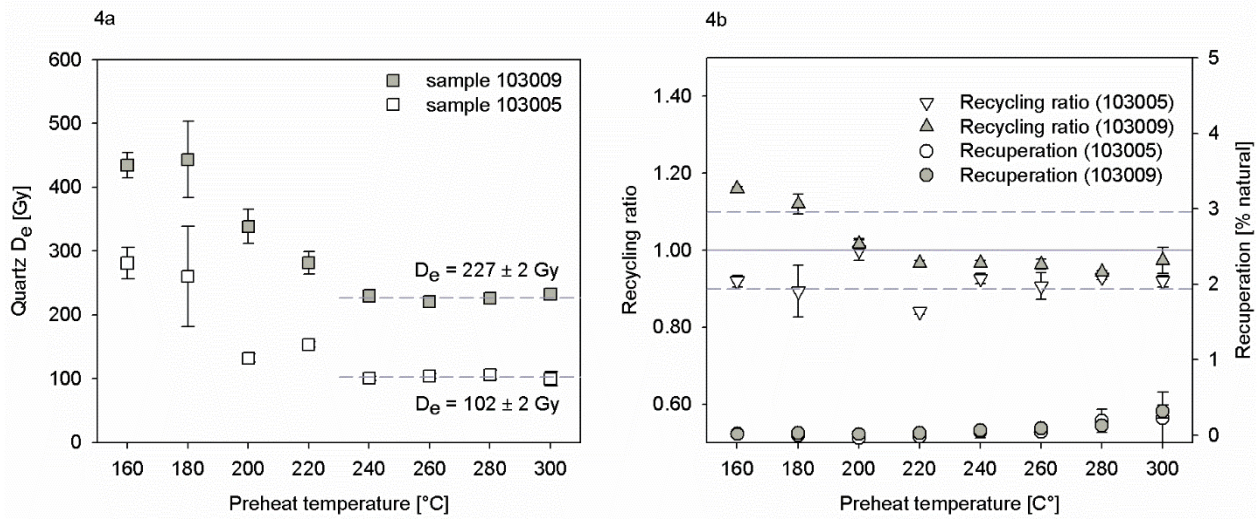

Fig. S4: a) Preheat plateaus for samples 103005 and 103009 (cut-heat 20°C below preheat). Three aliquots were measured per temperature step, error bars represent 1s.e. b) Recycling ratio (triangles) and recuperation (circles) for the same aliquots. Solid line at 1.00 represents perfect recycling and dashed lines denote 10% of unity.

Sample	Depth [m]	Measurement	n	De [Gy]	Recycling	Recuperation [%]	Dose recovery	g-value [%]	uncorrected age [ka]	uncorrected age [ka] residual subtracted	corrected age [ka]	corrected age [ka] residual subtracted
103001	0.80	OSL	11	71.4 ± 2.5	0.94 ± 0.02	0.2 ± 0.2	1.04 ± 0.05	-	21.2 ± 1.5	-	-	-
		IR50	4	60.5 ± 2.1	0.98 ± 0.01	2.5 ± 0.4	0.86 ± 0.01	1.9 ± 0.2	15.9 ± 1.4	14.9 ± 1.4	19.0 ± 1.6	17.7 ± 1.7
		pIR/IRSL290	4	104.6 ± 1.3	1.00 ± 0.02	2.1 ± 0.3	1.08 ± 0.01	1.1 ± 0.09	27.6 ± 2.2	24.9 ± 2.2	30.4 ± 2.4	27.5 ± 2.5
103002	3.00	OSL	5	85.0 ± 2.7	0.96 ± 0.02	0.1 ± 0.04		-	27.1 ± 1.9	-	-	-
		IR50	4	63.1 ± 2.0	0.98 ± 0.01	2.7 ± 0.3		1.9 ± 0.2	17.9 ± 1.5	16.8 ± 1.5	21.3 ± 1.8	20.0 ± 1.9
		pIR/IRSL290	4	107.4 ± 0.6	0.97 ± 0.01	2.2 ± 0.1		0.8 ± 0.04	30.5 ± 2.4	27.6 ± 2.4	32.8 ± 2.5	29.8 ± 2.6
103003	3.75	OSL	4	95.5 ± 3.7	0.92 ± 0.01	0.3 ± 0.3		-	30.5 ± 2.3	-	-	-
		IR50	4	62.1 ± 2.1	0.97 ± 0.01	2.1 ± 0.3		2.3 ± 0.4	17.5 ± 1.5	16.4 ± 1.5	21.6 ± 2.1	20.2 ± 2.1
		pIR/IRSL290	4	100.3 ± 0.8	0.98 ± 0.01	2.3 ± 0.2		1.0 ± 0.18	28.3 ± 2.3	25.5 ± 2.3	30.9 ± 2.5	27.8 ± 2.6
103004	5.45	OSL	12	89.1 ± 3.1	1.01 ± 0.04	0.2 ± 0.4		-	26.8 ± 2.0	-	-	-
		IR50	4	68.7 ± 3.9	0.97 ± 0.01	2.3 ± 0.5		2.2 ± 0.5	18.3 ± 1.8	17.2 ± 1.8	22.4 ± 2.5	21.1 ± 2.4
		pIR/IRSL290	4	114.4 ± 1.8	0.98 ± 0.01	2.1 ± 0.1		1.1 ± 0.13	30.5 ± 2.5	27.8 ± 2.5	33.7 ± 2.7	30.7 ± 2.8
103005	6.25	OSL	12	97.9 ± 3.3	0.98 ± 0.05	0.3 ± 0.5		-	27.3 ± 2.0	-	-	-
		IR50	3	95.2 ± 3.8	1.02 ± 0.02	1.5 ± 0.2		2.4 ± 0.2	23.3 ± 2.1	22.3 ± 2.1	29.0 ± 2.7	27.8 ± 2.7
		pIR/IRSL290	3	132.9 ± 3.2	0.98 ± 0.01	1.7 ± 0.01		0.3 ± 0.25	32.6 ± 2.8	30.1 ± 2.7	33.4 ± 2.9	30.9 ± 2.9
103006	7.75	OSL	12	130.4 ± 3.4	0.99 ± 0.02	0.1 ± 0.2		-	38.6 ± 2.8	-	-	-
		IR50	3	114.7 ± 1.6	1.02 ± 0.04	0.9 ± 0.8		3.5 ± 0.4	29.7 ± 2.6	28.7 ± 2.5	41.6 ± 4.0	40.1 ± 3.9
		pIR/IRSL290	3	161.1 ± 1.5	0.96 ± 0.00	1.6 ± 0.3		1.6 ± 0.49	41.8 ± 3.6	39.2 ± 3.4	48.3 ± 4.7	45.3 ± 4.5
103007	11.00	OSL	10	191.5 ± 8.3	0.98 ± 0.03	0.1 ± 0.2		-	53.3 ± 4.3	-	-	-
		IR50	3	165.3 ± 5.7	1.07 ± 0.05	1.2 ± 0.4		2.8 ± 1.1	40.1 ± 3.8	39.1 ± 3.6	52.2 ± 8.0	50.9 ± 7.9
		pIR/IRSL290	3	204.7 ± 8.4	0.96 ± 0.05	1.3 ± 0.3		1.1 ± 0.22	49.6 ± 4.8	47.2 ± 4.6	54.6 ± 5.3	51.9 ± 5.2
103008	13.25	OSL	11	184.4 ± 8.9	0.99 ± 0.03	0.1 ± 0.2		-	56.7 ± 4.7	-	-	-
		IR50	3	152.1 ± 8.8	0.97 ± 0.03	1.2 ± 0.2		2.8 ± 0.5	40.8 ± 4.3	39.7 ± 4.1	53.3 ± 6.4	51.9 ± 6.3
		pIR/IRSL290	3	205.1 ± 10.0	0.98 ± 0.01	1.0 ± 0.1		1.4 ± 0.86	55.0 ± 5.5	52.3 ± 5.3	62.2 ± 8.0	59.2 ± 7.8
103009	14.50	OSL	6	201.6 ± 4.2	1.01 ± 0.03	0.1 ± 0.1		-	62.0 ± 4.4	-	-	-
		IR50	3	184.6 ± 2.8	0.93 ± 0.03	0.9 ± 0.04		1.4 ± 0.2	49.9 ± 4.3	48.8 ± 4.1	56.4 ± 4.9	55.2 ± 4.8
		pIR/IRSL290	3	220.5 ± 2.7	0.97 ± 0.02	1.2 ± 0.1		1.3 ± 0.33	59.6 ± 5.1	56.9 ± 4.8	67.0 ± 5.9	64.0 ± 5.8

Table S5: Summary table of D_e results, luminescence characteristics, g_{2days}-values and corrected and uncorrected age estimates for the three signals under investigation (errors are 1s.e.). For details see text.

Step	Treatment	Observed
1	Give dose D_i	
2	Preheat, 320°C, 60s	
3	IR stimulation, 50°C, 200s	L_{50}
4	IR stimulation, 290°C, 200s	L_{290}
5	Give test dose D_t	
6	Preheat, 320°C, 60s	
7	IR stimulation, 50°C, 200s	T_{50}
8	IR stimulation, 290°C, 200s	T_{290}
9	IR stimulation, 325°C, 100s	
10	Return to 1	

Table S6: post-IR/IRSL protocol after Thiel et al. (2011a).

References

Aitken, M.J., 1985. Thermoluminescence Dating. Academic Press, London.

Ballarini, M., Wallinga, J., Wintle, A.G., Bos, A.J.J., 2007. A modified SAR protocol for optical dating of individual grains from young quartz samples. Radiation Measurements 42, 360-369.

Buylaert, J.-P., Thiel, C., Murray, A., Vandenberghe, D., Yi, S., Lu, H., 2011. IRSL and post-IR IRSL residual doses recorded in modern dust samples from the Chinese Loess Plateau. Geochronometria 38, 432-440.

Buylaert, J.P., Jain, M., Murray, A.S., Thomsen, K.J., Thiel, C., Sohbati, R., 2012. A robust feldspar luminescence dating method for Middle and Late Pleistocene sediments. Boreas. doi: 10.1111/j.1502-3885.2012.00248.x

Buylaert, J.P., Murray, A.S., Vandenberghe, D., Vriend, M., De Corte, F., Van den haute, P., 2008. Optical dating of Chinese loess using sand-sized quartz: Establishing a time frame for Late Pleistocene climate changes in the western part of the Chinese Loess Plateau. Quaternary Geochronology 3, 99-113.

Danzeglocke, U., Jöris, O., Wenninger, B., 2011. CalPal-2007 online.

Duller, G.A.T., 2003. Distinguishing quartz and feldspar in single grain luminescence measurements. Radiation Measurements 37, 161-165.

Frechen, M., Horváth, E., Gábris, Gy., 1997. Geochronology of Middle and Upper Pleistocene loess sections in Hungary. Quaternary Research 48, 291–312.

Frechen, M., Dodonov, A.E., 1998. Loess chronology of the Middle and Upper Pleistocene in Tadjikistan. Geologische Rundschau 87, 2-20.

Frechen, M., Kehl, M., Rolf, C., Sarvati, R., Skowronek, A., 2009. Loess chronology of the Caspian Lowland in Northern Iran. Quaternary International 198, 220-233.

Fuchs, M., Rousseau, D.-D., Antoine, P., Hatté, C., Gauthier, C., Marković, S., Zoeller, L., 2008. Chronology of the Last Climatic Cycle (Upper Pleistocene) of the Surduk loess sequence, Vojvodina, Serbia. Boreas 37, 66-73.

Huntley, D.J., Lamothe, M., 2001. Ubiquity of anomalous fading in K-feldspars and the measurement and correction for it in optical dating. Canadian Journal of Earth Sciences 38, 1093-1106.

Machalett, B., Oches, E.A., Frechen, M., Zöller, L., Hambach, U., Mavlyanova, N.G., Markovi, B., S., Endlicher, W., 2008. Aeolian dust dynamics in central Asia during the Pleistocene: Driven by the long-term migration, seasonality, and permanency of the Asiatic polar front. Geochem. Geophys. Geosyst. 9, Q08Q09.

Marković, S.B., Bokhorst, M.P., Vandenberghe, J., McCoy, W.D., Oches, E.A., Hambach, U., Gaudenyi, T., Jovanović, M., Zöller, L., Stevens, T., Machalett, B., 2008. Late Pleistocene loess-palaeosol sequences in the Vojvodina region, north Serbia. Journal of Quaternary Science 23, 73-84.

Marković, S.B., Hambach, U., Stevens, T., Kukla, G.J., Heller, F., McCoy, W.D., Oches, E.A., Buggle, B., Zöller, L., 2011. The last million years recorded at the Stari Slankamen (Northern Serbia) loess-palaeosol sequence: revised chronostratigraphy and long-term environmental trends. Quaternary Science Reviews 30, 1142-1154.

Murray, A., Marten, R., Johnston, A., Martin, P., 1987. Analysis for naturally occuring radionuclides at environmental concentrations by gamma spectrometry. Journal of Radioanalytical and Nuclear Chemistry 115, 263-288.

Murray, A.S., Wintle, A.G., 2003. The single aliquot regenerative dose protocol: potential for improvements in reliability. Radiation Measurements 37, 377-381.

Novothny, Á., Frechen, M., Horváth, E., Bradák, B., Oches, E.A., McCoy, W.D., Stevens, T., 2009. Luminescence and amino acid racemization chronology of the loess–paleosol sequence at Süttő, Hungary. Quaternary International 198, 62-76.

Novothny, Á., Frechen, M., Horváth, E., Krbetschek, M., Tsukamoto, S., 2010. Infrared stimulated luminescence and radiofluorescence dating of aeolian sediments from Hungary. Quaternary Geochronology 5, 114-119.

Novothny, Á., Frechen, M., Horváth, E., Wacha, L., Rolf, C., 2011. Investigating the penultimate and last glacial cycles of the Süttő loess section (Hungary) using luminescence dating, high-resolution grain size, and magnetic susceptibility data. Quaternary International 234, 75-85.

Olley, J.M., Murray, A., Roberts, R.G., 1996. The effects of disequilibria in the uranium and thorium decay chains on burial dose rates in fluvial sediments. Quaternary Science Reviews 15, 751-760.

Rees-Jones, J., 1995. Optical dating of young sediments using fine-grain quartz. Ancient TL 13, 9-14.

Rudner, Z.E., Sümegi, P., 2001. Recurring Taiga forest-steppe habitats in the Carpathian Basin in the Upper Weichselian. Quaternary International 76-77, 177-189.

Schatz, A.-K., Zech, M., Buggle, B., Gulyás, S., Hambach, U., Marković, S.B., Sümegi, P., Scholten, T., 2011. The late Quaternary loess record of Tokaj, Hungary: Reconstructing palaeoenvironment, vegetation and climate using stable C and N isotopes and biomarkers. Quaternary International 240, 52-61.

Schmidt, E.D., Machalett, B., Marković, S.B., Tsukamoto, S., Frechen, M., 2010. Luminescence chronology of the upper part of the Stari Slankamen loess sequence (Vojvodina, Serbia). Quaternary Geochronology 5, 137-142.

Sohbati, R., Murray, A.S., Buylaert, J.-P., Ortuño, M., Cunha, P.P., Masana, E., 2011. Luminescence dating of Pleistocene alluvial sediments affected by the Alhama de Murcia fault (eastern Betics, Spain) – a comparison between OSL, IRSL and post-IRIRSL ages. Boreas. 10.1111/j.1502-3885.2012.00249.x

Stevens, T., Armitage, S.J., Lu, H., Thomas, D.S.G., 2006. Sedimentation and diagenesis of Chinese loess: Implications for the preservation of continuous, high-resolution climate records. Geology 34, 849-852.

Stevens, T., Lu, H., 2009. Optically stimulated luminescence dating as a tool for calculating sedimentation rates in Chinese loess: comparisons with grain-size records. Sedimentology 56, 911-934.

Stevens, T., Lu, H., Thomas, D.S.G., Armitage, S.J., 2008. Optical dating of abrupt shifts in the late Pleistocene East Asian monsoon. Geology 36, 415-418.

Stevens, T., Marković, S.B., Zech, M., Hambach, U., Sümegi, P., 2011. Dust deposition and climate in the Carpathian Basin over an independently dated last glacial–interglacial cycle. Quaternary Science Reviews 30, 662-681.

Stevens, T., Thomas, D.S.G., Armitage, S.J., Lunn, H.R., Lu, H., 2007. Reinterpreting climate proxy records from late Quaternary Chinese loess: A detailed OSL investigation. Earth Science Reviews 80, 111-136.

Sümegi, P., Hertelendi, E., 1998. Reconstruction of microenvironmental changes in the Kopasz Hill loess area at Tokaj (Hungary) between 15 and 70 ka BP. Radiocarbon 40, 855-863.

Sümegi, P., Krolopp, E., 2002. Quatermalacological analyses for modeling of the Upper Weichselian palaeoenvironmental changes in the Carpathian Basin. Quaternary International 91, 53-63.

Sümegi, P., Rudner, Z.E., 2001. In situ charcoal fragments as remains of natural wild fires in the upper Würm of the Carpathian Basin. Quaternary International 76-77, 165-176.

Thiel, C., Buylaert, J.-P., Murray, A., Terhorst, B., Hofer, I., Tsukamoto, S., Frechen, M., 2011a. Luminescence dating of the Stratzing loess profile (Austria) – Testing the potential of an elevated temperature post-IR IRSL protocol. Quaternary International 234, 23-31.

Thiel, C., Buylaert, J.-P., Murray, A., Tsukamoto, S., 2011b. On the applicability of post-IR IRSL dating to Japanese loess. Geochronometria 38, 369-378.

Thomsen, K.J., Murray, A.S., Jain, M., Bøtter-Jensen, L., 2008. Laboratory fading rates of various luminescence signals from feldspar-rich sediment extracts. Radiation Measurements 43, 1474-1486.

Thomsen, K.J., Murray, A.S., Jain, M., 2011. Stability of IRSL signals from sedimentary K-feldspar samples. Geochronometria 38, 1-13.

Újvári, G., Kovács, J., Varga, G., Raucsik, B., Marković, S.B., 2010. Dust flux estimates for the Last Glacial Period in East Central Europe based on terrestrial records of loess deposits: a review. Quaternary Science Reviews 29, 3157-3166.

Willis, K.J., Rudner, E., Sümegi, P., 2000. The Full-Glacial Forests of Central and Southeastern Europe. Quaternary Research 53, 203-213.

Study 2: Paleoclimate and weathering of the Tokaj (NE Hungary) loess-paleosol sequence: a comparison of geochemical weathering indices and paleoclimate parameters

Ann-Kathrin Schatz, Thomas Scholten, Peter Kühn

Soil Science and Geomorphology Group, Department of Geosciences, Faculty of Science, University of Tübingen, Rümelinstrasse 19-23, 72072 Tübingen, Germany

Published in: Climate of the Past Discussions (CPD) 10/1 (2014), p. 469-507, doi: 10.5194/cpd-10-469-2014

Resubmitted and under review for publication in Climate of the Past (CP)

The original publication is available at: http://www.clim-past-discuss.net/10/469/2014/cpd-10-469-2014.html

Abstract

The Tokaj loess-paleosol sequence in NE Hungary is one of the key sites for detailed paleoclimate reconstructions of the Quaternary in SE Europe. In this study, the geochemical composition of samples from the upper part of the sequence (45-21 ka) was analyzed and a variety of commonly used weathering indices and element ratios were applied to estimate weathering intensity. Further, similarities and differences between these weathering indices and their sensitivity to changes in paleoclimatic conditions were assessed. Results indicate that all of them accurately track changes in weathering intensity and are, with minor exceptions, very similar to each other.

Based on different transfer functions for major and trace element concentrations (XRF), mass-specific magnetic susceptibility (*X*) and $\delta^{13}C$ data, we calculated mean annual paleotemperature (MAT) and mean annual paleoprecipitation (MAP) for the time intervals of paleosol formation (45-27 ka) and dust deposition (27-21 ka). Results differ depending on the respective transfer function and method but largely agree with previously published paleoclimate data of the region. XRF- and $\delta^{13}C$-based results converge to a MAT of 8-10 °C (paleosol) and 8-9 °C (loess) and show a MAP range of 685-879 mm a^{-1} (paleosol) and 572-700 mm a^{-1} (loess). *X*-based results are probably more consistent with the literature with MATs of 8.4 °C (paleosol) and 6.6 °C (loess) and MAPs of 258-390 mm a^{-1} (paleosol) and 222 mm a^{-1} (loess).

1. Introduction

Loess paleosol sequences are important terrestrial archives of Quaternary climate changes (An et al., 1990; Catt, 1991; Catt et al., 2000; Kemp, 2001; Porter, 2001). Geochronological techniques have provided valuable insights into sediment dynamics and helped establish a general chronologic framework of loess-paleosol sequences as a basis for all subsequent climate studies. Geophysical and sedimentological methods, such as grain size analyses and magnetic susceptibility (e.g. Evans and Heller, 2001; Lu et al., 1999; Terhorst et al., in press) have contributed to an improved understanding of past climate fluctuations, whereas paleontological findings have added unique paleoenvironmental information (Kovács et al., 2012; Sümegi and Krolopp, 2002). Spatially and temporally higher resolved micromorphological studies of soils and sediments provide complementary insights to past climate, landscape and environment (Kühn et al., 2013; Pietsch et al., 2014). An additional source of more quantitative environmental and climate data are the wide range of organic geochemical methods such as biomarkers and stable isotopes (e.g. Hatté et al., 1999; Schatz et al., 2011; Zech et al., 2007; Zech et al., 2010).

Besides providing provenance information (Muhs et al., 2013; Újvári et al., 2008; Újvári et al., 2014), loess and paleosol inorganic geochemistry generally reflects paleoweathering conditions and contributes to paleoclimate reconstructions as well. To quantify absolute and relative changes of paleoweathering intensity, a variety of different geochemical weathering indices (WIs) and element ratios have been introduced (e.g. Buggle et al., 2011; Sheldon and Tabor, 2009). Despite the debate about the reliability of these indices (Buggle et al., 2011; Li and Yang, 2010; Xiao et al., 2010), many successful applications can be found in the literature, mainly, but not limited to, Quaternary loess and paleosols in Europe (Buggle et al., 2011; Kovács, 2007; Kühn et al., 2013; Újvári et al., 2008; Újvári et al., 2014; Vancampenhout et al., 2013), North and South America (Goldberg and Humayun, 2010; Hall and Penner, 2013; Meier et al., 2014), China (Baumann et al., 2014; Chen et al., 1999; Xiong et al., 2010), Southern Arabia (Pietsch and Kühn, 2012) and Siberia (Zech et al., 2008).

Yet weathering indices may not only serve to quantify paleoweathering intensity, but also to estimate paleoclimate parameters, i.e. mean annual temperature (MAT) and mean annual precipitation (MAP) via specifically calibrated empirical transfer functions (Sheldon and Tabor, 2009). Although having been published for several years, these transfer functions based on weathering indices (Sheldon and Tabor, 2009), magnetic susceptibility (Han et al., 1996; Maher et al., 1994; Maher et al., 2003) and stable carbon isotopes (Nordt et al., 2007) are still to gain

more attention in loess-paleosol studies, especially for SE Europe since most successful studies have been conducted elsewhere (Kühn et al., 2013; Meier et al., 2014; Pietsch and Kühn, 2012).

Against this background, our study investigates one of the most extensively studied loess paleosol profiles in Tokaj, SE Hungary (NE Europe). The goals are (a) to apply a variety of geochemical weathering indices and element ratios to estimate weathering intensity (b) to assess and compare similarities and differences between these weathering indices as well as their sensitivity to changes in paleoclimatic conditions and (c) to apply transfer functions to derive MAT and MAP estimates from different proxy records and to discuss and compare the results with local climate data from the literature and the results of global climate models.

The results of this study will broaden our understanding of the late Quaternary paleoclimate of SE Europe and contribute to the current debate about full-glacial refugia of thermophilous plants (Willis et al., 2000; Willis and van Andel, 2004). Furthermore, this study may serve as an encouragement of future applications of these methods to examine and quantify paleoclimate records at other locations.

2. Study area

Tokaj (NE Hungary) is situated in the NE Carpathian Basin, a region of approximately 300,000 km^2 that is surrounded by major mountain ranges (Carpathian Mts., Alps, Dinaric Mts.; Fig. 1a). The area around Tokaj has been suggested as one of the rare refuges for deciduous and coniferous trees during the last glacial and has, as a result, received considerable attention (e.eg. Rudner and Sümegi, 2001; Schatz et al., 2011; Schatz et al., 2012; Sümegi and Hertelendi, 1998; Sümegi and Rudner, 2001; Sümegi and Krolopp, 2002; Willis et al., 2000). Today, NE Hungary is part of the continental climate zone (Dfb, warm summer subtype), with a large seasonal temperature variance (mean January T:-3 °C; mean July T: 20.6 °C; mean annual T: 9.8 °C) and a mean annual precipitation of 546 mm a^{-1} (World Data Center for Meteorology, 2011).

The loess-paleosol sequence at Patkó quarry is situated on the eastern slopes of Kopasz Hill (100 m a.s.l., 48°07’ N, 21°24’ E), in the southernmost part of the Tokaj Mountains at the confluence of the Bodrog and Tisza rivers. A 15 m high loess-paleosol sequence with two well-developed paleosols and three loess layers is exposed on top of an approximately 40 m high wall cut into the flanks of Kopasz Hill. The investigated section and the results of sedimentological,

geochronological, geophysical and geochemical investigations have been described in detail by Sümegi and Rudner (2001), Sümegi and Hertelendi (1998) and Schatz et al. (2011, 2012).

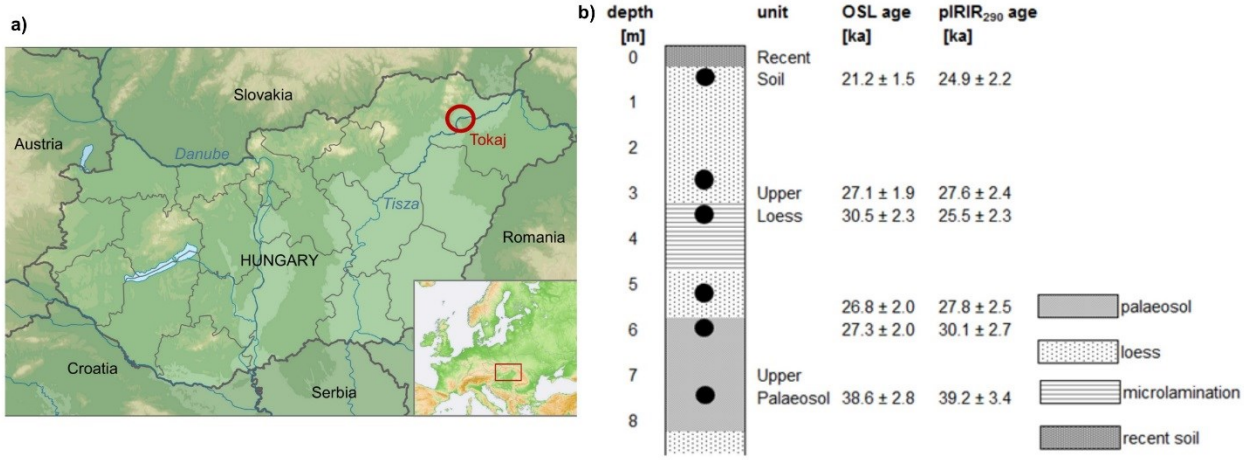

Fig. 1: a) Map of the study area, Tokaj in NE Hungary. b) Chronostratigraphy of the upper half of the paleosol-loess profile at Tokaj (Schatz et al., 2012).

In this study, we decided to focus exclusively on the upper part of the loess-paleosol sequence for two reasons: (i) the only paleotemperature data for the Northeastern part of Hungary and Tokaj, specifically, are the malacothermometer paleotemperatures from Sümegi and Hertelendi (1998) but they are only available for the upper half of the Tokaj loess-paleosol sequence. (ii) The chronostratigraphy (Schatz et al., 2012) for the upper half of the loess-paleosol sequence is more detailed than for the lower half, for which only rough age estimates exist. Paleoclimate information for a part of the sequence that is not well-constrained with regard to age does not yield much scientific value and lacks context. Therefore, only samples from the upper loess layer and the upper paleosol were included in our analyses (Fig. 1b).

The upper paleosol developed on top of a ca. 50-60 ka old loess layer which corresponds to the MIS3 'VL1L2' loess layer in the adjacent Vojvodina region in Serbia (e.g. Marković et al., 2008). It shows a reddish-brown, humic horizon with signs of podsolization in the upper part (Sümegi and Rudner, 2001). This soil formed in the latter stages of MIS3 between ca. 45-27 ka and may be classified as a weakly developed type of 'VL1S1' soil in the Vojvodina system. A charcoal layer directly on top of the paleosol, found in a similar stratigraphic position in an adjacent profile, was dated to 28-26 ka BP and has been interpreted as the result of extensive natural wildfires occurring after pedogenesis ceased and the climate became extremely dry (Sümegi and Hertelendi, 1998; Sümegi and Rudner, 2001). The upper loess layer was deposited in MIS 2 between 27-21 ka and

corresponds to the 'VL1L1' loess. Dust deposition may have ceased afterwards, or younger loess may have been eroded or overprinted by pedogenesis. The recent soil is only weakly developed and affected by recent bioturbation. Samples of the recent soil are not included in our analyses.

3. Methods

3.1 Laboratory analyses

Standard procedures were followed for sampling and sample handling in the field and lab. The section was cleaned and 35 bulk samples for geochemical analyses were taken in depth increments of 25 cm and air-dried at 40 °C. For all analyses, representative aliquots from homogenized and sieved (<2 mm) sample material were used.

XRF measurements were carried out on ball-milled subsamples. For the fused beads 1.5 g of dried sample powder (at 105 °C) is mixed with 7.5 g MERCK spectromelt A12 (mixture of 66% Li-tetraborate and 34% Li-metaborate) and melted at 1200 °C to fused beads using an Oxiflux system from CBR analytical service. Measurements were done with a Bruker AXS S4 Pioneer wavelength dispersive XRF device (Rh-tube at 4kW) and 32 standardized samples, using the traces program. Loss on ignition (LOI) was determined externally at 1000 °C. The element concentrations are expressed as wt.-% or ppm and were recalculated on a volatile-free basis.

Total organic carbon (TOC) was measured on decalcified subsamples (50 mg) using an NA 1108 Elementar Analyzer (CE Instruments, Milan, Italy). $CaCO_3$ was measured gasvolumetrically (DIN ISO 10693) and served as a basis for the calculation of total inorganic carbon (TIC). TIC and calcite-bound CaO were calculated stoichiometrically (wt.-%):

$$TIC = CaCO_3 * 0.12 \quad (1)$$

$$CaO_{calcite} = [(TIC * 3.6641) – (MgO * 2.092) * 0.522] * 2.2743 * 0.5603 \quad (2)$$

$$CaO^* = CaO\ tot – CaO\ calcite \quad (3)$$

In samples with low carbonate and high Mg concentrations (dolomite, mafic minerals), $CaO_{calcite}$ calculations can yield negative results. In this case, values are set to 0. Results are roughly similar to those obtained with McLennan's correction, which may support their validity. If CaO is corrected after McLennan (1993), the CaO* (henceforth called CaO**) concentration is calculated based on the ratio of Ca and Na: if the concentration of CaO is less or equal to the concentration of Na_2O,

the CaO value remains unaltered. If the CaO concentration is higher than Na_2O, the CaO** value is set equal to Na_2O. Apatite-bound Ca is assumed to be negligible.

3.2 Weathering indices

A variety of WI were calculated (for equations, see Table 1). Traditional, multi-element weathering indices are calculated from the concentrations of several mobile and immobile elements (in molar portions), thus providing a quantitative measure of mineral weathering. They are usually based on the enrichment of Al and the depletion of cations as Ca, K, Na or Mg. Common multi-element WIs are ΣBases/Al ratio (Retallack, 2001) and, more recently, the Paleosol Weathering Index (PWI, Gallagher and Sheldon, 2013). Other ratios are based on a more limited selection of elements (Al, K, Na, Ca) to focus on the weathering behavior of the feldspar group. An advantage of these feldspar indices is the fact that all index elements are hosted in the same mineral group, which helps minimizing the effects of variations in mineralogy. Common feldspar indices are the widely used Chemical Index of Alteration (CIA, Nesbitt and Young, 1982) and the Indices A and B after Kronberg and Nesbitt (1981).

In order to exclude potential effects arising from the inconsistency in K weathering (Buggle et al., 2011), several indices without K were developed, most prominently the Chemical Index of Weathering (CIW, also called CIA-K, Harnois, 1988), which is the K-free equivalent of the CIA, and the Plagioclase Index of Alteration (PIA, Fedo et al., 1995), a further modification of CIA and CIW that adjusts for Al contained in K-feldspar and results in purely plagioclase weathering. The WI after Yang et al. (2006) index uses Ti instead of Al as a refractory element and has been developed specifically for loess-paleosol studies, whereas WI-1 and WI-2 after Darmody et al. (2005) have not been widely applied to loess and paleosols yet.

Due to problems associated with determining the correct amount of silicate-bound Ca, indices that do not rely on Ca might be preferable, such as the index of Feng (1997) or the Chemical Proxy of Alteration (CPA, also known as CIW', Cullers, 2000, Buggle et al., 2011), which factors out both Ca and K, thus attempting to avoid all potential biases due to these cations.

Trace element indices are the last group of commonly employed weathering indices (Table 1). Both Ba/Sr and Rb/Sr represent leaching behavior during weathering with Ba and Rb being less soluble than Sr. Potential weakness in these indices are the poorly understood behavior of Rb and Ba in the sediment (Gallet et al., 1996; Sheldon and Tabor, 2009), grain-size dependence and the

Table 1: Overview of weathering indices and empirical climate transfer functions for MAT, MAP and MJT (mean July temperature): a) Mollisol-specific, b) Inceptisol-specific, c) forest soil-specific, d) X_{B-C} = [(mean mass-specific magnetic susceptibility X of B horizon)-(mean mass-specific magnetic susceptibility X of loess)], X [$10^{-8}m^3kg^{-1}$], e) X = mean mass-specific magnetic susceptibility of B horizon or loess, f) the $\delta^{13}C$ transfer function results in a mean July paleotemperature (MJT) which needs to be converted to MAT (see 5.3.1 for details).

Weathering index		**Equation**	**Reference**
multi-element	CIA	=[Al/(Al+Na+Ca*+K)]*100	Nesbitt & Young, 1982
	Index A	=(Si+Ca*+K+Na)/(Al+Si+Ca*+K+Na)	Kronberg & Nesbitt, 1981
	Index B	=(Ca*+Na+K)/(Al+Ca*+Na+K)	Kronberg & Nesbitt, 1981
	PWI	=[(4,20*Na)+(1,66*Mg)+(5,54*K)+(2,05*Ca)]*100	Gallagher & Sheldon, 2013
	Σbases/Al	=(Ca*+Mg+Na+K)/Al	Retallack, 2001
K-free	CIW (CIA-K)	=[Al/(Al+Na+Ca*)]*100	Harnois, 1988; Maynard, 1992
	PIA	=[(Al-K)/(Al+Ca*+Na-K)]*100	Fedo et al., 1995
	YANG	=(Ca*+Na+Mg)/Ti	Yang et al., 2006
	WI-1	=(Si+Ca*)/(Fe+Ti)	Darmody et al., 2005
	WI-2	=(Si+Ca*)/(Fe+Ti+Al)	Darmody et al., 2005
Ca-free	CPA (CIW')	=[Al/(Al+Na)]*100	Cullers, 2000; Buggle et al., 2011
	FENG	=(Al+Fe)/(Na+K+Mg+P)	Feng, 1997
trace element	Ba/Sr		
	Rb/Sr		

Climate parameter		**Equation**	**Reference**
XRF-based	XRF1-MAP	=-259,3 Ln(Σ bases/Al)+759	Sheldon et al., 2002
	XRF2-MAP [a)]	=-130,9 Ln(Ca/Al)+467	Sheldon et al., 2002
	XRF3-MAP	$=221,1e^{0,0179(CIA-K)}$	Sheldon et al., 2002
	XRF1-MAT [b)]	=46,9(Al/Si)+4	Sheldon, 2006
	XRF2-MAT	=-18,5* [(K+Na)/Al]+17,3	Sheldon et al., 2002
	XRF3-MAT [c)]	=-2,74Ln(PWI)+21,39	Gallagher & Sheldon, 2013
MS-based	X1-MAP [d)]	$=222+199 \log (X_{B-C})$,	Maher et al., 1994
	X2-MAP [e)]	$=-22,7+11,6X-6,7*10^{-2}X^2+1,9*10^{-4}X^3-1,9*10^{-7}X^4$	Han et al., 1996
	X3-MAP [d)]	$=86,4*\mathrm{Ln}(X_{B-C})+90,1$	Maher et al., 2003
	X-MAT [e)]	$=-2,4+0,2X-1,1*10^{-3}X^2+2,7*10^{-6}X^3-2,7*10^{-9}X^4$	Han et al., 1996
$\delta^{13}C$-based	$\delta^{13}C$-MJT [f)]	$=[0,685(\delta^{13}C)+34,9]$	Nordt et al., 2007

fact that variable and low initial concentrations may result in erroneously high weathering intensities. In addition to that, Sr substitutes for Ca (Wedepohl, 1987) and is therefore controlled by calcite and dolomite behavior.

3.3 Paleoclimate information

Some of the weathering indices listed above may also be used to estimate paleoprecipitation and paleotemperature based on empirical relationships between MAT or MAP and the geochemical composition of soils. We calculated MAP in three different ways after Sheldon et al. (2002). MAT was calculated after Sheldon et al. (2002), Sheldon (2006) and Gallagher and Sheldon (2013). These equations (Table 1) were mostly derived from a large database of North American soils (Marbut, 1935) and modern climate data. Ideally, a dataset used as a basis for transfer functions specifically for (SE) Europe would contain local soil data but such a dataset is not available. The North American soils used to derive the transfer functions, however, have both a very large variety in formation times, formation processes and parent materials. We therefore assume that they are representative for European (paleo-)sols as well and, consequentially, the transfer functions can be applied to those, too.

In this study, an important conceptual assumption needs to be made if we want to apply the XRF-based transfer functions to the paleosol and loess from the upper half of the Tokaj sequence. In order to be able to compare the results, we have to assume that the upper loess is geochemically identical to the middle loess (not included in our analyses) from which the paleosol has developed. A detailed geochemical analysis is beyond the scope of this study but the results of a forthcoming study support this assumption (Schatz et al., submitted). Sr-Nd isotopic analyses suggest a stable sediment source over time and elemental fingerprints confirm the geochemical homogeneity of the both loess layers.

With regard to the validity of using the transfer functions not only for paleosols, but also for loess, Kühn et al. (2013) have argued that they can indeed be used for both materials. Since loess is the parent material of the paleosol, it should include a genuine climate signal as well. In their study, Kühn et al. (2013) used two different equations and received similar MAP and MAT results for loess. Their results show a clear trend towards lower temperatures for loess than for the paleosol and MAT/MAP estimates that are comparable to those obtained from other proxies. These observations encourage the application of the transfer functions to loess.

For comparison with XRF-based reconstructions, we also calculated MAT and MAP based on mass-specific magnetic susceptibility X (henceforth called "X-based") following Maher et al. (1994), Maher et al. (2003) and Han et al. (1996). Equations are given in Table 1. Unlike XRF, magnetic susceptibility data are available for the entire profile, including the middle loess (Schatz et al., 2011; see appendix) from which the upper paleosol has developed. This middle loess was

used to calculate *X*1- and *X*2-MAP, which require a 'background' or baseline *X* signal of the parent material of a paleosol.

Table 2: Overview of weathering index results. Arrows indicate if WI increases or decreases with increasing weathering intensity. CaO* and CaO** denote the type of CaO correction (see text). The min/max values obtained for the study area are shown, together with results from previous studies at other locations: a) Loess from southwest Hungary (Újvári et al., 2008), b) Loess from Paks, Hungary (Újvári et al., 2012), c) Loess from Stari Slankamen, Serbia (Buggle et al., 2011), d) Loess from Beremend, Hungary (Varga et al., 2011), e) Average Loess Composition (AVL^3, Újvári et al., 2008), f) Red Clay from SW Hungary (Kovacs, 2007). Caution is required when comparing WIs in absolute numbers because results differ depending on the CaO correction used.

Index	↑↓	CaO	Results min/max	Loess [a)] HU	Loess [b)] HU	Loess [c)] RSB	Loess [d)] HU	AVL^3 [e)] global	Red Clay [f)] HU
CIA	↑	CaO*	49-67	-	-	-	-	-	79.3
		CaO**	57-67	58-66	60-70	57-76	67-78	41	-
Index A	↓	CaO*	0.91-0.923	-	-	-	-	-	-
		CaO**	0.91-0.923	-	-	-	-	0.922	-
Index B	↓	CaO*	0.33-0.51	-	-	-	-	-	-
		CaO**	0.33-0.43	-	-	0.24-0.43	-	0.59	-
PWI	↓	CaO*	11.6-13.4	-	-	-	-	-	-
		CaO**	11.6-13.4	-	-	-	-	11.9	-
Σbases/Al	↓	CaO*	0.76-1.5	-	-	-	-	-	-
		CaO**	0.75-1.18	-	-	-	-	1.94	-
CIW	↑	CaO*	54-75	-	-	-	-	-	-
		CaO**	64-75	-	67-80	64-86	76-88	45	-
PIA	↑	CaO*	48-72	-	-	-	-	-	-
		CaO**	59-72	-	-	60-85	-	39	-
YANG	↓	CaO*	6.4-14	-	6-23	-	-	-	-
		CaO**	6.3-10.6	-	-	-	-	22	-
WI-1	↓	CaO*	31-36	-	-	-	-	-	-
		CaO**	31-35	-	-	-	-	41	-
WI-2	↓	CaO*	7.3-8.7	-	-	-	-	-	-
		CaO**	7.3-8.7	-	-	-	-	9	-
CPA	↑		78-83	-	81-89	78-91	86-94	81	-
FENG	↑		1.3-1.9	-	-	-	-	1.34	-
Ba/Sr	↑		1.5-2.5	2.1-2.8	1.0-3.7	1.0-3.2	1.0-5.0	1.3	1.1
Rb/Sr	↑		0.51-0.87	0.2-0.7	0.2-0.9	0.4-1.2	0.3-1.4	0.38	0.46

Although the *X*-based equations have been derived from local datasets – the Chinese Loess Plateau (Maher et al., 1994; Han et al., 1996) and the Russian steppe (Maher et al., 2003) – it has been argued that they can be applied elsewhere as well. Panaiotu et al. (2001) have successfully used the *X*1-MAP equation to calculate MAP for a paleosol-loess sequence in SE Europe. Using an extensive dataset of well-drained paleosols developed on loess from the Northern Hemisphere temperate zone, Maher and Thompson (1995) and Maher et al. (2002) have shown that these

soils follow a similar magnetic enhancement trend as soils from the Chinese Loess Plateau. Maher et al. (2003) proposed an adjusted equation derived from Russian steppe soils, which is applicable to well-drained soils in a MAP range of 100-2000 mm a^{-1}. Again, they confirm the similarities in magnetic enhancement mechanisms of such soils from the Northern hemisphere temperate zone. Similar observations have been made by Forster and Heller (1997) for paleosols from SE Europe and Asia. Based on a quantitative model of magnetic enhancement, Orgeira et al. (2011) demonstrate that enhancement is mainly controlled by the ratio of MAP and evapotranspiration and identify world regions where *X*-based transfer functions can be applied, including the E Carpathian Basin. These results encourage us to apply the *X*-based transfer functions to our samples, although a truly 'global' transfer function is still missing.

A third, independent method to reconstruct paleoclimatic information are carbon isotopes ($\delta^{13}C$). Mean July paleotemperature was calculated based on $\delta^{13}C$ (Schatz et al., 2011; see appendix) following Nordt et al. (2007). This transfer function is based on differences in the isotopic composition of C3 and C4 plants and their dependence on temperature and climate and has successfully been applied to reconstruct paleotemperatures in semiarid grasslands (Hall and Penner, 2013; Meier et al., 2014). However, this equation may not be suitable for samples outside a mean July temperature range of ca. 16-26 °C, i.e. minimum and maximum temperatures that result from the highest and lowest naturally occurring plant $\delta^{13}C$ values (-13 ‰ for C4, -26 ‰ for C3 plants). Therefore, $\delta^{13}C$-based mean July paleotemperature was only calculated for the paleosol.

4. Results

4.1 General geochemistry

Loss on ignition (LOI, see Table S1 in the supplementary section) reflects variable amounts of carbonate, hydrous phases (e.g. clay minerals) and organic matter in the samples. Average LOI of the Tokaj samples is 6.48 wt.-%, ±0.83; highest LOI tends to be found in loess, paleosol samples have overall lower values. There is a positive correlation of LOI with $CaCO_3$ and CaO (r=0.66 and 0.73, respectively), indicating that LOI is mainly associated with carbonates. Average total inorganic carbon (TIC) is 0.56 wt.-% ±0.32; average values are higher for loess than for paleosol samples, whereas organic carbon (TOC; Ø 0.15 wt.-% ±0.33) is lower in loess. $CaCO_3$ (4.71 wt.-% ±2.63) is higher in loess (5.88 wt.-%) than in paleosol samples (1.77 wt.-%). Carbonate is

strongly correlated with uncorrected CaO (r=0.99), indicating that CaO contents are strongly dependent on $CaCO_3$, therefore, a correction is needed to obtain non-calcitic, silicate-bound CaO* only. Uncorrected CaO is highly negatively correlated with CaO-based weathering indices such as CIA (r=-0.99), which suggests that CIA variation is strongly influenced by uncorrected CaO and hence by $CaCO_3$, instead of reflecting a change in non-calcitic CaO. If corrected, the correlation coefficients of CaO* and $CaCO_3$ decrease (CaO*/$CaCO_3$: r=0.90, CaO*/CIA: r=-0.95).

Corrected CaO values differ systematically according to the correction method used. Measured CaO* values range from 2.17 wt.-% to 3.85 wt.-% (Ø 2.92 wt.-% ±0.4; loess: 3.02 wt.-%, paleosol: 2.68 wt.-%). Using McLennan‘s (1993) correction method, CaO** is significantly lower, ranging from 0.65 wt.-% to 1.83 wt.-% (Ø 1.50 wt.-% ± 0.37, loess: 1.63 wt.-%, paleosol: 1.18 wt.-%).

4.2 Major elements

An overview of the results of the XRF measurements is given in table S1 in the supplementary section. Compared with average loess composition (AVL[3], Újvári et al., 2008) and literature data, the samples contain a rather high amount, but narrow range, of SiO_2 (73.4 wt.-% ± 1.4), above-average amounts of Al_2O_3 (12.20 wt.-%±0.52), TiO_2 (0.88 wt.-%±0.04) and Fe_2O_3 (4.26 wt.-% ±0.21), while MgO (1.78 wt.-% ±0.24), Na_2O (1.84 wt.-% ± 0.07) and K_2O (2.11 wt.-% ± 0.14) contents are comparable to or slightly below average. Down-section compositional variability among samples is low to moderate. Paleosols can be differentiated from loess by slightly higher contents of SiO_2 (74.3 wt.-% vs. 73.11 wt.-%), Al_2O_3 (12.88 wt.-% vs. 11.9 wt.-%) and Fe_2O_3 (4.5 wt.-% vs. 4.2 wt.-%) and slightly lower contents of MgO (1.5 wt.-% vs. 1.9 wt.-%), CaO* (2.68 wt.-% vs. 3.02 wt.-%) and Na_2O (1.8 wt.-% vs. 1.9 wt.-%). In addition, paleosol samples have substantially lower $CaCO_3$ values than loess. The chemical differences between loess and paleosol samples are similar to the results of other studies and were probably caused by dissolution of soluble /mobile elements during pedogenesis.

4.3 Weathering

The changes in elemental compositions due to pedogenesis can also be visualized in X/Y elemental plots. In Fig. 2 a)-c), Al_2O_3/SiO_2, Fe_2O_3/TiO_2 and ΣBases/TiO_2 plots illustrate the relative enrichment of Al and Fe during pedogenesis, whereas bases are depleted during the process.

This depletion is further illustrated in the Na_2O/Al_2O_3 vs. K_2O/Al_2O_3 plot (Fig. 2d), Garrels and Mackenzie, 1971), which shows that chemical weathering leads to the removal of more soluble components such as Na and K compared to UCC and AVL[3] (i.e. lower left corner), but also within the Tokaj dataset with paleosol samples being more depleted than loess samples.

The Tokaj samples plot in the A-CN-K diagram (Fig. 2f; Nesbitt and Young, 1984) in a less-weathered region compared to PAAS (Taylor and McLennan, 1985) and NASC (Gromet et al., 1984) - both are standard samples for weathered continental sediments - and nearly parallel to the A-CN line, i.e. they follow the plagioclase weathering trend with a constant K-feldspar/plagioclase ratio. The degree of weathering is variable, with paleosol samples plotting closer to the CN corner and PAAS, indicating the progressive enrichment of Al and depletion of Ca and Na (plagioclase weathering) with increasing weathering intensity, while the K content (K-feldspar, micas) remains constant. The weathering trend originates close to the UCC composition (Taylor and McLennan, 1985), which equals a granodioritic composition and suggests that the samples have been derived from a felsic source, which has most likely remained constant over time. The location of the samples in the A-CN-K diagram changes, if CN is calculated with CaO** based on McLennan's correction instead of the measured CaO* values. This underestimation results in a shift along the plagioclase weathering trend towards the CN corner, parallel to the A-CN line. However, both datasets still plot on a line between UCC and PAAS, comparable with other paleosol and loess samples in the literature (Újvári et al., 2008, 2012; Buggle et al, 2011). Since the weathering trend is the same, an uncertainty in CaO composition does not affect the interpretation.

Fig. 2 (next page): a)-d): Al_2O_3/SiO_2 [wt.-%], Fe_2O_3/TiO_2 [wt.-%], $\Sigma bases/TiO_2$ [wt.-%], and Na_2O/Al_2O_3 vs. K_2O/Al_2O_3 [mol] plots illustrate geochemical weathering behavior. Grey open squares denote loess, black open triangles paleosol samples from Tokaj. The composition of the upper continental crust (UCC, Taylor and McLennan, 1985) and of average loess (AVL[3], Újvári et al., 2008) are indicated for comparison. See text for details. e) Comparison of the CIA weathering index computed with CaO* (corrected via measured $CaCO_3$ content and TIC) and based on CaO** (corrected after McLennan, 1993). f) Ternary A-CN-K diagram of the Tokaj paleosol and loess samples, UCC, AVL[3] and post-Archean Australian shale (PAAS, Taylor and McLennan, 1985). The samples plot parallel to the A-CN join, following an ideal weathering trend from less weathered UCC to highly weathered PAAS.

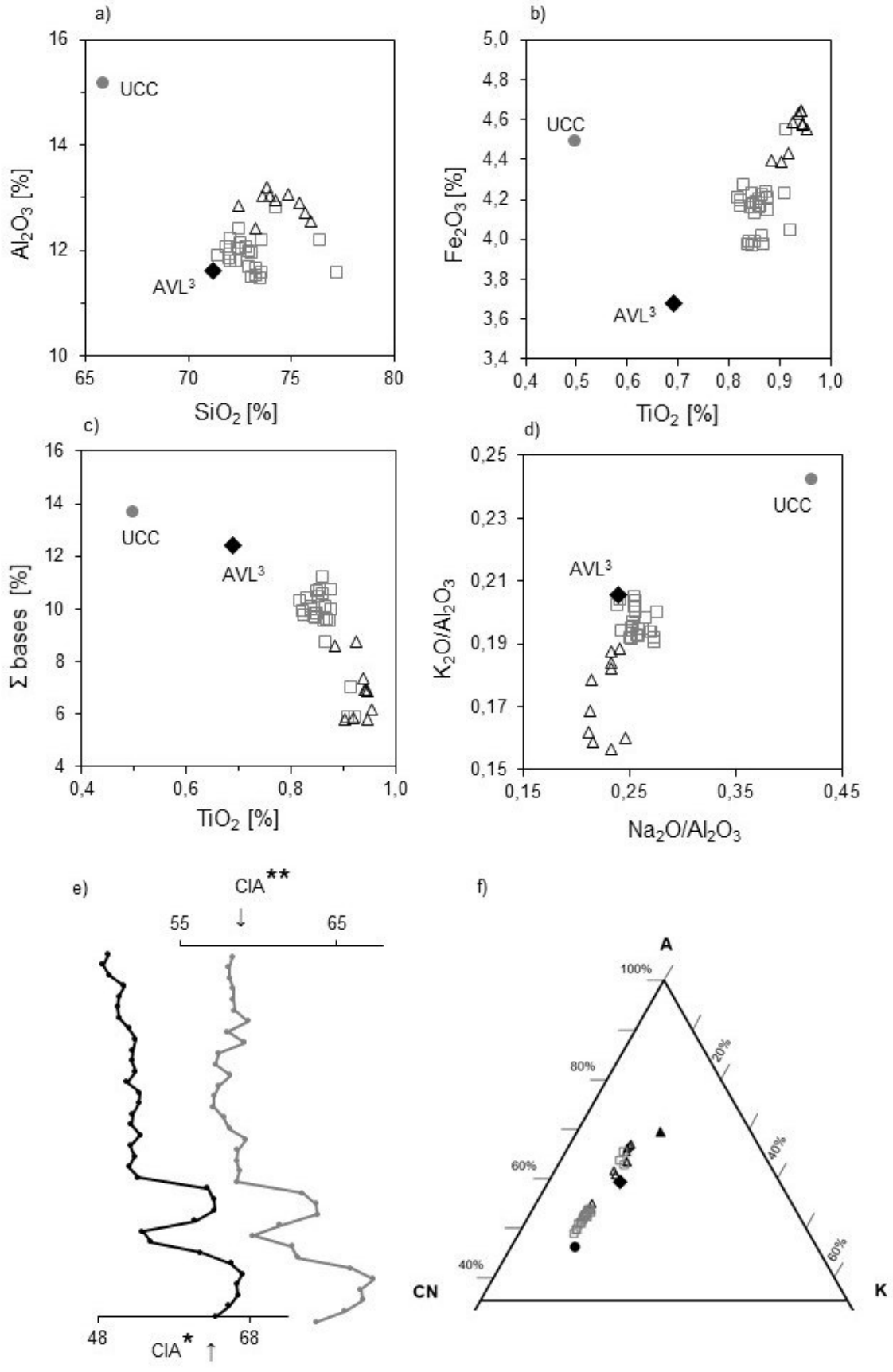
a)
UCC
AVL3
Al2O3 [%]
SiO2 [%]
b)
UCC
AVL3
Fe2O3 [%]
TiO2 [%]
c)
UCC
AVL3
Σ bases [%]
TiO2 [%]
d)
UCC
AVL3
K2O/Al2O3
Na2O/Al2O3
e)
CIA**
CIA*
f)
A
CN
K
100%
80%
60%
40%
20%
40%
60%

14 weathering indices were calculated (Table 2, Fig. 3) and compared with literature data. As most published weathering index data are predominantly based on McLennan's CaO correction, both CaO* and CaO**-based values are listed in Table 2. The comparison shows that CIA, CIW, CPA, Index B, PIA and Yang results are comparable to those of other loess studies, with the exception of Varga et al. (2011), who tend to report values associated with a higher degree of weathering. The results of Kovács (2007) clearly deviate from the Tokaj results since Red Clay is stronger weathered than paleosols and loess. AVL[3] generally shows less intense weathering but some indices are similar (CIW, WI-2), depending on the elements used for calculation.

Whereas the absolute results of the weathering indices calculated with either CaO* or CaO** differ systematically, the shape of the WI depth plots, i.e. the relative changes of weathering intensity, does not vary much (Fig. 3). Correlation is between r=0.93 (CIA-K) and r=0.98 (WI-1). Hence, for comparisons regarding relative changes in weathering intensity due to pedogenesis and climatic variations, the uncertainty introduced by different CaO corrections is negligible. For comparisons of absolute WI values, however, caution is required, as the results differ depending on the CaO correction used. To further illustrate this observation, CIA (CaO*) and CIA (CaO**) are shown in Figure 2e.

A large group of WI plots are surprisingly parallel and have correlation coefficients of well above 0.85 (CIA, CIA-K, PIA, CALMAG, Index B, Yang, Feng, Σbases/Al, Rb/Sr, Ba/Sr; Table 3). A second group of highly correlated WIs (r >0.95) with similar shape includes WI-1, WI-2 and Index A; CPA and particularly PWI are least correlated with the other indices.

4.4 Paleoclimatic data

The results of the MAP transfer functions are generally in a range of several hundred mm a^{-1} and 6-15 °C for all methods and equations (Table 4). Absolute values vary depending on the method used and the sample material. Paleosols have consistently higher MAP (Δ=100-200 mm a^{-1}) and MAT (Δ= 0.1-2 °C; Table 4). Both MAP and MAT calculated from geochemical and *X* data indicate warmer and wetter conditions during the time of paleosol formation (~45-27 ka) and colder, drier climate during dust deposition in MIS 2 (27-21 ka), including the LGM. *X*-based MAP is significantly lower than XRF-based MAP, but MAT values usually agree within error. XRF3 (Gallagher and Sheldon, 2013) is an exception and yields consistently higher MAT and MAP than all other methods and shows only little variation between loess and paleosol. Both XRF3-MAP

and XRF3-MAT seem erroneously high, especially if compared to literature data (see below), and are therefore excluded from further interpretations.

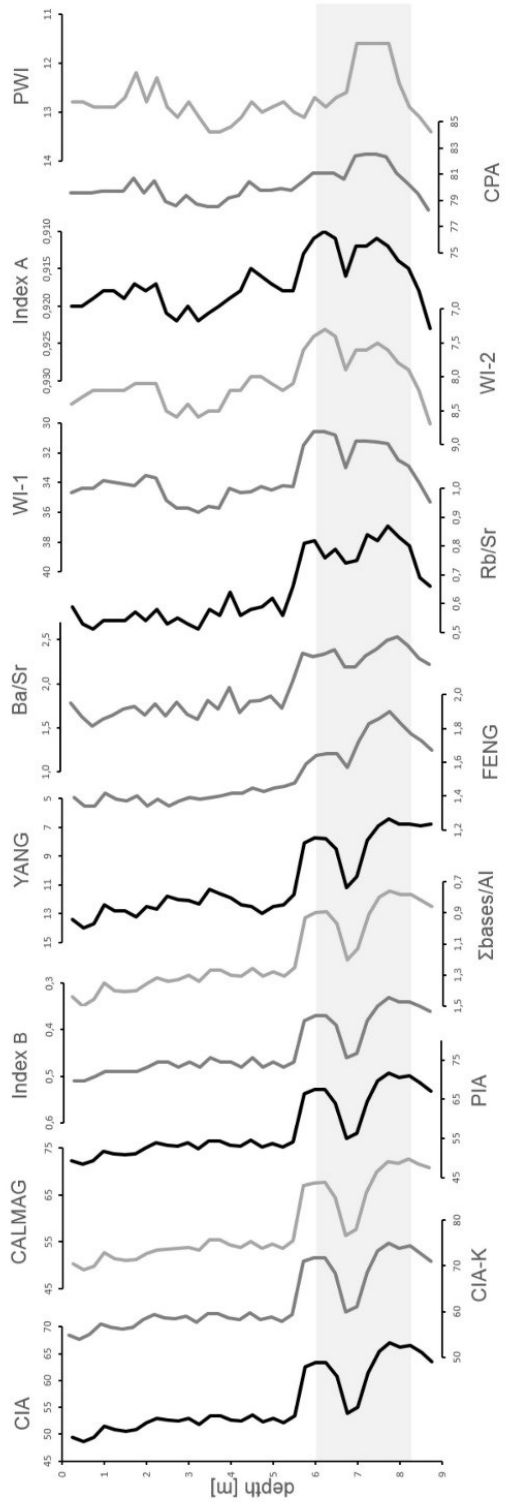

Fig. 3 (previous page): Overview of all weathering indices versus depth (for details, see Table 1). The paleosol (6-8.25 m) is indicated by a grey shade. A large group of WIs plot surprisingly parallel and are highly correlated (CIA, CIA-K, PIA, CALMAG, Index B, YANG, FENG, (Σbases/Al), Rb/Sr, Ba/Sr). A second group of highly correlated WIs with similar shape include WI-1, WI-2 and Index A; a third group consists of PWI and CPA. See Table 3 for a correlation matrix of the indices.

5. Discussion

5.1 Comparison of weathering indices, recommendations and the CaO* controversy

The majority of WIs is highly correlated (Table 3), indicating that there are equally well-suited to detect changes in the weathering intensity within the Tokaj loess-paleosol sequence. Anomalies and divergences associated with the use of K in these equations, resulting in differences between K-free and K-based indices, cannot be observed in our dataset. This might be due to the stronger weathering resistance of K-bearing minerals in low to moderately weathered samples and to the predominance of plagioclase (K-free feldspar) in the Tokaj samples, as inferred from the A-CN-K diagram. If Ca is corrected for calcite-bound Ca, as discussed above, WIs are not biased by $CaCO_3$ content and yield more reliable results, similar to Ca-free indices as FENG.

Thus, as long as any type of correction is applied, it is not necessary to use Ca-free indices. While we do acknowledge the geochemical considerations that led to the recommendations of K- and Ca-free indices, our results indicate that that these limitations might be overcautious. It is even possible that, by limiting an index to very few contributing elements such as Al and Na in the CPA, specific element concentrations, as e.g. introduced by secondary Na-salts at sites with negative water balance, are easily overemphasized and may lead to a bias in the results (Baumann et al., 2014).

Table 3 (next page): Correlation matrix of all weathering indices computed in this study (n=35). The main group of weathering indices is highly correlated (CIA, CIA-K, CALMAG, PIA, Index B, (Σbases/Al), YANG, FENG, Ba/Sr, Rb/Sr). The Si-based subgroup (WI-1, WI-2, Index A) differs slightly; CPA and PWI are least correlated with all other indices.

PWI	CPA	Index A	WI-2	WI-1	Rb/Sr	Ba/Sr	FENG	YANG	Σbases /Al	Index B	PIA	CAL-MAG	CIA-K	CIA	
-0.31	0.52	-0.62	-0.56	-0.66	0.86	0.92	0.91	-0.99	-0.99	-0.99	1.00	0.99	0.99	1.00	CIA
-0.30	0.52	-0.63	-0.61	-0.67	0.88	0.92	0.91	-0.99	-0.99	-0.99	1.00	0.99	1.00		CIA-K
-0.27	0.48	-0.58	-0.56	-0.62	0.87	0.92	0.92	-0.99	-0.99	-0.99	0.99	1.00			CAL-MAG
-0.30	0.52	-0.63	-0.60	-0.66	0.88	0.92	0.91	-0.99	-0.99	-0.99	1.00				PIA
0.31	-0.52	0.61	0.59	0.65	-0.87	-0.92	-0.92	0.99	0.99	1.00					Index B
0.33	-0.55	0.64	0.61	0.67	-0.90	-0.94	-0.94	0.99	1.00						Σbases /Al
0.30	-0.49	0.58	0.56	0.65	-0.88	-0.93	-0.92	1.00							YANG
-0.57	0.73	-0.71	-0.66	-0.73	0.93	0.94	1.00								FENG
-0.40	0.65	-0.72	-0.72	-0.76	0.97	1.00									Ba/Sr
-0.51	0.76	-0.81	-0.81	-0.85	1.00										Rb/Sr
0.63	-0.88	0.95	0.96	1.00											WI-1
0.60	-0.88	0.99	1.00												WI-2
0.63	-0.90	1.00													Index A
-0.89	1.00														CPA
1.00															PWI

Table 3 shows that the two WIs based on trace elements are highly correlated with the majority of the WIs based on main elements. The ratios Ba/Sr and Rb/Sr are frequently used in paleosol and loess weathering studies (e.g. Chen et al., 1999; Varga et al., 2011). There is, however, an ongoing debate about the reliability of trace element indices due to a lack of understanding of their weathering behavior, especially under strong weathering conditions, and the fact that they are controlled by $CaCO_3$ dynamics (Buggle et al., 2011). Furthermore, Sr and Rb contents – and consequently Rb- and Sr-based indices – are strongly grain-size dependent since these trace elements are primarily enriched in micas and clay minerals. Grain size is influenced by weathering but also by other factors such as e.g. climate, sediment source, transport etc. and can therefore not be considered as a direct or first-order weathering proxy (Újvári, 2014). In our data, Rb/Sr and Ba/Sr are highly correlated with the majority of the WIs (r=0.92-0.97) but given the discussion about trace element indices, the results should not encourage the use of these indices as reliable weathering indicators.

There are two subgroups of WIs which, although moderately to well correlated with other indices, show slightly different depth plots. WI-1, WI-2 and Index A indicate a decrease in weathering intensity between 2.5-4.0 m in the L1L1 loess layer that is not displayed by the main group of WIs. All three indices include Si as an additional element in their calculations, which might explain this minor deviation and decrease in correlation coefficients (r=0.8-0.85). PWI and, to a lesser extent, CPA are particularly weakly correlated with all other indices. Both indices point to an increase in weathering intensity between 1.75-2.25 m and seem to underestimate the weathering intensity for the upper half of the paleosol, which is significantly lower that the lower half. This might be due to the relative overemphasis of Na in the equations.

5.2 Sensitivity of weathering indices

In order to decide which WI is most sensitive to variations in the paleoweathering intensity, one approach may be to compare and correlate the WI results with a first-order, direct weathering proxy. Such a validation step has not been included in previous studies, which demonstrated and discussed various WI data without examining correlations with other weathering proxies (e.g. Buggle et al., 2011; Varga et al., 2011). Both *X* and grain size distribution are commonly applied as indicators of weathering intensity (e.g. Buggle et al., 2009; Marković et al., 2008; Terhorst et al., in press) but as discussed above, grain size is an 'integrated' index of both weathering and other factors such as climate, source distance and aridity and wind speed. Mass-specific magnetic

susceptibility (Schatz et al., 2011; see appendix) is more directly linked to weathering and will therefore be used to evaluate the WIs in this study.

Table 4: Mean annual temperature (MAT, °C) and mean annual precipitation (MAP, mm a^{-1}) for the Tokaj loess-paleosol profile, including coefficients of determination (R^2) and standard errors (S.E.) of the equations listed in Table 1. The R^2s and S.E.s are from the original publications, except those of XRF1-, XRF2- and XRF3-MAP, as well as of XRF1- and XRF2-MAT, which are from Sheldon and Tabor (2009).

Method		**R^2**	**S.E.**	**CaO**	**Loess**	**Paleosol**
geochemistry-based	XRF1-MAP	0.66	±235	CaO*	687	785
				CaO**	729	798
	XRF2-MAP	0.59	±156	CaO*	572	685
				CaO**	644	708
	XRF3-MAP	0.72	±181	CaO*	700	879
				CaO**	811	912
	XRF1-MAT	0.96	±0.6	-	8.5	8.8
	XRF2-MAT	0.37	±4.4	-	8.9	9.9
	XRF3-MAT	0.57	±2.1	CaO*	14.4	14.5
				CaO**	14.4	14.5
MS-based	*X*1-MAP	n.a.	n.a.	-	-	390
	*X*2-MAP	0.66	±11%	-	222	325
	*X*3-MAP	0.92	n.a.			258
	X-MAT	0.72	±11%	-	6.6	8.4
$\delta^{13}C$-based	$\delta^{13}C$-MAT	0.67	±1.4	-	-	8.8

Table 5 shows an overview of the correlation coefficients between the WIs and *X*. They are all moderately to well correlated with *X* (r=0.68-0.87). The FENG index is highest correlated with *X*, followed by the trace-element indices. PWI is least correlated with *X* but the correlation is too high to reject the index based on this result alone. The evaluation of the sensitivity of different WIs implies that the use of FENG is most desirable since it most accurately tracks changes in weathering intensity. This is surprising because multi-element indices (e.g. FENG) have come under suspicion due to their reliance on elements such as Na and Ca, which may bias results if secondary carbonates or Na salts are present (Baumann et al., 2014; Buggle et al., 2011). Yet for the Tokaj loess paleosol section the FENG index yields the best result. This might be due to the fact that the profile is not affected by secondary Na salt formation. For future loess paleosol studies at other locations, an individual evaluation of the WI sensitivity and the suitability of the best-performing index is recommended since weathering conditions vary through time and space.

Table 5: Correlation chart of weathering indices and mass-specific magnetic susceptibility (*X*) as a direct weathering proxy. Highest correlation coefficients are marked in bold print. FENG overall correlates best with the proxy records, PWI has the lowest correlation coefficient.

	X
CIA	0.71
CIA-K	0.70
CALMAG	0.70
PIA	0.71
Index B	0.72
(Σbases/Al)	0.75
YANG	0.75
FENG	**0.87**
Ba/Sr	**0.80**
Rb/Sr	**0.85**
WI-1	0.78
WI-2	0.70
Index A	0.72
CPA	0.79
PWI	0.68

5.3 Paleoclimatic reconstruction

5.3.1 Limitations and uncertainties of the paleoclimate transfer functions

The quantification of paleoclimate parameters from paleosols and loess is still a relatively new field, so neither has one function evolved as the most suitable one nor have there been larger discussions on quality, associated uncertainties and potential improvements.

One fundamental point that needs to be examined is the quality of the regressions used as transfer functions. Regressions, especially from large and highly diverse datasets with a variety of different soils, are certainly not perfect. One might speculate that the regression quality would improve if we use a dataset of regional and/or loess and paleosol samples only, but there are no published transfer functions specifically for SE European loess yet. The individual coefficients of determination (R^2) of the transfer functions used in this study vary and reach from rather low values (Table 4; XRF2-MAP: 0.59, XRF2-MAT: 0.37) to high or very high ones (*X*3-MAP: 0.92, XRF1-MAT: 0.96). Lower regression quality generally leads to larger uncertainties of the resulting MAP and MAT, something that has to be kept in mind when evaluating the paleoclimate estimates.

A major obstacle in these evaluations are missing or misleading information on how the regression models describe the data and their variability, as well as on associated errors. While R^2s are

always indicated (except for *X*1-MAP), a measure of uncertainty is not always given. Usually, standard errors (S.E.) are provided, either absolute or relative, but it is not always clear how they have been calculated. As pointed out by Újvári (2014), who recalculated the regression of Gallagher and Sheldon (2013), the S.E. or root mean squared error (RMSE) of the regression should not be used for estimating the errors of MAT and MAP. Instead, for an independent estimation of the uncertainties, the 95% prediction intervals have to be calculated (details and equations can be found in Újvári, 2014). We followed this approach and calculated errors of ±4.3 °C for XRF3-MAT instead of the ±2.1 °C reported in Gallagher and Sheldon (2013). This suggests that more rigorous and statistically sound error calculations have to be applied to the transfer functions and that published S.E. have to be used with cautions as they probably underestimate the uncertainties.

Despite these limitations, the transfer functions may still yield useful quantitative paleoclimate information from paleosols and loess. Due to the large errors, MAP and MAT estimates may be considered as semi-quantitative indicators only, but they nevertheless provide relative temperature and precipitation trends. The combination of transfer functions based on independent input data, such as XRF, *X* and carbon isotopes in this study, and independent paleoclimatic data from the literature, should lead to more robust and reliable paleotemperature and -precipitation estimates.

5.3.2 Mean annual temperature (MAT)

MAT during the time of paleosol formation (~45-27 ka)

For this paleosol formation interval, geochemistry-based MAT results in a temperature range of 8.8 ±0.6 °C (XRF1-MAT) to 9.9 ±4.4 °C (XRF2-MAT). *X*-MAT of 8.4 ±0.9 °C is slightly lower, but agrees within the XRF error limits (Table 4, Fig. 4a). Current MAT at the nearest weather station, Miskolc (Hungary), is 9.8 °C with a mean July temperature of 20.6 °C (1991-2000 average; World Data Center for Meteorology, 2011).

It has been proposed by various researchers that the Carpathian Basin was warmer and drier than elsewhere in Europe during MIS 3 and with patchy, mosaic-like variations in local climates, creating refugia for thermophilous species (Willis et al., 2000; Willis and van Andel, 2004; Fitzsimmons and Hambach, in press).

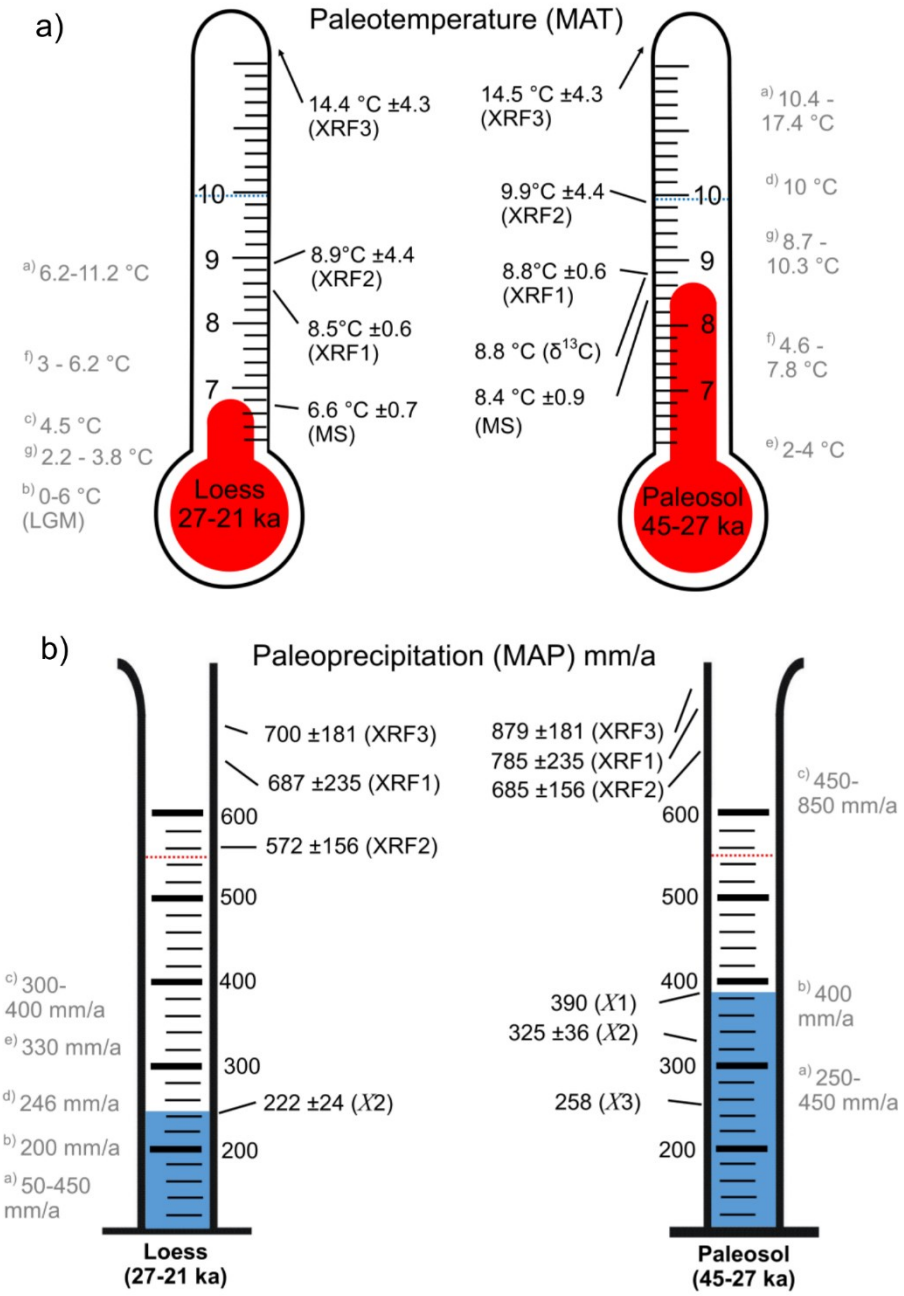

Fig. 4: a) Reconstructed MAT for loess and paleosol based on geochemical data (XRF1-MAT, XRF2-MAT, XRF3-MAT), magnetic susceptibility (*X*-MAT) and stable carbon isotopic data ($\delta^{13}C$-MAT). Grey arrows denote present MAT (9.8 °C). Selected regional temperature estimates from the literature are shown for comparison (see text for details): [a)] Kovács et al. (2012), [b)] Strandberg et al. (2011), [c)] Corcho Alvarado et al. (2011), [d)] e.g. Krolopp and Sümegi (1995), [e)] Frenzel et al. (1992), [f)] Sümegi and Hertelendi (1998), [g)] e.g. Sümegi and Krolopp (2002).
b) Reconstructed mean annual precipitation for loess and paleosol based on geochemical data (XRF1-MAP, XRF2-MAP, XRF3-MAP) and magnetic susceptibility (*X*1-MAP, *X*2-MAP, *X*3-MAP). Grey arrows denote present MAP (550 mm/a). Selected regional precipitation estimates from the literature are shown for comparison: [a)] Frenzel et al. (1992), [b)] Hatté and Guiot (2005), [c)] Kühn et al. (2013), [d)] Fitzsimmons and Hambach (2013), [e)] Strandberg et al. (2011).

Regional paleotemperature estimates for this period of time are scarce, but Kovács et al. (2012) reported MATs of 10.4–17.4 °C at several locations in the Czech Republic and Slovakia based on isotope analyses of mammoth teeth enamel. Several studies in Hungary and Serbia using the malacothermometer method (Sümegi, 1989) suggested mean July paleotemperatures of 16-19 °C and MAT similar to that of today, i.e. around 10 °C (Marković et al., 2007; Krolopp and Sümegi, 1995; Sümegi and Krolopp, 2002; Hertelendi et al., 1992). Specifically for the Tokaj hills, Sümegi and Hertelendi (1998) reported mean July summer paleotemperatures of 14-18 °C (malacothermometer), depending on topography and aspect.

Further insights may come from the $\delta^{13}C$-derived mean July paleotemperature, resulting in 18.0 ±1.4 °C, which is consistent with previous malacothermometer results. A novel approach to convert mean July paleotemperatures into MAT has recently been proposed by Hall and Penner (2013). It requires a simple linear regression calculated from modern MAT and modern mean July temperature. We used input data from the Hungarian Meteorological Survey for the nearest weather station, Debrecen (1901-2000, 10-year intervals; Hungarian Meteorological Service, 2013), and derived an empirical conversion formula following their approach ($y= 0.3507x+2.5117$; $R^2=0.42$). If applied to the present mean July temperature of 20.6 °C from Miskolc, the resulting 9.7 °C are almost identical to the measured MAT of 9.8 °C, which provides evidence for the validity of the method and encourages a tentative application to the paleotemperatures cited above. A MAT range of 9.2-9.9 °C can be derived from the Hungarian mean July malacothermometer temperatures of 19-21 °C. The proposed temperatures for Tokaj, 14-18 °C from the malacothermometer method and 18.0 °C from $\delta^{13}C$, result in a MAT of 7.4-8.8 °C or 8.8 °C.

The regional temperature estimates from the literature largely correspond to our data and converge towards a MAT of ca. 8 °C for the period of 45 to 27 ka. However, these paleotemperature estimates are consistently higher than those proposed in large-scale paleoclimatic reconstructions as e.g. in the Paleoclimatic Atlas of the Northern Hemisphere with a MAT of 2-4 °C and a mean July temperature of 14-16 °C (Frenzel et al., 1992). Contradictions between proxy data and climate models have been observed e.g. by Kageyama et al. (2006), Strandberg et al. (2011) and Mairesse et al. (2013). Among the factors discussed are e.g. a higher atmospheric and oceanic variability during the LGM, large uncertainty ranges in proxy data, a too coarse spatial resolution of model data, complex terrain and the sensitivity of regional climate to vegetation cover. Besides this deviation of model and proxy data, a higher regional MAT in the Carpathian Basin would result in a very large climatic gradient between SE and NW Europe. For this hypothetic gradient, evidence can be found in the literature: Huijzer and Vandenberghe (1998)

have proposed a MAT of -2 °C and mean July temperature of 10°C for NW Europe; a NW/SE climatic gradient was also observed by Heyman et al. (2013) in their glacier modeling data. To clarify and further explore these (apparent) contradictions, more and detailed quantitative data from different archives and proxies are required.

MAT during the time of dust deposition (27-21 ka)

For the time of dust deposition in MIS 2, geochemistry-based XRF-1-MAT and XRF2-MAT result in a temperature range of 8.5 ±0.6 °C to 8.9 ±4.4 °C. *X*-based MAT is lower with a MAT of 6.6 ±0.7 °C (Table 4, Fig. 4a). For the period of maximum cooling of the LGM (21 ka; Clark et al., 2009), regional mean annual temperatures of 2-3 °C (Kovács et al., 2012), 3.3 °C (Varsányi et al., 2011), 0.8 °C (Corcho Alvarado et al., 2011) and 1 °C (Stute and Deák, 1989) have been reported. These values are largely consistent with those from large-scale models, e.g. 0-2 °C and a mean July temperature of 8-10 °C (Frenzel et al., 1992), a MAT of 0°C (Peyron et al., 1998) or a mean July temperature of 10 °C (Kageyama et al., 2006). More recent climate modeling results show a decrease in MAT of -8 to -15 °C for Central European upland regions (Heyman et al., 2013) and global cooling of -1.9 to -9.1 °C (Strandberg et al., 2011) or -5.8 ± 1.4 °C (Schneider von Deimling et al., 2006) compared to modern MAT (9.8 °C), resulting in an absolute LGM MAT range of -5.2 to 7.9 °C. An atmospheric circulation model yields a MAT of 0-6 °C for the Carpathian Basin (Strandberg et al., 2011). While some of these estimates are consistent with our data, most of them are slightly or considerably lower than our temperatures. However, we did not specifically sample the peak LGM loess layer, nor are we certain if our samples even include loess deposited during this specific cold peak, since OSL and $pIRIR_{290}$ ages differ for the youngest loess of the section (Fig. 1b; Schatz et al., 2012). We therefore do not consider our results to be peak LGM temperatures but rather mean temperatures during dust deposition in MIS 2. Model and proxy temperature estimates for the peak LGM are accordingly considered as minimum temperatures.

Regional temperature estimates for the MIS 2 before the LGM peak have been reconstructed from oxygen isotopes in mammoth tooth enamel (Kovács et al., 2012), ranging from 6.2 °C to 11.2 °C in the Czech Republic and Slovakia. Corcho Alvarado et al. (2011) report a MAT of 4.5 °C using noble gas thermometry (NGT). Based on the malacothermometer method, Krolopp and Sümegi (1995), Hertelendi et al. (1992) and Sümegi and Krolopp (2002) propose a mean July temperature of 11-14 °C in Hungary, and generally cooler and drier temperatures compared to MIS 3. Sümegi and Hertelendi (1998) have reconstructed mean July temperatures of 12-16 °C - related to

topography and particularly aspect – for Tokaj. Using the conversion for mean July temperatures (Hall and Penner, 2013), these malacothermometer results probably correspond to a Hungarian MAT range of 6.4-7.1 °C and a Tokaj-specific MAT of 6.7-8.1 °C. Although there is singular evidence for permafrost activity in North-Central Hungary, which would require MAT to be as low as -12 to -20 °C (Kovács, 2007), the vast majority of studies conducted in the Carpathian Basin indicates that, on the contrary, the region sustained milder climatic conditions than comparable latitudes further west and might have been a possible location for the hypothesized cold stage refugia of temperate flora and fauna (Fitzsimmons and Hambach, in press; Willis et al., 2000; Willis and van Andel, 2004).

Our MATs of 6.6 ±0.7 °C (*X*), 8.5 ±0.6 °C (XRF-1) and 8.9 ±4.4 °C (XRF-2) seem to be slightly too high although they are overall comparable with the literature data, especially the *X*-based MAT. The same problem with XRF-MAT has been observed by Kühn et al. (2013) who considered the temperatures calculated for loess as too high, but the temperatures calculated from the paleosols as plausible.

5.3.3 Mean annual precipitation (MAP)

Current mean annual precipitation (MAP) of the region around Tokaj is 546 mm a^{-1} (1991-2000 average, Miskolc, World Data Center for Meteorology, 2011). Quantitative regional paleoprecipitation estimates from the literature are scarce. There seems to be an agreement on the fact that MIS 3 was wetter, while MIS 2 was dry or very dry (Fitzsimmons et al., 2012 and all malacology studies cited above).

For the paleosol (45-27 ka), our *X*-based MAP yields 258 mm a^{-1}, 325 ±36 mm a^{-1} and 390 mm a^{-1}, depending on the equation used (Table 4). XRF-based MAP results in 685 ±156 mm a^{-1} and 785 ±235 mm a^{-1} (XRF2-MAP, XRF1-MAP; Table 4, Fig. 4b). The use of XRF2-MAP is only recommended for Mollisols, but still included for comparison. Frenzel et al. (1992) suggested a MAP range of 250-450 mm a^{-1} for SE Europe during a corresponding timespan. Hatté and Guiot (2005) reported 240-360 mm a^{-1} for the paleosol-loess section at Nussloch, SW Germany, based on inverse modelling of carbon isotopic data. A range of 450-850 mm a^{-1} has been proposed by Kühn et al. (2013) for Alsheim, SW Germany, using the same XRF-based transfer functions as in this study.

For the loess layer (27-21 ka), our XRF data result in a range of 572 ±156 mm a^{-1} to 687 ±235 mm a^{-1}, while the *X*-MAP is again lower (222 ±24 mm a^{-1}; Table 4, Fig. 4b). Frenzel et al. (1992) propose a range of 50-450 mm a^{-1} for the LGM. Peyron et al. (1998) suggest a decrease of 800 mm a^{-1} compared to the modern MAP of 546 mm a^{-1}, which would result in negative values for our data. Hatté and Guiot (2005) report 220-400 mm a^{-1} for Nussloch and Kühn et al. (2013) 300-400 mm a^{-1} for Alsheim. Specifically for the LGM in upland regions, Heyman et al. (2013) propose a precipitation decrease of 25-75% compared to modern MAP. Strandberg et al.'s (2011) European circulation model returns a decrease in precipitation of about 300 mm a^{-1}, but with substantial regional variations. Fitzsimmons and Hambach (in press) suggest a decrease of about 60% for the Carpathian Basin based on a review of other studies. For both paleosol and loess samples, our *X*-MAPs are more consistent with the literature, whereas XRF1- and XRF2-MAP are probably too high. XRF2-MAP has lower values, which might still be acceptable considering the large errors associated with such calculations.

As discussed for MAT above, the paleoclimate in the Carpathian Basin was probably spatially highly diverse and differed from the surrounding regions. Large-scale models may not (yet) be able to express these heterogeneous conditions in their predicted MATs and MAPs, a fact that is also reflected in the wide range of predicted model MAPs in the literature. Consequently, the results from large-scale models for specific locations tend to differ from those obtained by local proxy reconstructions.

6. Summary and conclusions

We calculated and compared 14 WIs from loess and paleosol samples from the upper part of the Tokaj profile. The results are basically similar and show almost no variation with depth for the different WIs, leading us to the conclusion that restricting the choice of suitable weathering indices to those containing only a few elements (e.g. CPA, as proposed by Buggle et al., 2011) is probably overcautious and potentially introduces additional sources of error, mainly effects of recent weathering processes soil formation like accumulation of salts under dry climate conditions. We recommend to calculate a selection of weathering indices from different generic groups, i.e. multi-element, Ca-free, K-free, evaluate their sensitivity towards changes in weathering intensity and compare the results; if similar, it is not necessary to present more than one index in the publication.

The climate of the past in NE Hungary was described by MAT and MAP. MAT was calculated based on XRF, $\delta^{13}C$ and *X* data since errors of the transfer functions are large and more robust information can only be obtained by combining several independent methods and literature data. For the time of soil formation (45-27 ka), XRF-, *X*- and $\delta^{13}C$-based results converge to a MAT of 8-10°C, similar to, or slightly lower than today. This temperature range corresponds to the majority of the literature data for the region, but is systematically higher than proposed by large-scale climate models, which are probably not (yet) able to reflect the highly diverse paleoclimate of the Carpathian Basin. The locally reconstructed paleoclimate data may serve to refine these models. For the time of dust deposition (27-21 ka), XRF-based MAT results in a temperature range of 8-9 °C, which is probably too high, compared to other loess studies. Agreement with the literature data is best achieved with the *X*-based MAT of 6.6 °C.

For MAP we estimate a range of 685-879 mm a^{-1} for the time of paleosol formation using XRF transfer functions. *X*-based results are consistently lower (258-390 mm a^{-1}). For the time of loess deposition, both XRF- and *X*-based results are significantly lower with 572-700 mm a^{-1} vs. 222 mm a^{-1}. *X*-based MAP reconstructions are generally consistent with the literature, whereas most XRF-based results are probably too high.

Acknowledgements

This research was funded by a graduation fellowship from the state of Baden-Wuerttemberg, Germany. We acknowledge financial support by *Deutsche Forschungsgemeinschaft* and the Open Access Publishing Fund of Tübingen University. We are grateful to Gábor Újvári for valuable input and advice on critical aspects of the manuscript. We would like to thank Pál Sümegi (University of Szeged, Hungary) for his support during the field trip and an introduction to the site, as well as for comments on the manuscript, M. Zech, B. Buggle (University of Bayreuth, Germany), S. Gulyás, G.D. Páll and G. Persaits (University of Szeged) for help in the field, H. Taubald and team (University of Tübingen, Germany) for XRF measurements and the editor and the reviewers for their critical remarks, which greatly helped improving the manuscript.

Supplementary material

Table S1: XRF results (this study), as well as grain size and magnetic susceptibility data of Schatz et al. (2011) cited in this study. This table can be downloaded at http://www.clim-past-discuss.net/10/469/2014/cpd-10-469-2014.html

Fig. S1: Overview of regional paleoclimate proxy data from the literature cited in this study.


Alsheim
(Kühn et al., 2013)
Nussloch
(Hatté & Guiot, 2005)
N-Central CZ
(Corcho Alvarado et al., 2011)
CZ
CZ-SK-HU
(Kovács et al., 2012)
SK
Miskolc
Weather station
Tokaj
Gödöllő hills
(Kovács et al., 2007)
Debrecen
Weather station
D
A
H
SE Hungary
(Varsányi et al., 2011;
Stute & Deák, 1989)
Paks
(Újvári et al., 2014)
RO
SLO
Stari Slankamen
(Buggle et al., 2011)
Beremend
(Varga et al., 2011)
Surduk
(Hatté et al., 2013)
I
Irig
(Markovic et al., 2007)
HR
SRB
US Dept of State Geographer
© 2014 Google
© 2009 GeoBasis-DE/BKG
Image Landsat
Google earth
Imagery Date: 4/10/2013 lat 47.594642° lon 15.986929° elev 362 m eye alt 957.57 km

References

An, Z., Liu, T., Lu, Y., Porter, S. C., Kukla, G., Wu, X., Hua, Y., 1990: The long-term paleomonsoon variation recorded by the loess-paleosol sequence in Central China. Quaternary International 7-8, 91-95.

Baumann, F., Kühn, P., Dörfer, C., Schmidt, K., He, J.-S., Scholten, T., 2014: Pedogenesis, permafrost, substrate and topography: Plot and landscape scale interrelations of weathering processes on the central-eastern Qinghai-Tibet Plateau. Geoderma 226-227, 300-316.

Buggle, B., Hambach, U., Glaser, B., Gerasimenko, N., Marković, S., Glaser, I., Zöller, L., 2009: Stratigraphy, and spatial and temporal paleoclimatic trends in Southeastern/Eastern European loess-paleosol sequences. Quaternary International 196, 86-106.

Buggle, B., Glaser, B., Hambach, U., Gerasimenko, N., Marković, S., 2011: An evaluation of geochemical weathering indices in loess-paleosol studies. Quaternary International 240, 12-21.

Catt, J. A., 1991: Soils as indicators of quaternary climatic change in mid-latitude regions. Geoderma 51, 167-187.

Catt, J. A., Kemp, R., Felix-Henningsen, P., Scholten, T., 2000: Recent and paleo-pedogenesis as tools for modelling past and future global change. Preface. Catena 41, 1-2.

Chen, J., An, Z., Head, J., 1999: Variation of Rb/Sr Ratios in the Loess-Paleosol Sequences of Central China during the Last 130,000 Years and Their Implications for Monsoon Paleoclimatology. Quaternary Research 51, 215-219.

Clark, P. U., Dyke, A. S., Shakun, J. D., Carlson, A. E., Clark, J., Wohlfarth, B., Mitrovica, J. X., Hostetler, S. W., McCabe, A. M., 2009: The Last Glacial Maximum. Science 325, 710-714.

Corcho Alvarado, J. A., Leuenberger, M., Kipfer, R., Paces, T., Purtschert, R., 2011: Reconstruction of past climate conditions over central Europe from groundwater data. Quaternary Science Reviews 30, 3423-3429.

Cullers, R. L., 2000: The geochemistry of shales, siltstones and sandstones of Pennsylvanian–Permian age, Colorado, USA: implications for provenance and metamorphic studies. Lithos 51, 181-203.

Darmody, R. G., Thorn, C. E., Allen, C. E., 2005: Chemical weathering and boulder mantles, Kärkevagge, Swedish Lapland. Geomorphology 67, 159-170.

Evans, M. E., Heller, F., 2001: Magnetism of loess/palaeosol sequences: recent developments. Earth-Science Reviews 54, 129-144.

Fedo, C. M., Nesbitt, H. W., Young, G. M., 1995: Unraveling the effects of potassium metasomatism in sedimentary rocks and paleosols, with implications for paleoweathering conditions and provenance. Geology 23, 921-924.

Feng, Z.-D., 1997: Geochemical Characteristics of a Loess-Soil Sequence in Central Kansas. Soil Science Society of America Journal 61, 534-541.

Fitzsimmons, K. E., Marković, S. B., Hambach, U., 2012: Pleistocene environmental dynamics recorded in the loess of the middle and lower Danube basin. Quaternary Science Reviews 41, 104-118.

Fitzsimmons, K. E., Hambach, U., in press: Loess accumulation during the last glacial maximum: Evidence from Urluia, southeastern Romania. Quaternary International.

Forster, T., Heller, F., 1997: Magnetic enhancement paths in Loess sediments from Tajikistan, China and Hungary. Geophysical Research Letters 24, 17-20.

Frenzel, B., Pécsi, M., Velichko, A. A., 1992: Atlas of Paleoclimates and Paleoenvironments of the Northern Hemisphere, Late Pleistocene – Holocene. Geographical Institute, Hungarian Academy of Sciences and Gustav Fischer Verlag, Budapest, Stuttgart.

Gallagher, T. M., Sheldon, N. D., 2013: A new paleothermometer for forest paleosols and its implications for Cenozoic climate. Geology 41, 647-650.

Gallet, S., Jahn, B.-M., Torii, M., 1996: Geochemical characterization of the Luochuan loess-paleosol sequence, China, and paleoclimatic implications. Chemical Geology 133, 67-88.

Garrels, R. M., Mackenzie, F. T., 1971: Evolution of sedimentary rocks. Norton, New York.

Goldberg, K., Humayun, M., 2010: The applicability of the Chemical Index of Alteration as a paleoclimatic indicator: An example from the Permian of the Paraná Basin, Brazil. Palaeogeography, Palaeoclimatology, Palaeoecology 293, 175-183.

Gromet, L. P., Haskin, L. A., Korotev, R. L., Dymek, R. F., 1984: The “North American shale composite”: Its compilation, major and trace element characteristics. Geochimica et Cosmochimica Acta 48, 2469-2482.

Hall, S. A., Penner, W. L., 2013: Stable carbon isotopes, C3–C4 vegetation, and 12,800 years of climate change in central New Mexico, USA. Palaeogeography, Palaeoclimatology, Palaeoecology 369, 272-281.

Han, J., Lü, H., Wu, N., Guo, Z., 1996: The magnetic susceptibility of modern soils in China and its use for paleoclimate reconstruction. Studia Geophysica et Geodaetica 40, 262-275.

Harnois, L., 1988: The CIW index: A new chemical index of weathering. Sedimentary Geology 55, 319-322.

Hatté, C., Antoine, P., Fontugne, M., Rousseau, D.-D., Tisnérat-Laborde, N., Zöller, L., 1999: New chronology and organic matter δ13C paleoclimatic significance of Nußloch loess sequence (Rhine Valley, Germany). Quaternary International 62, 85-91.

Hatté, C., Guiot, J., 2005: Palaeoprecipitation reconstruction by inverse modelling using the isotopic signal of loess organic matter: application to the Nußloch loess sequence (Rhine Valley, Germany). Climate Dynamics 25, 315-327.

Hertelendi, E., Sümegi, P., Szöör, G., 1992: Geochronologic and Paleoclimatic Characterization of Quaternary Sediments in the Great Hugarian Plain. Radiocarbon 34, 833-839.

Heyman, B. M., Heyman, J., Fickert, T., Harbor, J. M. 2013: Paleo-climate of the central European uplands during the last glacial maximum based on glacier mass-balance modeling. Quaternary Research 79, 49-54.

Hungarian Meteorological Service, 2013: Climate Data Series 1901-2000. Hungarian Meteorological Service, Budapest.

Kageyama, M., Laîné, A., Abe-Ouchi, A., Braconnot, P., Cortijo, E., Crucifix, M., de Vernal, A., Guiot, J., Hewitt, C. D., Kitoh, A., Kucera, M., Marti, O., Ohgaito, R., Otto-Bliesner, B., Peltier, W. R., Rosell-Melé, A., Vettoretti, G., Weber, S. L., Yu, Y., 2006: Last Glacial Maximum temperatures over the North Atlantic, Europe and western Siberia: a comparison between PMIP models, MARGO sea–surface temperatures and pollen-based reconstructions. Quaternary Science Reviews 25, 2082-2102.

Kemp, R. A., 2001: Pedogenic modification of loess: significance for palaeoclimatic reconstructions. Earth-Science Reviews 54, 145-156.

Kovács, J., 2007: Chemical weathering intensity of the Late Cenozoic “Red Clay” deposits in the Carpathian Basin. Geochemistry International 45, 1056-1063.

Kovács, J., Moravcová, M., Újvári, G., Pintér, A. G., 2012: Reconstructing the paleoenvironment of East Central Europe in the Late Pleistocene using the oxygen and carbon isotopic signal of tooth in large mammal remains. Quaternary International 276–277, 145-154.

Krolopp, E., Sümegi, P., 1995: Palaeoecological reconstruction of the late pleistocene, based on loess malacofauna in Hungary. GeoJournal 36, 213-222.

Kronberg, B. I., Nesbitt, H. W., 1981: Quantification of weathering, soil geochemistry and soil fertility. Journal of Soil Science 32, 453-459.

Kühn, P., Techmer, A., Weidenfeller, M., 2013: Lower to middle Weichselian pedogenesis and palaeoclimate in Central Europe using combined micromorphology and geochemistry: the loess-paleosol sequence of Alsheim (Mainz Basin, Germany). Quaternary Science Reviews 75, 43-58.

Li, C., Yang, S., 2010: Is chemical index of alteration (CIA) a reliable proxy for chemical weathering in global drainage basins? American Journal of Science 310, 111-127.

Lu, H., Huissteden, K. V., An, Z., Nugteren, G., Vandenberghe, J., 1999: East Asia winter monsoon variations on a millennial time-scale before the last glacial–interglacial cycle. Journal of Quaternary Science 14, 101-110.

Maher, B. A., Thompson, R., Zhou, L. P., 1994: Spatial and temporal reconstructions of changes in the Asian palaeomonsoon: A new mineral magnetic approach. Earth and Planetary Science Letters 125, 461-471.

Maher, B. A., Thompson, R., 1995: Paleorainfall Reconstructions from Pedogenic Magnetic Susceptibility Variations in the Chinese Loess and Paleosols. Quaternary Research 44, 383-391.

Maher, B. A., Alekseev, A., Alekseeva, T., 2002: Variation of soil magnetism across the Russian steppe: its significance for use of soil magnetism as a palaeorainfall proxy. Quaternary Science Reviews 21, 1571-1576.

Maher, B. A., Alekseev, A., Alekseeva, T., 2003: Magnetic mineralogy of soils across the Russian Steppe: climatic dependence of pedogenic magnetite formation. Palaeogeography, Palaeoclimatology, Palaeoecology 201, 321-341.

Mairesse, A., Goosse, H., Mathiot, P., Wanner, H., Dubinkina, S., 2013: Investigating the consistency between proxy-based reconstructions and climate models using data assimilation: a mid-Holocene case study. Climate of the Past 9, 2741-2757.

Marbut, C. F., 1935: Atlas of American Agriculture, Part III, Soils of the United States. 8 ed., edited by: Agriculture, U. S. D. o., Advance Sheets, US Government Printing Office, Washington (D.C.).

Marković, S. B., Oches, E. A., McCoy, W. D., Frechen, M., Gaudenyi, T., 2007: Malacological and sedimentological evidence for “warm” glacial climate from the Irig loess sequence, Vojvodina, Serbia. Geochemistry, Geophysics, Geosystems 8, Q09008.

Marković, S. B., Bokhorst, M. P., Vandenberghe, J., McCoy, W. D., Oches, E. A., Hambach, U., Gaudenyi, T., Jovanović, M., Zöller, L., Stevens, T., Machalett, B., 2008: Late Pleistocene loess-palaeosol sequences in the Vojvodina region, north Serbia. Journal of Quaternary Science 23, 73-84.

Maynard, J. B., 1993: Chemistry of Modern Soils as a Guide to Interpreting Precambrian Paleosols. The Journal of Geology 100, 279-289.

McLennan, S. M., 1993: Weathering and global denudation. The Journal of Geology 101, 295-303.

Meier, H. A., Driese, S. G., Nordt, L. C., Forman, S. L., Dworkin, S. I., 2014: Interpretation of Late Quaternary climate and landscape variability based upon buried soil macro- and micromorphology, geochemistry, and stable isotopes of soil organic matter, Owl Creek, central Texas, USA. Catena 114, 157-168.

Muhs, D. R., Budahn, J. R., McGeehin, J. P., Bettis III, E. A., Skipp, G., Paces, J. B., Wheeler, E. A., 2013: Loess origin, transport, and deposition over the past 10,000 years, Wrangell-St. Elias National Park, Alaska. Aeolian Research 11, 85-99.

Nesbitt, H. W., Young, G. M., 1982: Early Proterozoic climates and plate motions inferred from major element chemistry of lutites. Nature 299, 715-717.

Nesbitt, H. W., Young, G. M., 1984: Prediction of some weathering trends of plutonic and volcanic rocks based on thermodynamic and kinetic considerations. Geochimica et Cosmochimica Acta 48, 1523-1534.

Nordt, L., von Fischer, J., Tieszen, L., 2007: Late Quaternary temperature record from buried soils of the North American Great Plains. Geology 35, 159-162.

Orgeira, M. J., Egli, R., Compagnucci, R. H., 2011: A Quantitative Model of Magnetic Enhancement in Loessic Soils. In: The Earth's Magnetic Interior. Edited by: Petrovský, E., Ivers, D., Harinarayana, T., and Herrero-Bervera, E., IAGA Special Sopron Book Series, Springer Netherlands, 361-397.

Panaiotu, C. G., Panaiotu, E. C., Grama, A., Necula, C., 2001: Paleoclimatic record from a loess-paleosol profile in southeastern Romania. Physics and Chemistry of the Earth, Part A: Solid Earth and Geodesy 26, 893-898.

Peyron, O., Guiot, J., Cheddadi, R., Tarasov, P., Reille, M., de Beaulieu, J.-L., Bottema, S., Andrieu, V., 1998: Climatic Reconstruction in Europe for 18,000 YR B.P. from Pollen Data. Quaternary Research 49, 183-196.

Pietsch, D., Kühn, P., 2012: Early Holocene paleosols at the southwestern Ramlat As-Sab'atayn desert margin: New climate proxies for southern Arabia. Palaeogeography, Palaeoclimatology, Palaeoecology 365–366, 154-165.

Pietsch, D., Kühn, P., Lisitsyn, S., Markova, A., Sinitsyn, A., 2014: Krotovinas, pedogenic processes and stratigraphic ambiguities of the Upper Palaeolithic sites Kostenki and Borshchevo (Russia). Quaternary International 324, 172-179.

Porter, S. C., 2001: Chinese loess record of monsoon climate during the last glacial–interglacial cycle. Earth-Science Reviews 54, 115-128.

Retallack, G. J., 2001: Soils of the past. Blackwell, Oxford, 600 pp.

Rudner, Z. E., Sümegi, P., 2001: Recurring Taiga forest-steppe habitats in the Carpathian Basin in the Upper Weichselian. Quaternary International 76–77, 177-189.

Schatz, A.-K., Zech, M., Buggle, B., Gulyás, S., Hambach, U., Marković, S. B., Sümegi, P., Scholten, T., 2011: The late Quaternary loess record of Tokaj, Hungary: Reconstructing palaeoenvironment, vegetation and climate using stable C and N isotopes and biomarkers. Quaternary International 240, 52-61.

Schatz, A.-K., Buylaert, J.-P., Murray, A., Stevens, T., Scholten, T., 2012: Establishing a luminescence chronology for a palaeosol-loess profile at Tokaj (Hungary): A comparison of quartz OSL and polymineral IRSL signals. Quaternary Geochronology 10, 68-74.

Schatz, A. K., Qi, Y., Siebel, W., Wu, J., Zöller, L., under review: Tracking potential source areas of Central and Southeast European loess: examples from Tokaj (HU), Nussloch (D) and Grub (AT). Central European Journal of Geosciences.

Schneider von Deimling, T., Ganopolski, A., Held, H., Rahmstorf, S., 2006: How cold was the Last Glacial Maximum? Geophysical Research Letters 33, L14709.

Sheldon, N. D., Retallack, G. J., Tanaka, S., 2002: Geochemical Climofunctions from North American Soils and Application to Paleosols across the Eocene-Oligocene Boundary in Oregon. The Journal of Geology 110, 687-696.

Sheldon, N. D., 2006: Quaternary Glacial-Interglacial Climate Cycles in Hawaii. The Journal of Geology 114, 367-376.

Sheldon, N. D., Tabor, N. J., 2009: Quantitative paleoenvironmental and paleoclimatic reconstruction using paleosols. Earth-Science Reviews 95, 1-52.

Strandberg, G., Brandefelt, J., Kjellström, E., Smith, B., 2011: High-resolution regional simulation of last glacial maximum climate in Europe. Tellus A 63, 107-125.

Stute, M., Deák, J., 1989: Environmental isotope study (14C, 13C, 18O, D, noble gases) on deep groundwater circulation systems in Hungary with reference to paleoclimate. Radiocarbon 31, 902-918.

Sümegi, P., 1989: Upper Pleistocene evolution history of the Hajdúság (Hungary) region on the basis of stratigraphical investigations. Ph.D. thesis, University of Debrecen, Hungary. Debrecen, 93 pp.

Sümegi, P., Hertelendi, E., 1998: Reconstruction of microenvironmental changes in the Kopasz Hill loess area at Tokaj (Hungary) between 15 and 70 ka BP. Radiocarbon 40, 855-863.

Sümegi, P., Rudner, Z. E., 2001: In situ charcoal fragments as remains of natural wild fires in the upper Würm of the Carpathian Basin. Quaternary International 76–77, 165-176.

Sümegi, P., Krolopp, E., 2002: Quatermalacological analyses for modeling of the Upper Weichselian palaeoenvironmental changes in the Carpathian Basin. Quaternary International 91, 53-63.

Taylor, S. R., McLennan, S. M., 1985: The continental crust: its composition and evolution. Blackwell Scientific Publications, Oxford.

Terhorst, B., Kühn, P., Damm, B., Hambach, U., Meyer-Heintze, S., Sedov, S., in press: Paleoenvironmental fluctuations as recorded in the loess-paleosol sequence of the Upper Paleolithic site Krems-Wachtberg. Quaternary International.

Újvári, G., Varga, A., Balogh-Brunstad, Z., 2008: Origin, weathering, and geochemical composition of loess in southwestern Hungary. Quaternary Research 69, 421-437.

Újvári, G., 2014: Interactive comment on “Paleoclimate and weathering of the Tokaj (NE Hungary) loess-paleosol sequence: a comparison of geochemical weathering indices and paleoclimate parameters” by A.-K. Schatz et al. Climate of the Past Discussions 10, C19-C26.

Újvári, G., Varga, A., Raucsik, B., Kovács, J., 2014: The Paks loess-paleosol sequence: A record of chemical weathering and provenance for the last 800 ka in the mid-Carpathian Basin. Quaternary International 319, 22-37.

Vancampenhout, K., Langohr, R., Slaets, J., Buurman, P., Swennen, R., Deckers, J., 2013: Paleo-pedological record of the Rocourt Pedosequence at Veldwezelt–Hezerwater (Belgian Pleistocene loess belt): Part 1 - Evolution of the parent material. Catena 107, 118-129.

Varga, A., Újvári, G., Raucsik, B., 2011: Tectonic versus climatic control on the evolution of a loess–paleosol sequence at Beremend, Hungary: an integrated approach based on paleoecological, clay mineralogical, and geochemical data. Quaternary International 240, 71-86.

Varsányi, I., Palcsu, L., Kovács, L. Ó., 2011: Groundwater flow system as an archive of palaeotemperature: Noble gas, radiocarbon, stable isotope and geochemical study in the Pannonian Basin, Hungary. Applied Geochemistry 26, 91-104.

Wedepohl, K. H., 1987: Handbook of Geochemistry. Springer, Berlin.

Willis, K. J., Rudner, E., Sümegi, P., 2000: The Full-Glacial Forests of Central and Southeastern Europe. Quaternary Research 53, 203-213.

Willis, K. J., van Andel, T. H., 2004: Trees or no trees? The environments of central and eastern Europe during the Last Glaciation. Quaternary Science Reviews 23, 2369-2387.

World Data Center for Meteorology, 2011: 9th Series World Weather Records (WWR) 1991-2000, Asheville.

Xiao, S., Liu, W., Li, A., Yang, S., Lai, Z., 2010: Pervasive autocorrelation of the chemical index of alteration in sedimentary profiles and its palaeoenvironmental implications. Sedimentology 57, 670-676.

Xiong, S., Ding, Z., Zhu, Y., Zhou, R., Lu, H., 2010: A ~6 Ma chemical weathering history, the grain size dependence of chemical weathering intensity, and its implications for provenance change of the Chinese loess–red clay deposit. Quaternary Science Reviews 29, 1911-1922.

Yang, S., Ding, F., Ding, Z., 2006: Pleistocene chemical weathering history of Asian arid and semi-arid regions recorded in loess deposits of China and Tajikistan. Geochimica et Cosmochimica Acta 70, 1695-1709.

Zech, M., Zech, R., Glaser, B., 2007: A 240,000-year stable carbon and nitrogen isotope record from a loess-like palaeosol sequence in the Tumara Valley, Northeast Siberia. Chemical Geology 242, 307-318.

Zech, M., Zech, R., Zech, W., Glaser, B., Brodowski, S., Amelung, W., 2008: Characterisation and palaeoclimate of a loess-like permafrost palaeosol sequence in NE Siberia. Geoderma 143, 281-295.

Zech, M., Andreev, A., Zech, R., Müller, S., Hambach, U., Frechen, M., Zech, W., 2010: Quaternary vegetation changes derived from a loess-like permafrost palaeosol sequence in northeast Siberia using alkane biomarker and pollen analyses. Boreas 39, 540-550.

Study 3: Tracking potential source areas of Central and Southeast European loess: examples from Tokaj (HU), Nussloch (D) and Grub (AT)

Ann-Kathrin Schatz [a], Yue Qi [b], Wolfgang Siebel [c], Jiade Wu [b], Ludwig Zöller [d]

a) Soil Science and Geomorphology Group, Department of Geosciences, Faculty of Science, University of Tübingen, Rümelinstr. 19-23, 72072 Tübingen, Germany

b) School of Earth and Space Sciences, University of Science and Technology of China, 230026 Hefei, China

c) Geochemistry Group, Department of Geosciences, Faculty of Science, University of Tübingen, Wilhelmstr. 56, 72074 Tübingen, Germany

d) Chair of Geomorphology, University of Bayreuth, Universitätsstr. 30, 95440 Bayreuth, Germany

Submitted to: Central European Journal of Geosciences (07/2014), currently under review

Abstract

There are several competing hypotheses for the origin of loess in Europe but quantitative evidence is still rare. Here, Sr-Nd isotopic and bulk elemental composition of loess from Marine Isotope Stages 2 and 3 from three study regions in Central and Southeast Europe – Nussloch (Germany), Grub (Austria) and Tokaj (Hungary) - are analyzed. This study aims at examining differences and similarities of loess deposits throughout Europe, correlating loess with potential source rocks from major mountain ranges and comparing loess with floodplain sediments from main rivers as integrated samples of the drainage areas. The results show that European loess deposits are largely uniform and that sediment sources have been rather stable in Southeast Europe and more variable in Central Europe. However, the methods used are not sufficient to unequivocally confirm and reject potential sediment sources but, in combination, help to identify the most likely sediment origins. While a direct correlation of loess and potential source rocks is difficult, the comparison with floodplain sediments is most promising and confirms previous hypotheses. Loess from Tokaj and Grub is most likely a mix of local sediments and material transported by the Danube River. Rhine River sediments are probably the main source of loess at Nussloch.

Keywords: Loess, Provenance, Sr-Nd, Geochemistry, Dust

1. Introduction

Dust is an integral part of the Earth's environment and terrestrial deposits of aeolian sediments, such as loess, are the most extensive Quaternary deposits of the surface of the Earth. Loess is recognized as an important archive of paleoclimatic and paleoenvironmental information that may be used to complement highly resolved, long-term marine records. As a primarily aeolian sediment, loess is one of the few direct proxies of paleowind direction and strength and thus constitutes an important component of detailed and comprehensive paleoclimatic studies. In order to understand and use the paleowind information contained in loess, it is, however, essential to identify the source sediments. For the extensively studied loess deposits along the two main rivers in Central and Southeast Europe - the Rhine and the Danube – Smalley and Leach's (1978) and Smalley et al.'s (2009) hypothesis of a primarily glacial, Alpine origin of loess has been widely accepted. While undoubtedly providing a valuable theoretical foundation, their assumptions are largely conceptual in nature and lack quantitative evidence. Recently, several studies have been published which employ quantitative geochemical methods to examine potential sediment source areas. Buggle et al. (2008) successfully used different major and trace elemental characterization methods to compare loess deposits from Serbia, Romania and Ukraine with floodplain sediments of Central and Southeast Europe. With the help of heavy mineral analyses, Thamó-Bozsó et al. (2014) were able to confirm earlier assumptions and identify new sources of loess in Hungary. Újvári et al. (2012) used a combination of Sr-Nd and U-Pb isotopic provenance indicators to characterize loess in the Carpathian Basin and compare with a large variety of potential source areas.

With this study, we aim to contribute to the increasing body of quantitative evidence for the origin of loess in Central and Southeast Europe. We focus on three loess sections - Nussloch (Southwest Germany), Grub (East Austria) and Tokaj (Northeast Hungary) - and combine two widely accepted methods from sedimentary provenance research. The abundances of major and trace elements, displayed as normalized diagrams of elemental variations ("spider diagrams") or ratios of selected elements, may serve as characteristic sediment 'fingerprints' and have successfully been used in the geochemical characterization of loess deposits and potential source areas (Buggle et al., 2008; Jahn et al., 2001; Muhs et al., 2013; Újvári et al., 2008; Újvári et al., 2014). Sr-Nd isotopic analyses may help identifying the parent rocks of sediments and have often served as a valuable tool for loess provenance studies in China and South America (Chen et al., 2007; Gallet et al., 1998; Smith et al., 2003; Sun, 2002, 2005; Zhang et al., 2012). With a combined elemental and isotopic approach and a large collection of literature data of potential source areas, we want to address four fundamental questions:

(i) Are loess deposits of Marine Isotope Stages (MIS) 2 and 3 homogenous, i.e. have sediment sources remained stable over time?

(ii) Are there regional similarities of loess deposits in Central and Southeast Europe, which may indicate common sediment sources and transport pathways?

(iii) Can loess be directly traced back to rocks from major and local mountain ranges and geological units (e.g. Alps, Carpathians, Bohemian Massif)?

(iv) Is loess genetically linked with floodplain and fluvial sediments of rivers in the vicinity of the deposits (e.g. Rhine, Danube, and Tisza)?

2. The Tokaj, Grub and Nussloch study sites and potential source areas of loess

The Tokaj site, located in the Northeast Carpathian Basin (Northeast Hungary; Fig. 1) at the confluence of the Bodrog and Tisza Rivers, has been intensively studied (Schatz et al., 2011; Schatz et al., 2014; Sümegi and Hertelendi, 1998; Sümegi and Rudner, 2001), including a chronostratigraphy based on optically and infrared stimulated luminescence (OSL, IRSL) ages (Schatz et al., 2012). A fundamental hypotheses on the origin of loess in the Carpathian Basin has been proposed by Smalley and Leach (1978), who classified the region around Tokaj and in the vicinity of the Tisza River as “D4 loess region”, consisting of wind-blown material from three main loess sources: (i) North European glacial debris carried through the Moravian Depression, (ii) glacial material from the Alps transported by the Danube River, and (iii) silt-sized material from weathered flysch rocks in the Carpathian Mountains. There is a general consensus in the literature on Smalley and Leach’s hypotheses. Other studies suggest a contribution of local materials such as loosely consolidated Miocene/Pliocene material in the Great Hungarian Plain ("Pannonian sands"; Smith et al., 1991) and Miocene flysch and molasse rocks (Pécsi, 1993), and a contribution of distal sediments as e.g. North African dust (Stuut et al., 2009; Varga, 2011). Recent studies, however, limit the contribution of African dust to <10 % (Újvári et al., 2012). Based on a heavy mineral study (Thamó-Bozsó et al., 2014), a mixture of fluvial sediments from the Danube and local Transdanubian rivers and local Cenozoic sandstones has been proposed. A geochemical study of Serbian loess (Buggle et al., 2008) showed a major contribution of material from the Carpathians, transported by the Tisza and smaller Danube tributaries, and sediment carried by the Danube, the Drava (metamorphic crystalline Alps) and probably also by the Inn River. This study did not find evidence for a significant contribution of Austroalpine (Eastern Alps, cover nappes) and Bohemian Massif (transported through the Moravian Depression) sediments.

A recent isotopic study (Újvári et al., 2012) proposes a mixture of Quaternary Danube sediments, Pannonian sands and local rocks (e.g. Transdanubian Range). Paleowind reconstructions for the Carpathian Basin are in line with most of these assumptions and indicate wind directions between north and northwest for the Carpathian Basin (Marković et al., 2008; Rousseau et al., 2007; Sebe et al., 2011).

The Grub-Kranawetberg site near Stillfried (Lower Austria; Fig. 1), on the banks of the Morava River and close to the Austrian-Slovakian boarder, has less extensively been studied (Antl, 2013; Zöller et al., 2013). We follow the stratigraphic framework of Zöller et al. (2013). Grub is part of the "D2 loess region" (Smalley and Leach, 1978), for which two main loess sources have been proposed: (i) glacial material from the Alps, carried by the Danube River, (ii) glacial material from northern Europe transported by the Morava River. To our knowledge, quantitative geochemical provenance studies for this region are lacking.

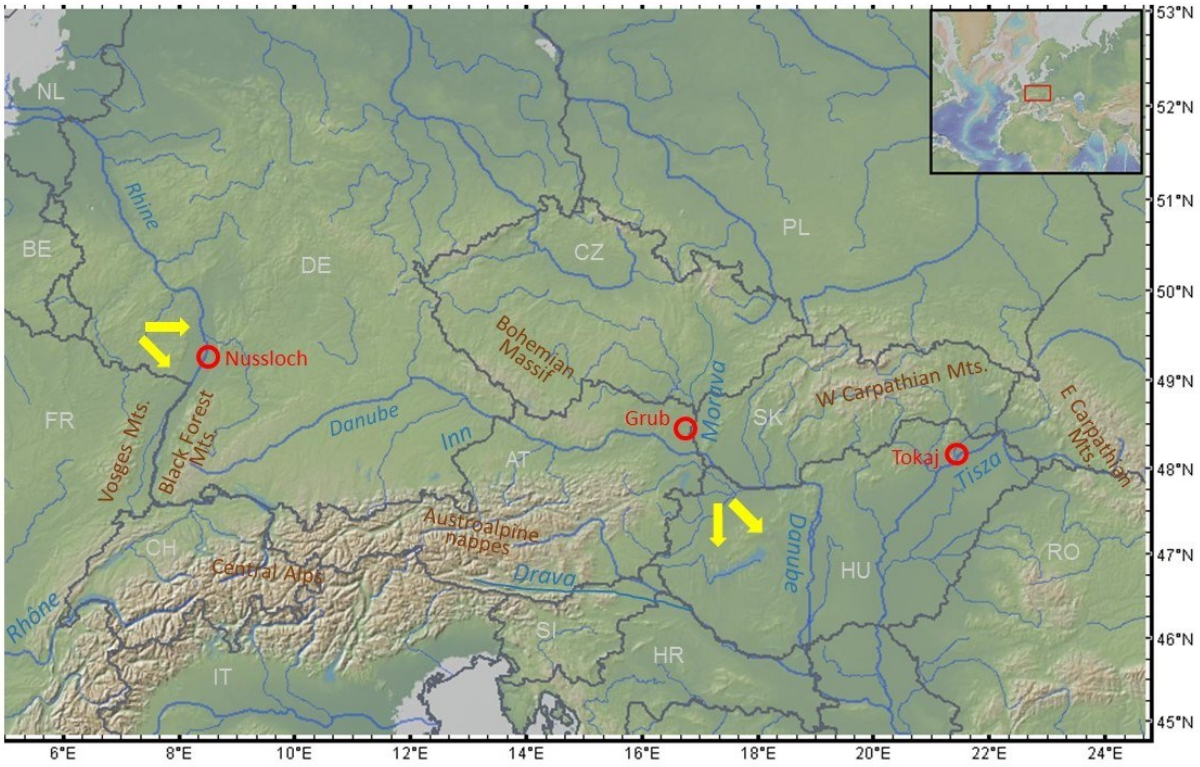

Fig. 1: Map showing the location of the study areas Nussloch, Grub and Tokaj, major mountain ranges, geological units and rivers, as well as paleowind directions (yellow arrows).

The Nussloch site, ca 10 km south of the city of Heidelberg (Germany; Fig. 1) and ca. 20 km southeast of the Neckar-Rhine confluence, is one of the most extensively studied loess sites in

the Upper Rhine Valley (e.g. Antoine et al., 2009; Gocke et al., 2010; Hatté et al., 1999; Hatté and Guiot, 2005; Moine et al., 2005; Rousseau et al., 2002). We use samples from the P4 section and follow the chronostratigraphy of Antoine et al. (2009). Nussloch is part of Smalley and Leach's "D1 loess region", which should predominantly consist of Alpine glacial material. Smalley et al. (2009) and Hill (2005) propose sediments from the Central Alps in Switzerland, transported by the Rhine River, as the main source of Tertiary and Quaternary sediments in the Upper Rhine Graben, which in turn is the most likely major source of loess along the Rhine River. Broad alluvial plains and a braided river system in the Rhine valley, transported by strong NW and W winds, have also been proposed by Antoine et al. (2009; 2001) and Zech et al. (2012) as the main source of loess at Nussloch.

3. Materials and methods

3.1 Sampling

Standard procedures were followed for sampling and sample handling during field and laboratory work. Homogenized and sieved (<2 mm) representative aliquots from 20 bulk loess and paleosol samples from Tokaj, 10 samples from Nussloch and 7 samples from Grub were used for geochemical analyses.

3.2 Bulk geochemistry

X-ray fluorescence (XRF) analyses were carried out on ball-milled subsamples. 1.5 g of dried sample powder (at 105°C) was mixed with 7,5 g MERCK spectromelt A12 (mixture of 66% Li-tetraborate and 34% Li-metaborate) and melted at 1200°C to fused beads using an Oxiflux system from CBR analytical service. Measurements were done with a Bruker AXS S4 Pioneer wavelength dispersive XRF device (Rh-tube at 4kW) and 32 standardized samples, using the traces program. Loss on ignition (LOI) was determined externally at 1000°C. The element concentrations are expressed as wt.-% or ppm and were recalculated on a volatile-free basis. Elements with missing data due to the detection limit were excluded from the analyses.

3.3 $^{87}Sr/^{86}Sr$ and $^{143}Nd/^{144}Nd$ isotope geochemistry

Analyses of the $^{87}Sr/^{86}Sr$ and $^{143}Nd/^{144}Nd$ ratios on the lithogenic fractions of the loess samples

were performed at the Key Laboratory of Crust-Mantle Materials and Environments, University of Science and Technology of China (USTC), Hefei. In order to remove organic material, impurities and carbonates (Smith et al., 2003; Újvári et al., 2012), 100 mg of sample powder were leached with 4 ml 0.5 N acetic acid (CH_3COOH) at 50 °C for 4 hours. The detrital residual was rinsed 3 times with ultrapure water, transferred into Teflon vessels and dissolved using HF and $HClO_4$ (120 °C, 3 days). The digested samples were evaporated at 130 °C and dissolved in $HClO_4$, and subsequently evaporated at 150 °C and redissolved in 6 N HCl twice to remove fluorides. In a final step the samples were redissolved in 1 ml of 3N HCl and centrifuged. Sr and light rare-earth elements were isolated on quartz columns by conventional ion exchange chromatography with a 5 ml resin bed of Bio Rad AG 50W-X12, 200-400 mesh. Nd was separated from other rare-earth elements on quartz columns using 1.7 ml Teflon powder coated with HDEHP, di(2-ethylhexyl)orthophosphoric acid, as cation exchange medium. Isotope analyses were conducted on a Finnigan MAT 262 mass spectrometer using static collection mode. Sr was loaded with a Ta-HF activator on pre-conditioned Ta filaments and was measured in double-filament mode. Nd was loaded as phosphate on pre-conditioned Re filaments and measurements were performed in a Re double filament configuration. The $^{143}Nd/^{144}Nd$ ratios are expressed as ε_{Nd}, where ε_{Nd} is the analyzed $^{143}Nd/^{144}Nd$ ratio normalized to the chondritic uniform reservoir value (CHUR, 0.512638; Jacobsen and Wasserburg, 1980). Analyses of NBS-SRM 987 and La Jolla Nd standards during this study yielded an average values of $^{87}Sr/^{86}Sr = 0.710244 \pm 15$ and $^{143}Nd/^{144}Nd = 0.511823 \pm 15$. $^{87}Sr/^{86}Sr$ ratios are normalized to $^{86}Sr/^{88}Sr = 0.1194$ and the $^{143}Nd/^{144}Nd$ ratios to $^{146}Nd/^{144}Nd = 0.7219$. Results of Nd and Sr in blank measurements are 80 pg and 65 pg, respectively. Relative errors of the samples are ≤0.0024% for Sr and ≤0.0022% for Nd.

4. Results

4.1 Bulk geochemistry

The results of the XRF measurements for the Tokaj (TO), Nussloch (NU) and Grub (GR) samples are listed in Table S1 in the appendix. The SiO_2 content of all samples is relatively low and narrow from 63.5 ± 1.2% (NU) to 74 ± 1.9 wt.-% (TO). TiO_2 is relatively high for TO (0.90 ± 0.06 wt.-%) and GR (0.89 ± 0.05 wt.-%) but much lower for NU (0.56 ± 0.02 wt.-%). Al_2O_3 and Fe_2O_3 contents of all samples show narrow ranges from 7.9 ± 0.2% (NU) to 12.5 ± 1.2 wt.-% (GR) for Al_2O_3 and 2.8 ± 0.2 wt.-% (NU) to 4.4 ± 0.5 wt.-% (GR) for Fe_2O_3. MgO is rather low and within a narrow range for all samples (TO: 1.7 ± 0.2 wt.-% - NU: 3.6 ± 0.3 wt.-%). CaO content varies widely. While percentages for TO and GR are rather low (3.0 ± 1.9 wt.-%, 5.9 ± 3.4 wt.-%, respectively), CaO of

NU is 18.3 ± 1.1 wt.-%. Na_2O (NU: 1.3 ± 0.1 wt.-% - TO: 1.8 ± 0.1 wt.-%) and K_2O (NU: 1.6 ± 0.1 wt.-% - GR: 2.3 ± 0.1 wt.-%) contents are both low and within a narrow range for all samples. Loss on ignition (LOI) varies from relatively low values for TO (5.7 ± 1.5 wt.-%) and GR (8.0 ± 2.7 wt.-%) to higher average values for NU (15.9 ± 0.8 wt.-%).

4.1.1 Major element ratios

An increase in SiO_2 content is correlated with an increase in Al_2O_3, which indicates the presence of alumosilicates containing both elements, such as feldspars and micas. This effect is most pronounced for the GR samples and least for the NU samples, which plot in the lower left corner of the Al_2O_3 vs. SiO_2 diagram (Fig. 2a). TO and GR samples overlap slightly and plot together with global average loess (GAL; Újvári et al., 2008). All samples have compositions near the upper continental crust (UCC), which represents a global average of slightly weathered crustal rocks, and are more different from highly altered sediments such as PAAS (Post-Archean Australian Shale; Taylor and McLennan, 1985). In the SiO_2 vs. TiO_2 diagram (Fig. 2b), the samples show a similar distribution as in the Al_2O_3 vs. SiO_2 diagram. Again, TO and GR samples show similar compositions, while NU samples are displaced to lower SiO_2 and Al_2O_3 values. NU samples plot close to UCC, but all samples are distinctly different from PAAS. There is no, or only a weak, linear correlation between Ti and Si for the NU and TO samples, indicating that Ti is probably present in different mineral groups such as silicates (e.g. chlorite, biotite) and oxides (e.g. rutile). This is different for the GR samples, which show a more pronounced linear trend, probably due to Ti being accommodated in a Ti-bearing mineral phase. In the K_2O vs. Al_2O_3 diagram (Fig. 2c), the TO and GR samples overlap again, while NU samples are displaced towards lower K_2O and Al_2O_3 contents. The samples show a clear linear trend, indicating that the Al abundance is mainly controlled by K-bearing minerals such as K-feldspar and phyllosilicates. In the Na_2O/Al_2O_3 vs. K_2O/Al_2O_3 diagram the samples show some overlap in composition (Fig. 2d). They are close to UCC and GAL, reflecting characteristics of depositional conditions of sedimentary rocks, whereas igneous rocks have much higher Na_2O/Al_2O_3 ratios (Garrels and Mackenzie, 1971).

Fig. 2 (next page): Diagrams of a) SiO_2 vs. Al_2O_3, b) SiO_2 vs. TiO_2, c) K_20 vs. Al_2O_3 and d) Na_2O/Al_2O_3 vs. K_2O/Al_2O_3 for loess samples from Tokaj (grey squares), Grub (grey triangles) and Nussloch (dark grey circles). For comparison, the Upper Continental Crust (UCC, black cross; Rudnick and Gao, 2003) and Post-Archean Australian Shale (PAAS, grey X; Taylor and McLennan, 1985) standards are shown, as well as Global Average Loess (GAL, grey open triangle; Újvári et al., 2008).

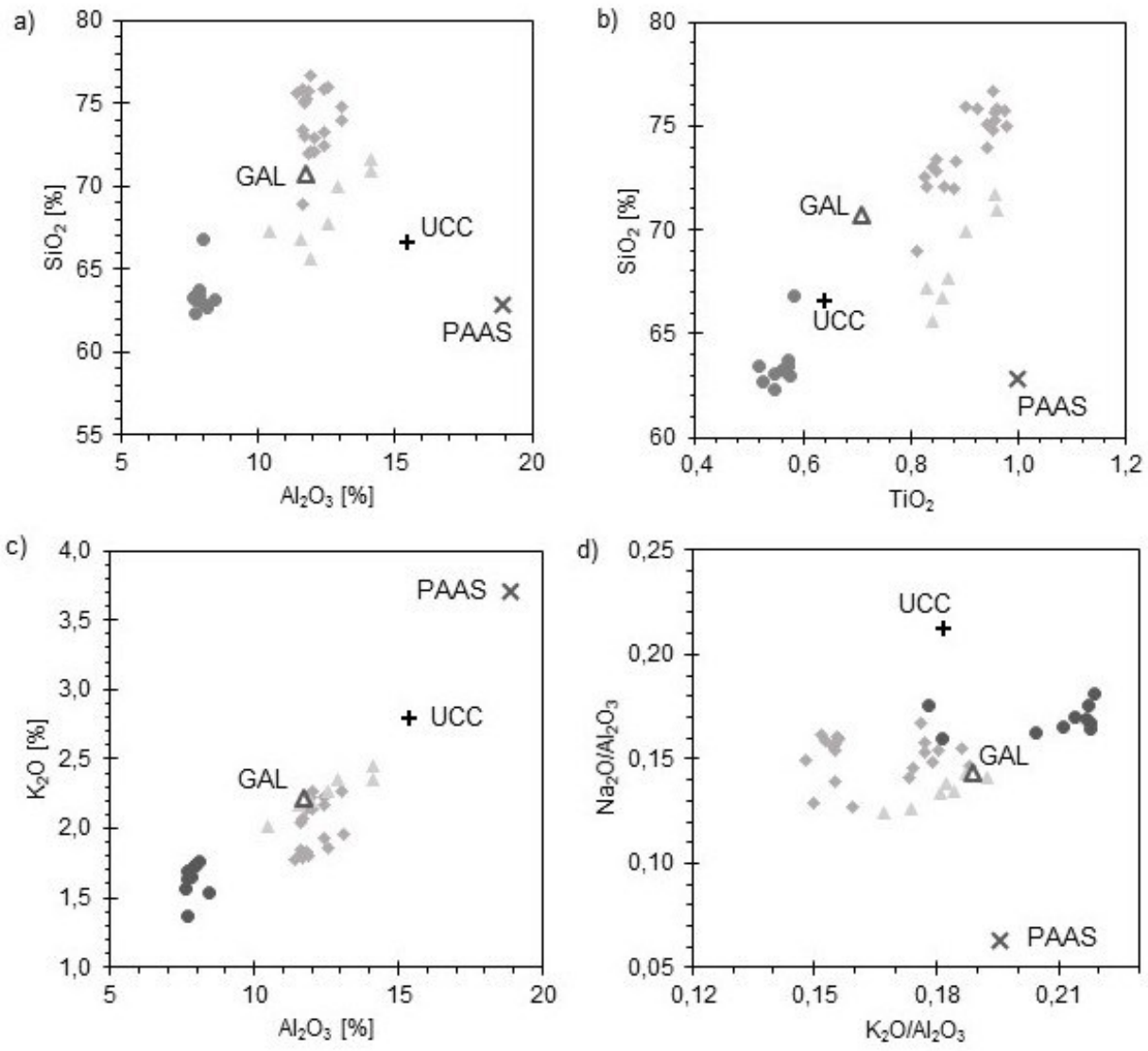

Discrimination between the three sample groups is best achieved in the SiO_2/TiO_2 vs. Al_2O_3/TiO_2 diagram (Fig. 3a). Furthermore, both Si and Al, as well as Ti, are hardly mobile in environments with pH >4. Therefore, these elements – and hence the Al_2O_3/TiO_2 vs. SiO_2/TiO_2 ratios – should not significantly be affected by weathering processes and pedogenesis. The TO, NU and GR samples plot mostly as discrete clusters. Again, the TO and GR data points are located closer together, while the NU samples plot in the upper left area due to their lower Ti content. GAL plots roughly half-way between NU and TO/GR, but all samples are distinctly different from both UCC and PAAS, probably as a consequence of weathering.

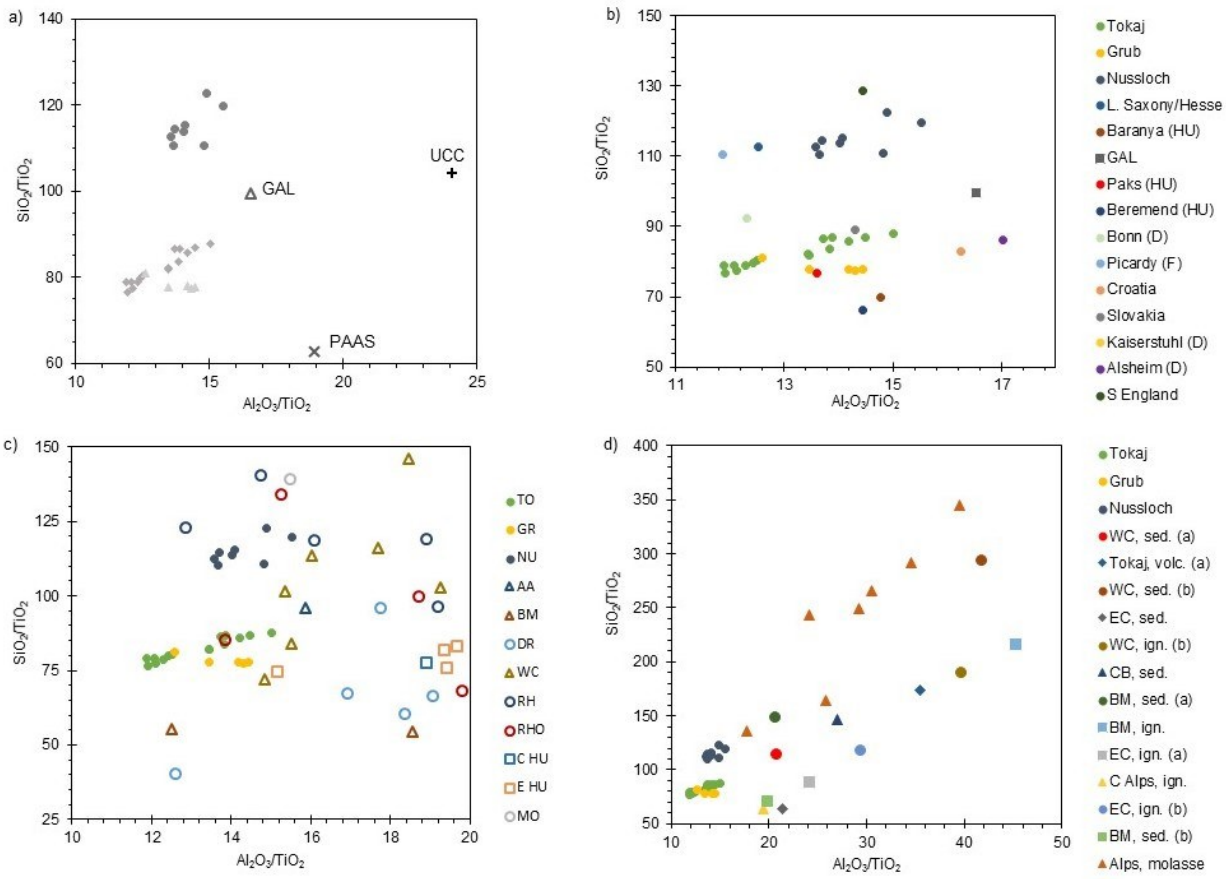

Fig. 3: SiO_2/TiO_2 vs. Al_2O_3/TiO_2 plots. a) Tokaj (grey squares), Grub (grey triangles) and Nussloch (grey circles) loess with UCC (Rudnick and Gao, 2003), PAAS (Taylor and McLennan, 1985) and GAL (Újvári et al., 2008).

b) Overview of Tokaj, Grub, Nussloch loess and loess from other localities in Europe. Data sources: Lower Saxony/Hesse (Northwest Germany; Schnetger, 1992), Baranya (Southwest Hungary; Újvári et al., 2008), GAL (Global Average Loess; Újvári et al., 2008), Paks (Central Hungary; Újvári et al., 2014), Beremend (South Hungary; Varga et al., 2011), Bonn (West Germany; Smykatz-Kloss, 2003), Picardy (North France; Smykatz-Kloss, 2003), Susak Island (West Croatia; Mikulčić Pavlaković et al., 2011), Slovakia (Nehyba et al., 2010), Kaiserstuhl (Southwest Germany; Taylor et al., 1983), Alsheim (West Germany; Kühn et al., 2013), South England (Parks and Rendell, 1992).

c) Overview of Tokaj, Grub and Nussloch loess and floodplain data (all: FOREGS data: Salminen et al., 2005; except MO: Nehyba et al., 2010) of major European drainage areas (AA: Austroalpine cover nappes area; BM: Bohemian Massif, DR: Drava, WC: Western Carpathians, RH: Rhine, RHO: Rhône, HU-M: Central Hungary, HU-E: East Hungary, MO: Morava).

d) Overview of Tokaj, Grub and Nussloch loess and rock data from major geologic units. Abbreviations: sed. - sedimentary rocks, volc. - volcanic rocks, ign. - igneous rocks, WC - West Carpathians, EC - East Carpathians, CB - local mountain ranges in the Carpathian Basin, BM - Bohemian Massif, C Alps - Central Alps. Sources: WC, sed. (a): Nehyba et al., 2010; Tokaj, volc. (a): Kiss et al., 2010; WC, sed. (b): Vďačný et al., 2013; EC, sed.: Mason et al., 1996; WC, ign. (b): Kohút and Nabelek, 2008; CB, sed.: Varga et al., 2007; BM, sed. (a): Drost et al., 2004; BM, ign.: Siebel et al., 2008; EC, ign. (a): Jurje et al., 2013; C Alps, ign.: Schaltegger et al., 2003; EC, ign. (b): Seghedi et al., 2004; BM, sed. (b): Drost et al., 2007; Alps, molasse: von Eynatten, 2003.

4.1.2 UCC-normalized spider diagrams

To minimize the effects of weathering and associated selective element depletion/enrichment, only pure loess samples are shown in the UCC-normalized element plots; paleosol samples were excluded. In these plots, the elemental concentrations of GAL are usually close to unity or slightly depleted compared to UCC, except Ca and Zr, which are enriched, and Na, which is depleted (Fig. 4a). The TO, NU and GR samples generally follow this trend, but show some distinct differences. TO samples largely follow the GAL pattern but are slightly enriched in Ti, Mn and Cr, whereas Mg and Sr are slightly and Ca strongly depleted, compared with GAL. The profile does not show much variation, except for Mg, Sr and Ca. NU samples are slightly depleted in most elements compared with GAL, except for Mg, Ca and Sr, which are enriched. Variation is generally lower than that of the other profiles. The GR profile is most similar to GAL composition, but slightly more enriched in Ti, Mn and Mg. Variation is very low except for Ca. Comparing all three profiles, the elemental compositions generally do not vary much within a profile, except for Ca and, to a lesser extent, Mg, Sr and Cr. This is probably due to the presence of secondary carbonates. Note that for the UCC-normalized compositions, Ca is expressed as total Ca (Ca_{tot}), not corrected, silicate-bound Ca*, in order to ensure comparability with GAL and the literature data. Ca_{tot} includes Ca from secondary carbonates. Therefore, the Ca/UCC ratio (as well as Mg/UCC, Sr/UCC) should be considered less diagnostic of the elemental composition of a sample or profile.

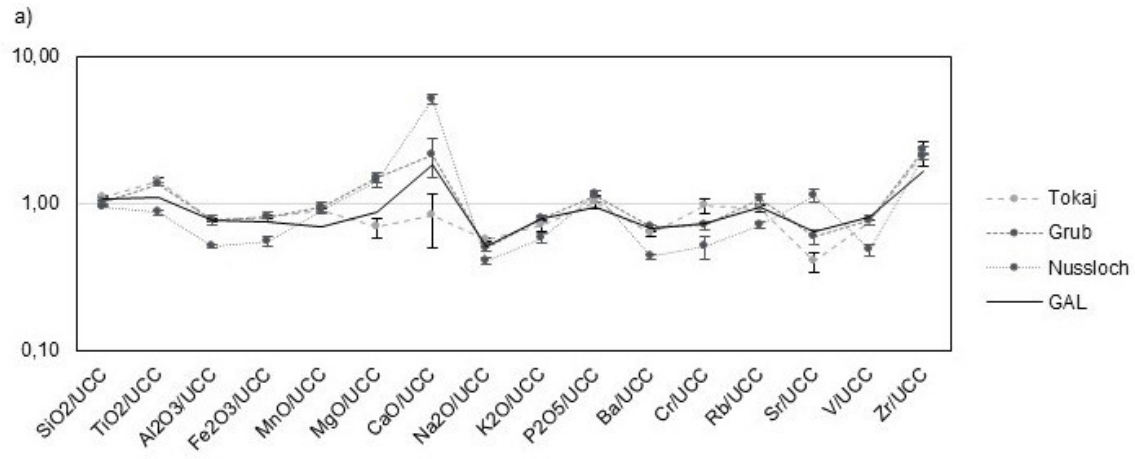

Fig. 4 (this and next page): UCC-normalized spider diagrams. For abbreviations and references, see Fig. 3. a) UCC-normalized elemental abundances (major and selected trace elements) and errors (standard deviations) of Tokaj, Grub, Nussloch and Global Average Loess. b-c) Comparison of Tokaj, Grub and Nussloch with loess from North, West, Central and Southeast Europe. d) Comparison of Tokaj and Grub with potential source rocks from SE Europe and the Alps. e) Comparison of Tokaj, Grub and Nussloch loess and Alpine potential source rocks. f-g) Tokaj, Grub and Nussloch loess and floodplain data of major European drainage areas.

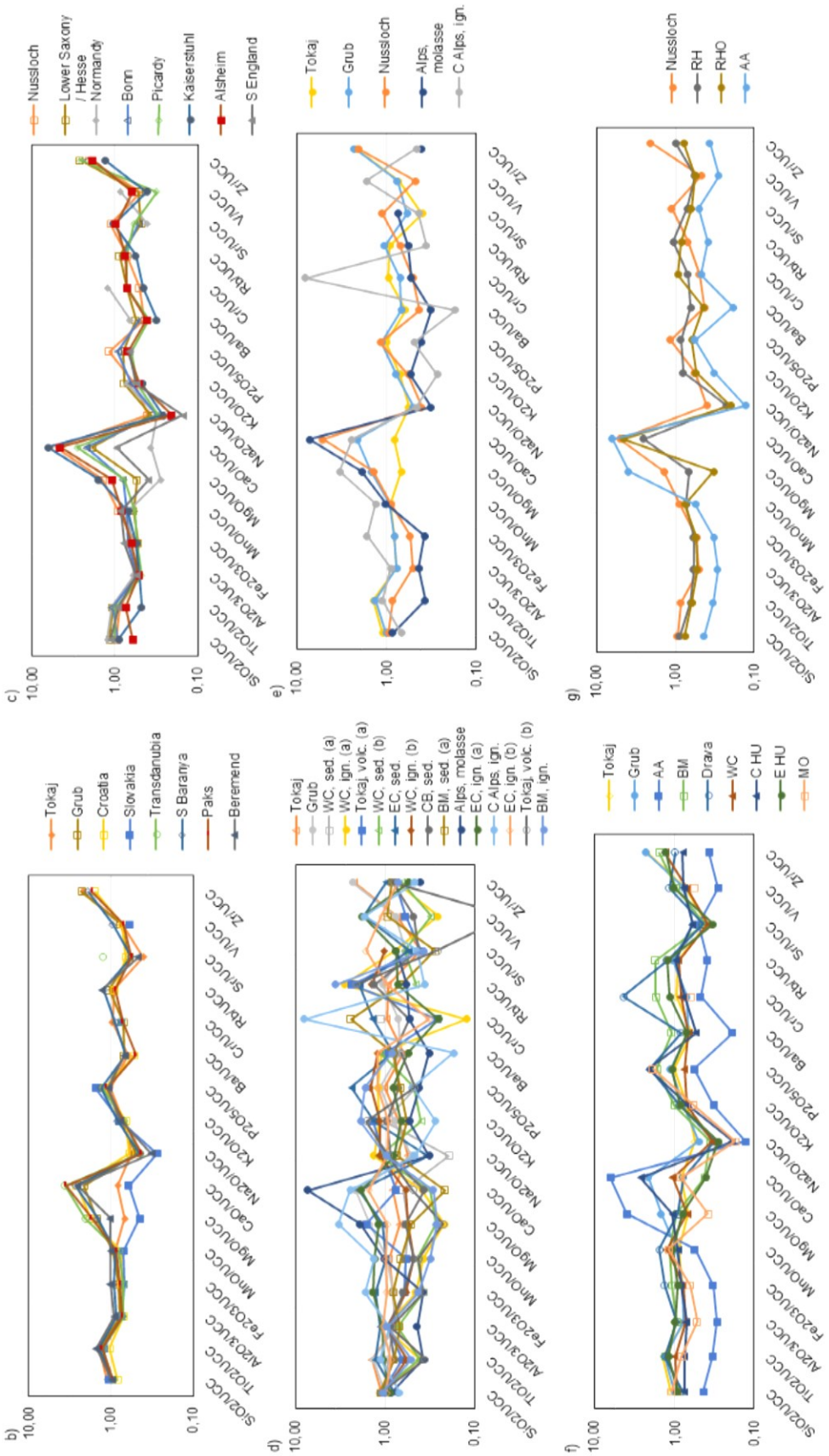
b)
c)
d)
e)
f)
g)
10,00
1,00
0,10
Tokaj
Grub
Croatia
Slovakia
Transdanubia
S Baranya
Paks
Berremend
Nussloch
Lower Saxony / Hesse
Normandy
Bonn
Picardy
Kaiserstuhl
Alsheim
S England
WC, sed. (a)
WC, ign. (a)
Tokaj, volc. (a)
WC, sed. (b)
EC, sed.
WC, ign. (b)
CB, sed.
BM, sed. (a)
Alps, molasse
EC, ign. (a)
C Alps, ign.
EC, ign. (b)
Tokaj, volc. (b)
BM, ign.
Alps, molasse
C Alps, ign.
RH
RHO
AA
BM
Drava
WC
C HU
E HU
MO

Table 1: Overview of $^{87}Sr/^{86}Sr$ and $^{143}Nd/^{144}Nd$ values and additional data. Chronostratigraphic information based on optically-stimulated and infrared-stimulated luminescence (OSL, IRSL) is according to (Zöller et al., 2013) for Grub, (Antoine et al., 2009) for Nussloch and (Schatz et al., 2012) for Tokaj. Paleosol samples are marked with an asterisk (*). Results of isotopic analyses are given with absolute and relative errors. >30 µm is the percentage of particles > 30 µm in the sample and represents grain size distribution.

Lab code	depth	OSL	IRSL	$^{87}Sr/^{86}Sr$	abs. e.	rel. e.	$^{143}Nd/^{144}Nd$	abs. e.	rel. e.	ε_{Nd}	>30 µm
	m	ka	Ka		±	%		±	%		%
Grub (Austria)											
GR 7	1.70	32	23	0.720091	13	0.0018	0.512143	7	0.0014	-9.7	n.a.
GR 6	2.40	30	28	0.719926	10	0.0014	0.512121	8	0.0015	-10.1	n.a.
GR 5	2.80	34		0.720137	15	0.0021	0.512197	5	0.0011	-8.6	n.a.
GR 4	3.10	33	30	0.720220	13	0.0018	0.512124	7	0.0014	-10.0	n.a.
GR 3	3.40	39	34	0.720063	15	0.0021	0.512116	8	0.0015	-10.2	n.a.
GR 2 *	3.70	40		0.719918	10	0.0013	0.512079	11	0.0021	-10.9	n.a.
GR 1 *	4.00	47	40	0.720138	10	0.0015	0.512073	11	0.0021	-11.0	n.a.
Nussloch, P4 section (Germany)											
NU 1	4.90		19	0.716552	13	0.0019	0.512164	8	0.0015	-9.2	n.a.
NU 2	5.60	23		0.716788	13	0.0018	0.512162	7	0.0014	-9.3	n.a.
NU 3	9.45			0.718051	12	0.0017	0.512162	8	0.0016	-9.3	n.a.
NU 4	11.10			0.718817	14	0.0020	0.512124	7	0.0013	-10.0	n.a.
NU 5	11.60			0.719320	13	0.0018	0.512110	8	0.0016	-10.3	n.a.
NU 6 *	12.90			0.718528	14	0.0020	0.512122	8	0.0015	-10.1	n.a.
NU 7 *	13.10		32	0.718888	12	0.0017	0.512119	5	0.0010	-10.1	n.a.
NU 8	15.30			0.718636	14	0.0019	0.512128	11	0.0022	-9.9	n.a.
NU 9	16.00			0.718916	17	0.0024	0.512095	6	0.0013	-10.6	n.a.
NU 10	17.00	< 54	< 57	0.719114	12	0.0017	0.512123	9	0.0017	-10.0	n.a.
Tokaj, Patkó quarry (Hungary)											
TO 20	0.75	21	25	0.719018	11	0.0015	0.512146	9	0.0018	-9.6	54.6
TO 19	1.5			0.718918	15	0.0021	0.512135	8	0.0015	-9.8	51.7
TO 18	2.25			0.719354	15	0.0021	0.512130	10	0.0019	-9.9	60.3
TO 17	3.00	27	28	0.718424	14	0.0019	0.512144	7	0.0014	-9.6	63.4
TO 16	3.75	31	26	0.718235	15	0.0021	0.512140	8	0.0015	-9.7	59.0
TO 15	4.50			0.719058	14	0.0019	0.512156	5	0.0011	-9.4	59.8
TO 14	5.25	27	28	0.718985	15	0.0020	0.512151	8	0.0015	-9.5	57.2
TO 13 *	6.00	27	30	0.719584	14	0.0019	0.512136	7	0.0014	-9.8	46.5
TO 12 *	6.75			0.718925	10	0.0014	0.512145	7	0.0014	-9.6	44.6
TO 11*	7.5	39	39	0.718860	14	0.0019	0.512117	11	0.0021	-10.2	36.9
TO 10 *	8.25			0.718396	14	0.0019	0.512145	7	0.0014	-9.6	40.2
TO 9	9.00			0.718194	12	0.0017	0.512104	9	0.0017	-10.4	48.3
TO 8	9.75			0.718663	14	0.0020	0.512131	6	0.0011	-9.9	48.9
TO 7	10.50	53	47	0.718754	14	0.0019	0.512	9	0.0017	-10.9	47.8
TO 6	11.25			0.718292	14	0.0019	0.512	8	0.0016	-10.1	46.5
TO 5	12.00			0.718304	12	0.0017	0.512	6	0.0012	-10.2	51.8
TO 4	12.75	57	52	0.718424	12	0.0017	0.512	6	0.0011	-10.2	47.8
TO 3	13.50	62	57	0.718351	13	0.0018	0.512	8	0.0015	-10.2	47.0
TO 2	14.25			0.719393	9	0.0013	0.512	8	0.0015	-10.7	44.6
TO 1 *	15.00			0.720358	11	0.0016	0.512	8	0.0016	-10.5	39.3

4.2 $^{87}Sr/^{86}Sr$ and $^{143}Nd/^{144}Nd$ isotope analyses

4.2.1 Grain-size dependence of $^{87}Sr/^{86}Sr$ and $^{143}Nd/^{144}Nd$ ratios and leaching experiments

Several studies have shown that strontium isotope ratios in aeolian sediments are grain-size dependent and increase with decreasing grain size, since more radiogenic Sr is present in the fine fraction (Feng et al., 2009). This coupling between grain size and $^{87}Sr/^{86}Sr$ ratio is usually not observed for $^{143}Nd/^{144}Nd$. The authors conclude that isotopic compositions should be measured on specific grain size fractions of the samples instead of using bulk material (Chen et al., 2007; Feng et al., 2009; Újvári et al., 2012). However, there is some debate on this topic and other authors have argued that it is only the bulk fraction that contains the entire source area information of a sample (Jahn et al., 2001; Smith et al., 2003; Zhang et al., 2012). For Tokaj, grain size data are available that were obtained from the same samples used for isotopic measurements (Schatz et al., 2011; Table 1). These data support that $^{143}Nd/^{144}Nd$ and grain size are only weakly correlated (R^2=0.234). The correlation between grain size and $^{87}Sr/^{86}Sr$ ratios is one order of magnitude lower, resulting in an R^2 of 0.038. Therefore, in this study, we present bulk $^{87}Sr/^{86}Sr$ and $^{143}Nd/^{144}Nd$ ratios since the correlation between grain size and isotopic ratios is weak to non-existent – at least for Tokaj - and therefore negligible.

The decision for a leaching pre-treatment of the isotopic samples and the choice of the leaching procedure may significantly influence the results of $^{87}Sr/^{86}Sr$ and $^{143}Nd/^{144}Nd$ measurements. We conducted an experiment with three samples (TO8, NU6, GR4). All of them were measured unleached and leached (4 ml 0.5 N acetic acid, 50 °C, 4 h). The results are shown in Fig. 5 and Table 2. For $^{143}Nd/^{144}Nd$ ratios, the difference between the leached and unleached samples ranges from 0.0015% to 0.0034%, which is within or slightly above the relative error from the measurement (0.0011-0.0018%). For $^{87}Sr/^{86}Sr$, the difference is 2 orders of magnitude higher (0.21%-0.79%) than the relative error from the measurement (0.0018-0.0020%). These results indicate that isotopic signatures depend at least partly on the respective leaching method used. Caution is required when comparing results obtained from samples with different pretreatments and careful documentation is needed when such results are reported.

Table 2 (next page): Results of the leaching experiment. 3 samples were used, one from each location. Results of isotopic analyses are given with absolute and relative errors. The difference between the leached and unleached sample is expressed as Δ (%).

Lab code	treatment	$^{87}Sr/^{86}Sr$	abs. e. ±	rel. e. %	Δ %	$^{143}Nd/^{144}Nd$ ±	abs. e. %	rel. e.	ε_{Nd}	Δ %
TO 8	unleached	0.716586	13	0.0018	0.21	0.512097	8	0.0016	-10.6	0.0034
	leached	0.718663	14	0.0020		0.512131	6	0.0011	-9.9	
NU 6	unleached	0.710606	14	0.0019	0.79	0.512127	6	0.0012	-10.0	0.0005
	leached	0.718528	14	0.0020		0.512122	8	0.0015	-10.1	
GR 4	unleached	0.716142	14	0.0020	0.41	0.512102	10	0.0018	-10.5	0.0022
	leached	0.720220	13	0.0018		0.512124	7	0.0014	-10.0	

4.2.2 $^{87}Sr/^{86}Sr$ and $^{143}Nd/^{144}Nd$ isotopic compositions

Strontium and neodymium isotopic compositions of the three localities are fairly uniform and do not vary much with depth (Table 1, Fig. 5, Fig. 6). For the majority of the samples from all three localities, ε_{Nd} values range from -9.25 to -11, with the exception of one GR outlier (GR5) which has an ε_{Nd} value of -8.6. Sr ratios are more variable but generally fall in a typical range of the weathering products of old continental crust. The majority of the samples overlap in an $^{87}Sr/^{86}Sr$ range of 0.718 to 0.7195. GR samples have slightly more radiogenic (i.e. higher) $^{87}Sr/^{86}Sr$ ratios (0.720), while 3 samples from the upper part of the Nussloch profile have clearly less radiogenic $^{87}Sr/^{86}Sr$ ratios for 3 samples from the upper part of the profile (0.716-0.718).

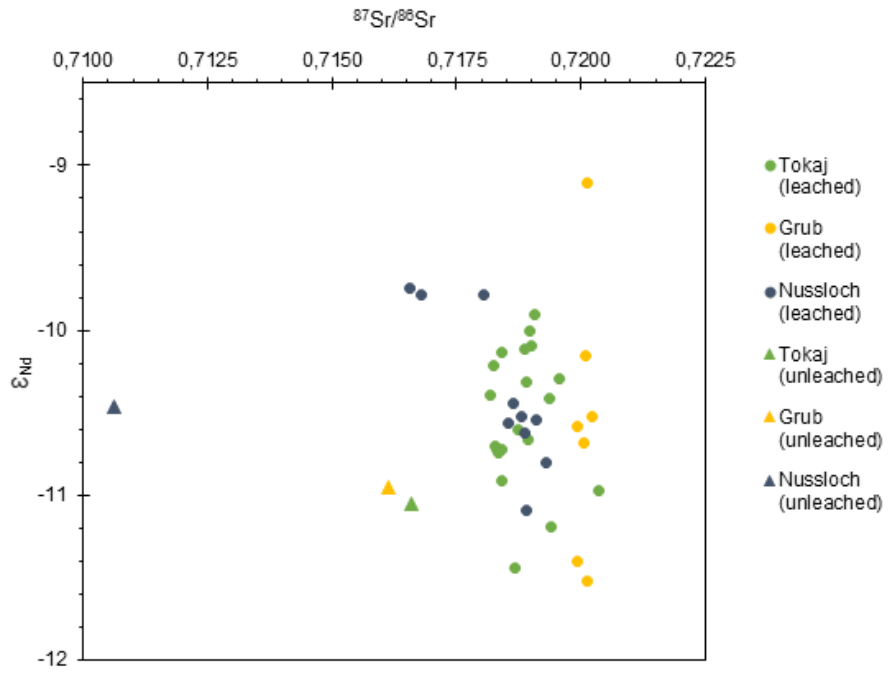

Fig. 5: $^{87}Sr/^{86}Sr$ vs. ε_{Nd} diagram of leached (circles) and unleached (triangles) Tokaj, Grub and Nussloch loess samples.

The $^{87}Sr/^{86}Sr$ ratios of 20 bulk loess and paleosol samples from Tokaj range from 0.7188 and 0.7203 and ε_{Nd} ratios range from -9.4 to -10.9. ε_{Nd} values are rather stable throughout the profile, with a possible weak trend to less radiogenic values with depth. The $^{87}Sr/^{86}Sr$ ratios show some variation in the upper part of the profile, but are generally constant. However, there is a pronounced shift towards more radiogenic ratios for the lowermost samples, which, however, is not manifested in the ε_{Nd} data. $^{87}Sr/^{86}Sr$ ratios of the Nussloch samples (n=10) range from 0.7166 to 0.7193 and Nd ratios from -9.2 to -10.6. ε_{Nd} values show a possible weak trend to less radiogenic values with depth, while there is a clear trend to more radiogenic Sr values with depth. For the Grub samples (n=7), $^{87}Sr/^{86}Sr$ ratios range from 0.7199 to 0.7202 and ε_{Nd} from -8.6 to -11. Sr ratios are very homogeneous with depth, but there is a weak trend to less radiogenic ε_{Nd} values with depth. One sample (GR5) has an exceptionally high ε_{Nd} value of -8.6. This strong deviation is not repeated in the Sr ratios and might be an outlier.

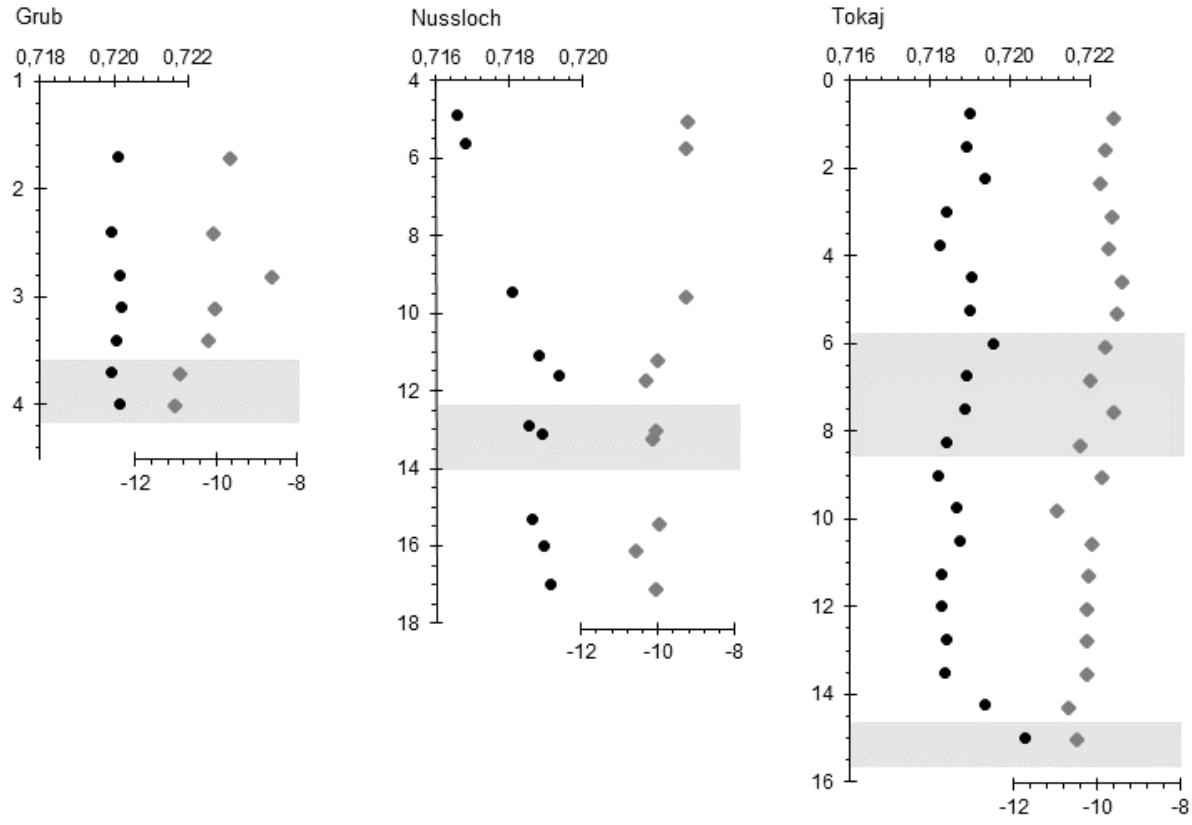

Fig. 6: $^{87}Sr/^{86}Sr$ and ε_{Nd} vs. depth (in meters) plots of the Tokaj, Nussloch and Grub profiles. Paleosols are indicated as grey shaded areas. Symbol size exceeds bars for analytical errors in all cases.

5. Discussion

5.1 Limitations of the methods used

Before discussing potential sediment sources, the main limitations and constraints of the Sr-Nd isotopic and element fingerprinting methods should be considered. First, processes such as weathering and pedogenesis, secondary carbonate formation and sorting via transport in air and water may alter both the isotopic signature and the element composition. These biasing effects can be controlled to some extent by limiting the samples to a similarly weathered selection (e.g. by excluding paleosol samples) and constraining the age range, as well as by removing secondary carbonates. Sorting effects, however, cannot be controlled for. In our study we used samples from MIS 2 and 3 (ca. 60-20 ka) and either excluded or paid special attention to possible biases introduced by paleosol samples. Samples were leached to remove secondary carbonates for isotopic measurements and ensure comparability with literature data. This was not the case for XRF analytical results that are usually reported as total CaO. Second, the signatures of multiple sources and/or the contribution of minor sediment sources will be obscured by mixing. This fact has been discussed previously (Buggle et al., 2008; Újvári et al., 2012) and is one of the main limitations of all fingerprinting methods. A third limitation is the fact that Danube loess contains a mixture of both detrital silicatic material and detrital carbonates, mainly dolomite (Újvári et al., 2012). Carbonates have low $^{87}Sr/^{86}Sr$ values and 'dilute' the isotopic signal, hence is it difficult to compare loess isotopic signatures with those of crystalline silicatic source rocks. While this is a major shortcoming for $^{87}Sr/^{86}Sr$, $^{143}Nd/^{144}Nd$ signatures will be less affected by a potential carbonate contribution. Fourth, fingerprinting requires that the composition of the possible source areas is both sufficiently well known and distinctive. While abundant XRF and isotopic data of possible source areas is available, the second criterion probably cannot always be fulfilled. If the geochemical characteristics of all potential source areas are not known and/or distinguishable from each other, certain sources can only be ruled out, but not confirmed. This has been discussed before (Újvári et al., 2012) for similarities between Greenland dust and Southeast European loess. While limiting the validity of the fingerprinting results, fingerprinting methods still provide valuable information by excluding potential source areas and uncovering similarities and differences of sediments and potential sources. Last, it is worth keeping in mind that some conflicting results in element and isotopic compositions from the literature may be attributed to different analytical methods or different measurement conditions.

5.2 Within-profile variation

All three profiles do not show much variation in $^{87}Sr/^{86}Sr$ and ε_{Nd} values with depth (Fig. 6, Fig. 5, Table 1). No systematic effects of paleosol formation and associated higher clay content containing more radiogenic Sr, such as shifts, peaks etc., on the composition of both isotopic systems can be observed. The Tokaj samples have the lowest internal variability for both $^{87}Sr/^{86}Sr$ and ε_{Nd}. Nussloch has a narrow range of ε_{Nd} and a wider $^{87}Sr/^{86}Sr$ range. Grub has constant $^{87}Sr/^{86}Sr$ values but a wider ε_{Nd} range, including one potential outlier. There is no evidence for a clear shift or trend in sediment isotopic composition in both isotopic systems at the same time. This is further supported by very low correlation coefficients between $^{87}Sr/^{86}Sr$ and ε_{Nd} for Tokaj (r^2=0.01) and Grub (r^2=0.11). An identifiable change of sediment source would ideally be characterized by a synchronous, inversely correlated shift in both isotopic signals. The Nussloch Sr-Nd correlation coefficient is higher (r^2=0.74), which might indicate an actual shift of the sediment source over time, albeit not pronounced. Due to the biasing influence of grain size and secondary carbonates on the $^{87}Sr/^{86}Sr$ composition, it has been argued that $^{143}Nd/^{144}Nd$ is a more reliable provenance indicator (Rao et al., 2006). Based on ε_{Nd} alone, our results indicate a stable sediment source for Tokaj from ca. 60-20 ka and strong sediment homogeneity within the profile. For Grub, a possible weak and gradual shift towards a less radiogenic sediment source from 50-30 ka can be observed. For Nussloch, the results indicate a small shift of about 1 ε_{Nd} unit in the upper part of the profile, at some time between ca. 20 and 30 ka.

5.3 Uniformity of Central and Southeast European loess and dust

In an overview of global loess and dust Sr-Nd isotopic signatures (Fig. 7) , the Tokaj, Grub and Nussloch samples have a distinct composition when compared to loess from other regions of the world such as Argentina, the U.S. and Alaska, Central Asia, China and Ukraine. $^{87}Sr/^{86}Sr$ vs. ε_{Nd} diagrams (DePaolo, 1988) are commonly used in petrological studies to identify the sources of igneous rocks. Samples derived from the depleted mantle of the Earth plot in the upper left quarter, whereas those derived from crustal material plot in the lower right quarter. Our samples cluster in the lower half of a mixing hyperbola defined by Svensson et al. (2000), close to, or overlapping with, several recent and last glacial maximum (LGM) Greenland dust samples, which indicates a common source or a genetic link between these sediments. The implications of this observation have been discussed previously for Southeast European loess (Újvári et al., 2012).

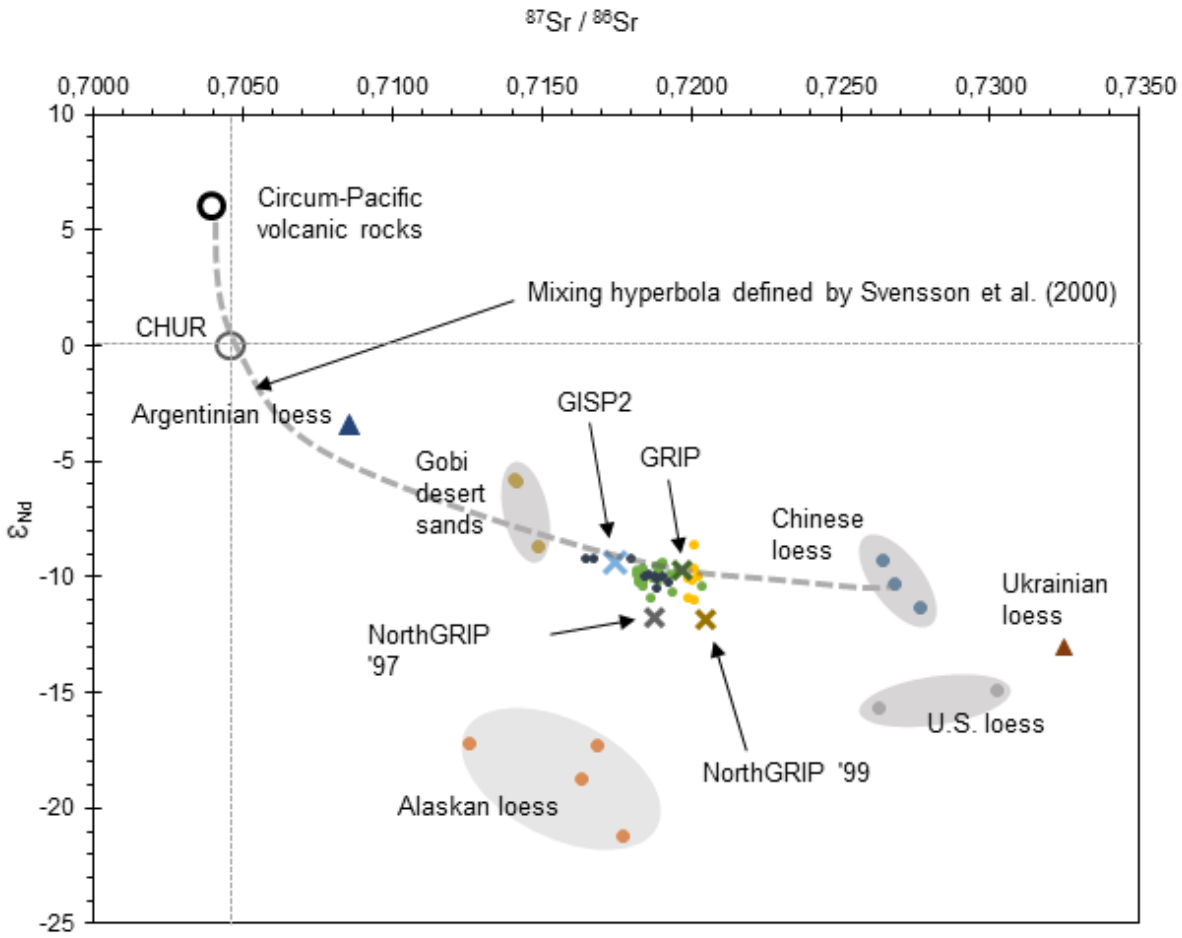

Fig. 7: Comparison of the Tokaj, Grub and Nussloch loess samples and selected global loess and dust data. GRIP is Greenland dust, references are given in Fig. 8. Sources: Argentinian loess data: Smith et al. (2003), Circum-Pacific average volcanic rock data: Svensson et al. (2000), US, China, Gobi and Ukraine data: Biscaye et al. (1997). CHUR is the chondritic uniform reservoir (Jacobsen and Wasserburg, 1980), indicated by a vertical and horizontal grey line.

Zooming into the region of weathered crustal rocks (Fig. 8) and our loss data, it is obvious that the majority of the Tokaj, Nussloch and Grub samples are isotopically very similar and has probably been derived from the same source or from several sources with roughly identical isotopic properties. Minor exceptions are the Grub outlier and the three youngest Nussloch samples which have unusually high ε_{Nd} values. Similarities, especially in ε_{Nd} values also exist between the analyzed samples and spatially close loess deposits in Southwest and Central Hungary and Croatia, and loess from France. However, the isotopic signatures of more distant loess from Morocco and Tunisia, from Spitsbergen, and of Mediterranean Sea sediments are similar as well. In contrast, Belgian loess plots further away from the Nussloch and the French loess samples,

towards Ukrainian loess. The same is true for loess from the Western UK (Scilly Islands) and the Canary Islands.

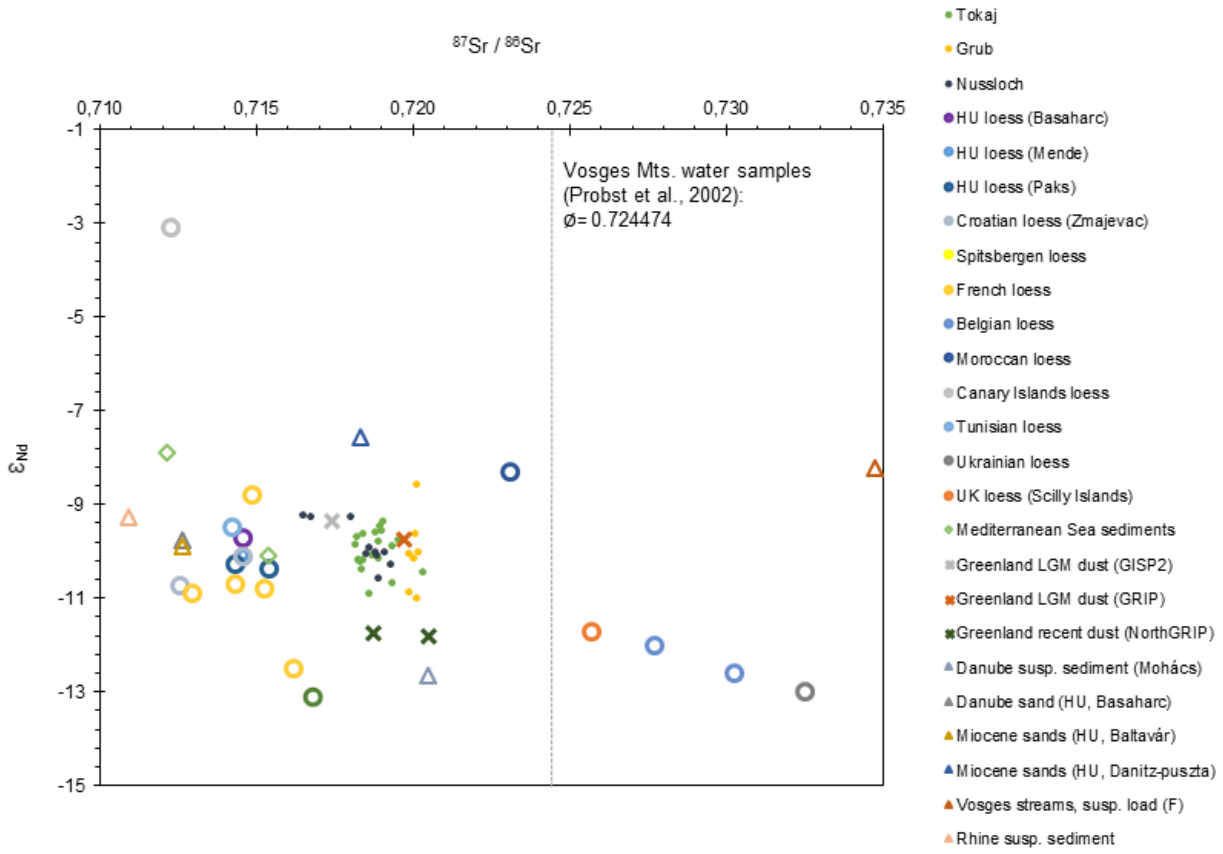

Fig. 8: Comparison of Tokaj, Grub and Nussloch loess, loess samples from various locations in Europe, Greenland dust, suspended and floodplain sediments of the Danube and Rhine Rivers and rivers in the Vosges Mts. and Miocene sands from Hungary (Pannonian Sands). Data sources: Basaharc, Mende, Paks and Zmajevac loess, Mohács and Basaharc fluvial sediments, Miocene sands (Újvári et al., 2012), Spitsbergen, French and Belgian loess (Gallet et al., 1998), Moroccan, Canary Island and Tunisian loess and Mediterranean Sea sediments (Grousset et al., 1992), Ukrainian loess and GRIP Greenland dust (Svensson et al., 2000), Scilly Islands (UK) loess (Gallet et al., 1998), GISP2 Greenland dust (Biscaye et al., 1997), NorthGRIP Greenland dust (Bory et al., 2002), fluvial sediments of the Rhine River and streams in the Vosges Mts. (Tricca et al., 1999).

Additional information of similarities and differences is provided by comparing the major and trace element spider diagrams and element ratio plots. In both the UCC-normalized spider diagrams (Fig. 4b) and the Al_2O_3/TiO_2 vs. SiO_2/TiO_2 plot (Fig. 3b), Tokaj and Grub samples show similar patterns, close to GAL, whereas samples from Nussloch reveal a different composition. Compared with geographically close loess data from Southeast Europe, all samples exhibit identical patterns in the spider diagrams, except for Mg, Ca and Sr. The latter three elements were probably

influenced by the presence of secondary carbonates and are therefore not indicative of potentially different sediment sources. A similar relationship is found in the Al_2O_3/TiO_2 vs. SiO_2/TiO_2 plot (Fig. 3b), where Tokaj and Grub samples plot close to Croatian loess (Susak Island; Mikulčić Pavlaković et al., 2011), Hungarian loess from South Baranya (Újvári et al., 2008), Beremend (Varga et al., 2011) and Paks (Újvári et al., 2014), and West German loess from Alsheim (Kühn et al., 2013) and east of Bonn (Smykatz-Kloss, 2003). Tokaj samples overlap with Slovakian loess (Nehyba et al., 2010), while Grub samples have identical ratios to loess from Paks in Hungary. The results, together with those from the Sr-Nd analyses, clearly show the genetic link between major loess deposits in Hungary, Croatia and probably Slovakia and Tokaj and Grub. Geochemical similarities of loess from Central Hungary/Croatia have been observed before (Újvári et al., 2012) and can now be expanded with results from East Hungary (Tokaj) and Austria (Grub). The overall uniformity of loess in the Northern Carpathian Basin and adjacent regions points to a common, distal source of sediment (or rather a mixture of multiple sources) and a common transport pathway but does not provide evidence for the idea of a significant contribution of local, proximal material, as e.g. Tokaj volcanic rocks, assuming a unique geochemical signature of the proximal sediment.

The situation in Nussloch and other, geographically close loess deposits in Western and Central Europe, however, is less clear. While samples from these regions show rather similar patterns in the spider diagram (Fig. 4c), variance is much higher than for the Southeast European loess samples. Nussloch loess is isotopically most similar to loess from Lower Saxony and Hesse (Schnetger, 1992), Bonn and Alsheim (West Germany), and shows different patterns than loess from Southeast England (Parks and Rendell, 1992), Kaiserstuhl in Southwest Germany (Taylor et al., 1983) and the Picardy (Smykatz-Kloss, 2003) and Normandy (Lautridou et al., 1984) regions in France. This is only partially supported by the Al_2O_3/TiO_2 vs. SiO_2/TiO_2 plot (Fig. 3b), in which Nussloch loess is most similar to Picardy and South England loess, and again to Lower Saxony and Hesse, but different from Alsheim and Bonn. This points to the conclusion that there are larger regional differences in the chemical and isotopic composition of Western and Central European loess deposits compared to those of Southeast Europe. The results from the different analyses are often ambiguous and do not clearly show similarities or differences between the localities. Both spider diagrams and Al_2O_3/TiO_2 vs. SiO_2/TiO_2 ratios indicate that Nussloch loess is similar to samples from Lower Saxony and Hesse. However, this observation is not confirmed by Sr-Nd data. Isotopic and elemental analyses show some similarities between Nussloch and French loess (Fig. 8), but the picture is less clear for Alsheim, Bonn and Kaiserstuhl, which we would expect to be similar as well, assuming a uniform sediment source and pathway, such as the Rhine River.

5.4 Rocks and floodplain sediments as potential sources of Tokaj, Nussloch and Grub loess

5.4.1 A comparison of loess and potential source rocks from the Alps and Southeast Europe

As discussed above, a direct comparison of elemental data of loess samples and potential crystalline silicatic source rocks will probably not result in valid matches due to the presence of detrital carbonates in the samples and the destruction of the source signal through weathering, sorting and transport processes. In the UCC-normalized spider and Al_2O_3/TiO_2 vs. SiO_2/TiO_2 diagrams (Fig. 4d, 4e, 3d), potential crystalline source rocks have different and much more heterogeneous compositions and generally possess no similarities with loess. Some East Carpathian flysch, Bohemian Massif and Alpine granitoid samples plot in the vicinity of the Tokaj and Grub samples, but do not overlap, indicating that there is probably no direct link between these rocks and the loess samples and that the source information may have been obscured by weathering. A comparison between Swiss molasse and igneous rock samples from the Swiss Alps reveals similarities between Nussloch loess and molasse, indicating that Rhine River sediments are the main source for loess from this locality (Hill, 2005; Smalley et al., 2009). This observation is confirmed by the Nd isotopic data, where Nussloch loess falls in the ε_{Nd} range of Alpine molasses samples (Henry et al., 1997).

As for elemental data, the same limitations due to weathering and sediment mixing apply for $^{87}Sr/^{86}Sr$, but $^{143}Nd/^{144}Nd$ ratios should be less affected by weathering processes and potentially carry a source signal. Compared to loess, many potential source rocks have a different isotopic signature with much higher ε_{Nd} values (Fig. 7, Fig. 9, Fig. 10), including basalts from Hungary and Austria (Carpathian Basin (CB); Embey-Isztin et al., 1993), igneous rocks from the Central Alps (Schaltegger et al., 2003), igneous rocks from Hungary and Romania (Eastern Carpathians (EC); Seghedi et al., 2004) and Bohemian Massif granites (BM; Siebel et al., 2008). Our loess samples plot close to, or within, the rectangles of East Carpathian flysch (Mason et al., 1996), granites from the Tisia terrane in Southwest Hungary (Carpathian Basin (CB); Klötzli et al., 2004), Bohemian Massif sedimentary rocks (Drost et al., 2007), Western Carpathian granites (WC; Kohút and Nabelek, 2008), and at some distance to Slovakian gneiss (WC; Gaab et al., 2006) and Czech metamorphic rocks (BM; Janousek et al., 2006). A more detailed analysis of single data points (Fig. 10) reveals that the loess samples overlap with several rock samples, most notably with East Carpathian flysch (Mason et al., 1996). Furthermore, all samples are located within the ε_{Nd} range

of Alpine molasses samples (Henry et al., 1997) and close to the $^{87}Sr/^{86}Sr$ range of igneous rocks from the Black Forest Mts. in Southwest Germany (Baumann and Hofmann, 1988).

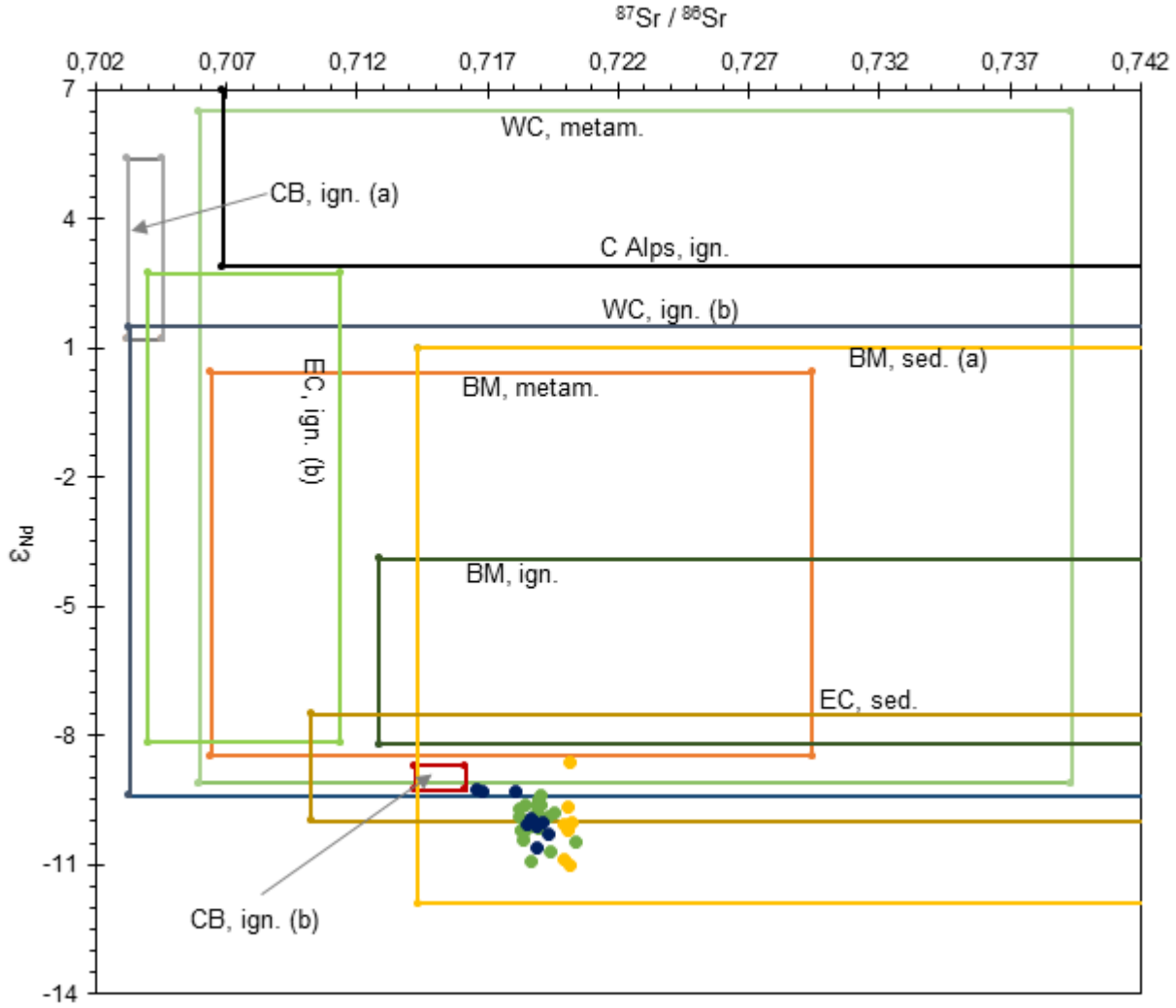

Fig. 9: Tokaj, Grub and Nussloch loess and potential source rocks from Southeast Europe and the Alps. Squares are drawn based on min/max values. Abbreviations: BM - Bohemian Massif, C Alps - Central Alps, CB - local rocks in the Carpathian Basin, EC - East Carpathians, WC - Western Carpathians, sed. - sedimentary rocks, ign. - igneous rocks, metam. - metamorphic rocks. Data sources: BM, sed. (a): Drost et al. (2004), BM, sed. (b): Drost et al. (2007), BM, ign.: Siebel et al. (2008), BM, metam.: Janousek et al. (2006), CB, ign. (a): Embey-Isztin et al. (1993), CB, ign. (b): Klötzli et al. (2004), EC, sed.: Mason et al., (1996), EC, ign. (b): Seghedi et al. (2004), WC, ign. (b): Kohút and Nabelek (2008), WC, metam.: Gaab et al. (2006).

These results also demonstrate the main shortcoming of the Sr-Nd fingerprinting method. There might be a contribution from the surrounding East and West Carpathian Mountains (WC, EC) or local rocks from the Carpathian Basin (CB) to the Tokaj (and possibly Grub) loess sites, but a contribution of southeast European material to the Nussloch site is highly unlikely since neither

rivers nor dominant wind systems exist and have existed throughout the Quaternary to constantly transport material from the Carpathian Basin to West Germany. Thus, sediment sources can only be ruled out, but not confirmed. However, a contribution of East Carpathian material to East Hungarian loess via the Tisza River has been discussed before (Smalley and Leach, 1978) and further investigations are encouraged by the isotopic and elemental data. Furthermore, Tokaj, Grub and Nussloch loess and Alpine molasses samples have several geochemical similarities and should be included in further analyses, since these sediments have probably been derived from the same initial source, i.e. the Alps, and may have supplied material for both Southeast and Central European loess via the Rhine and the Danube Rivers.

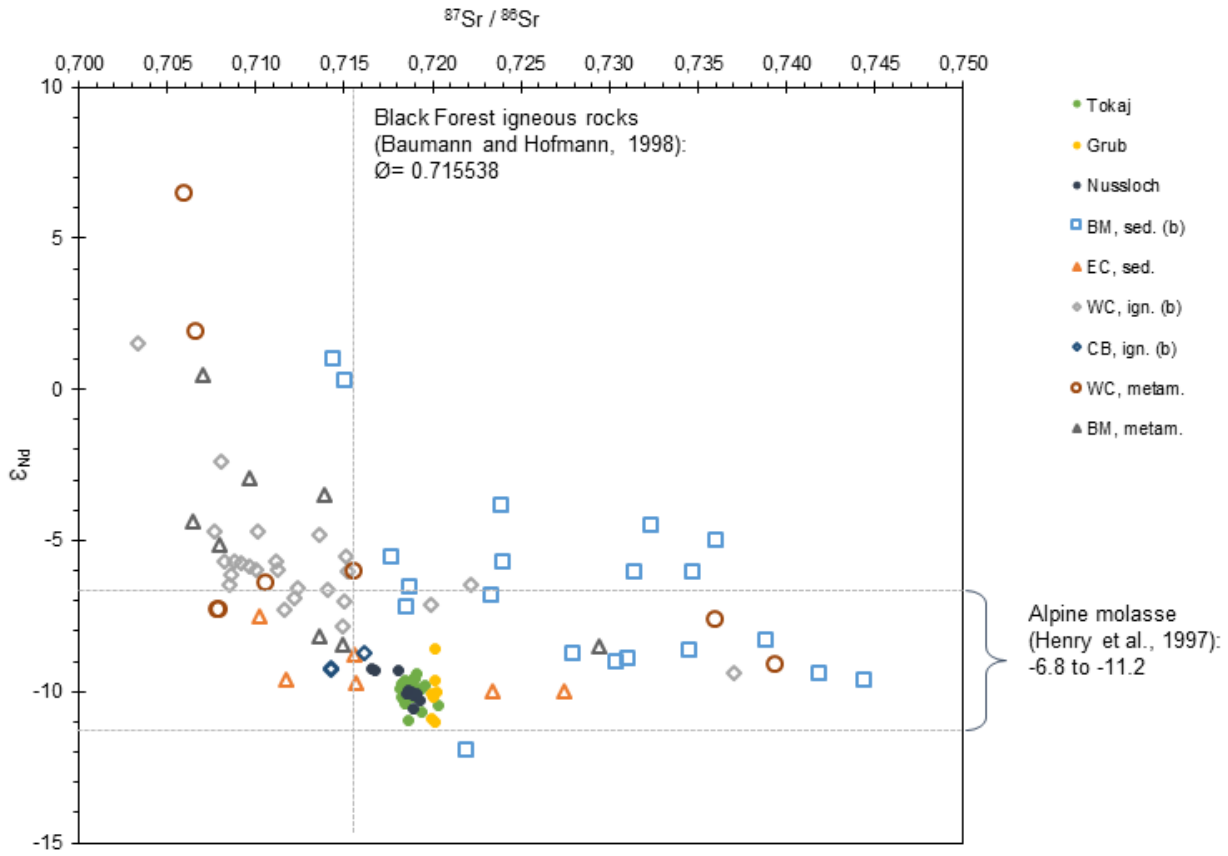

Fig. 10: Tokaj, Grub and Nussloch loess and potential source rocks from Southeast Europe and the Alps. This figure is a zoom-in of Fig. 9 with individual data points.

5.4.2 A comparison of loess and floodplain sediments in Central and Southeast Europe

It has often been argued that fluvial rather than aeolian processes acted as the main transport mechanism for material that later accumulated as loess. Smalley and Leach (1978) assume that glacial sediments from the Alps were transported to the North and Southeast by the Rhine and Danube Rivers, deposited in floodplains and river banks and subsequently transported by the wind to build proximal loess deposits. Several provenance studies have therefore focused on studying floodplain deposits as potential source materials of loess (Buggle et al., 2008; Muhs and Budahn, 2006; Újvári et al., 2012). Here we followed the approach by Buggle et al. (2008) who successfully compared their loess data with recent floodplain geochemical data from the FOREGS database (Salminen et al., 2005). We expanded their selection and classification (Austroalpine cover nappes, Bohemian Massif, Drava, Western Carpathians) with additional samples from the Rhine and Rhône Rivers and their tributaries, and Central and Eastern Hungary, representing the deposits of the Danube and Tisza and tributaries, respectively (all FOREGS; a complete list of samples can be found in the appendix). One additional sample is from the Dřevnice-Morava confluence in Slovakia (Nehyba et al., 2010). So far, Sr-Nd data is only available from the Danube River at Mohács and Basaharc (Hungary), from Miocene Pannonian sands in Hungary (all: Újvári et al., 2012) and from the Upper Rhine Valley (Tricca et al., 1999), but not from other locations across Europe or rivers as, e.g., the Tisza.

A comparison of these samples in the spider diagrams (Fig. 4f) shows similar patterns of Tokaj and Grub and floodplain sediments from Eastern Hungary (E-HU), the Bohemian Massif and the Western Carpathians and, to a lesser degree, Central Hungary (C-HU), and the Drava and Morava Rivers. Samples from the Austroalpine region (AA) deviate from Tokaj and Grub. This is confirmed in the Al_2O_3/TiO_2 vs. SiO_2/TiO_2 diagram (Fig. 3c), where Tokaj and Grub plot close to the Western Carpathians and East Hungary (Tisza), but plot away from the Drava and the Bohemian Massif. The Sr-Nd data (Fig. 8) from the suspended load and Pleistocene fluvial sediments of the Danube River, as well as of the Miocene Pannonian sands, plot around Tokaj and Grub. The ε_{Nd} values of the Pleistocene fluvial sediments and the Pannonian sands are identical with our loess samples, indicating that the loss and the fluvial sediments have probably been derived from the same source(s). These results are in line with previous findings for the Northwest and Central Carpathian Basin (Buggle et al., 2008; Thamó-Bozsó et al., 2014; Újvári et al., 2012) and confirm the fundamental theoretical hypotheses of loess origin (Smalley et al., 2009; Smalley and Leach, 1978). The high degree of similarity between Tokaj and Grub loess either implies that input from the East Carpathians and the Pannonian sands did not change the geochemical signature

significantly, or that material from East Hungary and Pannonian sands must have been transported to East Austria.

Very little floodplain data is available for Nussloch. A comparison with FOREGS data of Rhine, Rhône and Austroalpine floodplain sediments shows strong similarities with Rhine and Rhône samples in both the spider diagrams (Fig. 4g) and in the Al_2O_3/TiO_2 vs. SiO_2/TiO_2 plot (Fig. 3c), which supports the theory of fluvial transport from source regions in the Swiss Central Alps via the Rhine River, deposition and subsequent short aeolian transport, as suggested by previously (Antoine et al., 2001; Hill, 2005; Smalley et al., 2009). A comparison of isotopic signatures (Fig. 8) shows that river, spring and soil samples from the Vosges Mts. (Probst et al., 2000; Tricca et al., 1999) adjacent to the Upper Rhine Valley have more radiogenic Sr ratios than the Nussloch samples, but might result in a similar isotopic composition if mixed with sediments from the Black Forest (Fig. 10) from the opposite side of the Upper Rhine Valley, or with Rhine River sediments (Tricca et al., 1999). Such a mixture could provide an additional, minor contribution of sediment with a similar geochemical signature. However, more data from potential source rocks and from sediments in the Alps and along the Rhine River are needed to consolidate these findings.

6. Conclusions

The results of our combined geochemical and Sr-Nd isotopic study and MIS 2 and 3 loess samples from Tokaj (Hungary), Grub (Austria) and Nussloch (Germany) show that:

- The sediment source of the Tokaj loess-paleosol profile most likely remained stable between 60 to 20 ka. In contrast, the geochemical and isotopic composition of loess from Grub and Nussloch is less homogenous, indicating a weak change in the source from 50 to 30 ka in Grub and a more pronounced change between 30 to 20 ka at Nussloch.
- Overall, European loess has a rather similar geochemical and isotopic composition. This is especially true for loess from the Carpathian Basin and adjacent areas (Tokaj, Grub, Hungary, Croatia), where the uniformity is most pronounced, which indicates a common, distal sediment source and common transport pathways and weakens the theory of a significant contribution of local/proximal sediments. Geochemical and isotopic variance is higher in Central and Northern European loess (Nussloch, Germany, France, Benelux).
- A direct comparison of loess and possible source rocks is difficult due to weathering and mixing effects. The Tokaj and Grub samples show some similarities with sedimentary rocks

from the East Carpathians, the Bohemian Massif and Alpine molasse; Nussloch loess could have been derived from deposits of the Alpine molasse.

- The comparison of loess and floodplain and river sediments is most promising and confirms previous results and hypotheses. While Tokaj and Grub loess appear to be linked with Miocene local sands in Hungary and fluvial sediments from the Western Carpathians, the Bohemian Massif, the Danube and the Tisza Rivers, Nussloch loess may have been derived from Rhine River sediments or from a mixture of Black Forest and Vosges Mts. sedimentary material.
- There is a general lack of data, especially Sr-Nd data of floodplain sediments, and consistent datasets (XRF, isotopic data, measured on the same samples).
- Sr-Nd analyses and geochemical fingerprints alone are not sufficient to reliably identify the sediment sources of loess in Europe, but may provide indicators for further studies.
- In all cases, and especially with regard to isotopic analyses, the harmonization of sample pre-treatment (such as leaching and grain-size sorting) is desirable since results differ substantially depending on pre-treatment processes.

Acknowledgements

This research was funded by a graduation fellowship from the state of Baden-Wuerttemberg, Germany. We would like to thank P. Sümegi (University of Szeged, Hungary) for his support during the field trip and an introduction to the site, M. Zech, B. Buggle (University of Bayreuth, Germany), S. Gulyás, G. D. Páll and G. Persaits (University of Szeged) for help in the field and H. Taubald and team (University of Tübingen, Germany) for XRF measurements.

Supplementary material

A table containing the results of the XRF measurements can be found in the supplementary section of the journal, as well as a compilation of all literature data used in this study.

References

Antl, W., 2013. The inventories of archaeoligical horizons 4 and 3 and the loess section of Grub/Kranawetberg, a Gravettian site in Lower Austria. E&G Quaternary Science Journal 62, 120-126.

Antoine, P., Rousseau, D.-D., Moine, O., Kunesch, S., Hatté, C., Lang, A., Tissoux, H., Zöller, L., 2009. Rapid and cyclic aeolian deposition during the Last Glacial in European loess: a high-resolution record from Nussloch, Germany. Quaternary Science Reviews 28, 2955-2973.

Antoine, P., Rousseau, D.-D., Zöller, L., Lang, A., Munaut, A.-V., Hatté, C., Fontugne, M., 2001. High-resolution record of the last Interglacial–glacial cycle in the Nussloch loess–palaeosol sequences, Upper Rhine Area, Germany. Quaternary International 76–77, 211-229.

Baumann, A., Hofmann, R., 1988. Strontium isotope systematics of hydrothermal vein minerals in deposits of West Germany. Geol Rundsch 77, 747-762.

Bentley, R.A., Krause, R., Price, T.D., Kaufmann, B., 2003. Human Mobility at the Early Neolithic Settlement of Vaihingen, Germany: Evidence from Strontium Isotope Analysis. Archaeometry 45, 471-486.

Biscaye, P.E., Grousset, F.E., Revel, M., Van der Gaast, S., Zielinski, G.A., Vaars, A., Kukla, G., 1997. Asian provenance of glacial dust (stage 2) in the Greenland Ice Sheet Project 2 Ice Core, Summit, Greenland. Journal of Geophysical Research: Oceans 102, 26765-26781.

Bory, A.J.M., Biscaye, P.E., Svensson, A., Grousset, F.E., 2002. Seasonal variability in the origin of recent atmospheric mineral dust at NorthGRIP, Greenland. Earth and Planetary Science Letters 196, 123-134.

Buggle, B., Glaser, B., Zöller, L., Hambach, U., Marković, S., Glaser, I., Gerasimenko, N., 2008. Geochemical characterization and origin of Southeastern and Eastern European loesses (Serbia, Romania, Ukraine). Quaternary Science Reviews 27, 1058-1075.

Chen, J., Li, G., Yang, J., Rao, W., Lu, H., Balsam, W., Sun, Y., Ji, J., 2007. Nd and Sr isotopic characteristics of Chinese deserts: Implications for the provenances of Asian dust. Geochimica et Cosmochimica Acta 71, 3904-3914.

DePaolo, D.J., 1988. Neodymium isotope geochemistry : an introduction. Springer, Berlin, Heidelberg.

Drost, K., Linnemann, U., McNaughton, N., Fatka, O., Kraft, P., Gehmlich, M., Tonk, C., Marek, J., 2004. New data on the Neoproterozoic – Cambrian geotectonic setting of the Teplá-Barrandian volcano-sedimentary successions: geochemistry, U-Pb zircon ages, and provenance (Bohemian Massif, Czech Republic). Int J Earth Sci (Geol Rundsch) 93, 742-757.

Drost, K., Romer, R.L., Linnemann, U., Fatka, O., Kraft, P., Marek, J., 2007. Nd-Sr-Pb isotopic signatures of Neoproterozoic–Early Paleozoic siliciclastic rocks in response to changing geotectonic regimes: A case study from the Barrandian area (Bohemian Massif, Czech Republic). Geological Society of America Special Papers 423, 191-208.

Embey-Isztin, A., Downes, H., James, D.E., Upton, B.G.J., Dobosi, G., Ingram, G.A., Harmon, R.S., Scharbert, H.G., 1993. The Petrogenesis of Pliocene Alkaline Volcanic Rocks from the Pannonian Basin, Eastern Central Europe. Journal of Petrology 34, 317-343.

Feng, J.-L., Zhu, L.-P., Zhen, X.-L., Hu, Z.-G., 2009. Grain size effect on Sr and Nd isotopic compositions in eolian dust: Implications for tracing dust provenance and Nd model age. Geochemical Journal 43, 123-131.

Gaab, A.S., Janák, M., Poller, U., Todt, W., 2006. Alpine reworking of Ordovician protoliths in the Western Carpathians: Geochronological and geochemical data on the Muráñ Gneiss Complex, Slovakia. Lithos 87, 261-275.

Gallet, S., Jahn, B.-M., Van Vliet Lanoë, B., Dia, A., Rossello, E., 1998. Loess geochemistry and its implications for particle origin and composition of the upper continental crust. Earth and Planetary Science Letters 156, 157-172.

Garrels, R.M., Mackenzie, F.T., 1971. Evolution of sedimentary rocks. Norton, New York.

Gocke, M., Kuzyakov, Y., Wiesenberg, G.L.B., 2010. Rhizoliths in loess – evidence for post-sedimentary incorporation of root-derived organic matter in terrestrial sediments as assessed from molecular proxies. Organic Geochemistry 41, 1198-1206.

Grousset, F.E., Rognon, P., Coudé-Gaussen, G., Pédemay, P., 1992. Origins of peri-Saharan dust deposits traced by their Nd and Sr isotopic composition. Palaeogeography, Palaeoclimatology, Palaeoecology 93, 203-212.

Hatté, C., Antoine, P., Fontugne, M., Rousseau, D.-D., Tisnérat-Laborde, N., Zöller, L., 1999. New chronology and organic matter δ13C paleoclimatic significance of Nußloch loess sequence (Rhine Valley, Germany). Quaternary International 62, 85-91.

Hatté, C., Guiot, J., 2005. Palaeoprecipitation reconstruction by inverse modelling using the isotopic signal of loess organic matter: application to the Nußloch loess sequence (Rhine Valley, Germany). Clim Dyn 25, 315-327.

Henry, P., Deloule, E., Michard, A., 1997. The erosion of the Alps: Nd isotopic and geochemical constraints on the sources of the peri-Alpine molasse sediments. Earth and Planetary Science Letters 146, 627-644.

Hill, T.C., 2005. Geochemical evidence for weathering in NW European loess on a sub-millennial scale during the last Ice Age. University of Gloucestershire, Gloucestershire, p. 238.

Jacobsen, S.B., Wasserburg, G.J., 1980. Sm-Nd isotopic evolution of chondrites. Earth and Planetary Science Letters 50, 139-155.

Jahn, B.-M., Gallet, S., Han, J., 2001. Geochemistry of the Xining, Xifeng and Jixian sections, Loess Plateau of China: eolian dust provenance and paleosol evolution during the last 140 ka. Chemical Geology 178, 71-94.

Janousek, V., Gerdes, A., Vrána, S., Finger, F., Erban, V., Friedl, G., Braithwaite, C.J.R., 2006. Low-pressure Granulites of the Lišov Massif, Southern Bohemia: Viséan Metamorphism of Late Devonian Plutonic Arc Rocks. Journal of Petrology 47, 705-744.

Jurje, M., Ionescu, C., Hoeck, V., Kovacs, M., 2013. Geochemistry of Neogene quartz andesites from the Oaş and Gutâi Mountains, Eastern Carpathians (Romania): a complex magma genesis. Mineralogy and Petrology, 1-20.

Kiss, P., Gméling, K., Molnár, F., Pécskay, Z., 2010. Geochemistry of Sarmatian volcanic rocks in the Tokaj Mts (NE Hungary) and their relationship to hydrothermal mineralization. Central European Geology 53, 377-403.

Klötzli, U.S., Buda, G., Skiöld, T., 2004. Zircon typology, geochronology and whole rock Sr–Nd isotope systematics of the Mecsek Mountain granitoids in the Tisia Terrane (Hungary). Mineralogy and Petrology 81, 113-134.

Kohút, M., Nabelek, P.I., 2008. Geochemical and isotopic (Sr, Nd and O) constraints on sources for Variscan granites in the Western Carpathians - implications for crustal structure and tectonics. Journal of Geosciences 53, 307-322.

Kühn, P., Techmer, A., Weidenfeller, M., 2013. Lower to middle Weichselian pedogenesis and palaeoclimate in Central Europe using combined micromorphology and geochemistry: the loess-paleosol sequence of Alsheim (Mainz Basin, Germany). Quaternary Science Reviews 75, 43-58.

Lautridou, J.P., Sommé, J., Jamagne, M., 1984. Sedimentological, mineralogical and geochemical characteristics of the loesses of North-West France. Geographical Research Institute of the Hungarian Academy of Sciences, Budapest.

Marković, S.B., Bokhorst, M.P., Vandenberghe, J., McCoy, W.D., Oches, E.A., Hambach, U., Gaudenyi, T., Jovanović, M., Zöller, L., Stevens, T., Machalett, B., 2008. Late Pleistocene loess-palaeosol sequences in the Vojvodina region, north Serbia. Journal of Quaternary Science 23, 73-84.

Mason, P.R.D., Downes, H., Thirlwall, M.F., Seghedi, I., Szakacs, A., Lowry, D., Mattey, D., 1996. Crustal Assimilation as a Major Petrogenetic Process in the East Carpathian Neogene and Quaternary Continental Margin Arc, Romania. Journal of Petrology 37, 927-959.

Mikulčić Pavlaković, S., Crnjaković, M., Tibljaš, D., Šoufek, M., Wacha, L., Frechen, M., Lacković, D., 2011. Mineralogical and geochemical characteristics of Quaternary sediments from the Island of Susak (Northern Adriatic, Croatia). Quaternary International 234, 32-49.

Moine, O., Rousseau, D.-D., Antoine, P., 2005. Terrestrial molluscan records of Weichselian Lower to Middle Pleniglacial climatic changes from the Nussloch loess series (Rhine Valley, Germany): the impact of local factors. Boreas 34, 363-380.

Muhs, D.R., Budahn, J.R., 2006. Geochemical evidence for the origin of late Quaternary loess in central Alaska. Canadian Journal of Earth Sciences 43, 323-337.

Muhs, D.R., Budahn, J.R., McGeehin, J.P., Bettis III, E.A., Skipp, G., Paces, J.B., Wheeler, E.A., 2013. Loess origin, transport, and deposition over the past 10,000 years, Wrangell-St. Elias National Park, Alaska. Aeolian Research 11, 85-99.

Nehyba, S., Adamová, M., Faimon, J., Kuchovský, T., Holoubek, I., Zeman, J., 2010. Modern fluvial sediment provenance and pollutant tracing: a case study from the Dřevnice River Basin (eastern Moravia, Czech Republic). Geologica Carpathica 61, 147-162.

Parks, D.A., Rendell, H.M., 1992. Thermoluminescence dating and geochemistry of loessic deposits in southeast England. Journal of Quaternary Science 7, 99-107.

Pécsi, M., 1993. Negyedkor és löszkutatás (Loess and the Quaternary). Akadémiai Kiadó, Budapest, Hungary.

Probst, A., El Gh'mari, A., Aubert, D., Fritz, B., McNutt, R., 2000. Strontium as a tracer of weathering processes in a silicate catchment polluted by acid atmospheric inputs, Strengbach, France. Chemical Geology 170, 203-219.

Rao, W., Yang, J., Chen, J., Li, G., 2006. Sr-Nd isotope geochemistry of eolian dust of the arid-semiarid areas in China: Implications for loess provenance and monsoon evolution. CHINESE SCI BULL 51, 1401-1412.

Rousseau, D.D., Antoine, P., Hatté, C., Lang, A., Zöller, L., Fontugne, M., Othman, D.B., Luck, J.M., Moine, O., Labonne, M., Bentaleb, I., Jolly, D., 2002. Abrupt millennial climatic changes from Nussloch (Germany) Upper Weichselian eolian records during the Last Glaciation. Quaternary Science Reviews 21, 1577-1582.

Rousseau, D.D., Derbyshire, E., Antoine, P., Hatté, C., 2007. Loess Records: Europe, In: Elias, S.A. (Ed.), Encyclopedia of Quaternary Science. Elsevier, Oxford, pp. 1440-1456.

Rudnick, R.L., Gao, S., 2003. 3.01 - Composition of the Continental Crust, In: Holland, H.D., Turekian, K.K. (Eds.), Treatise on Geochemistry. Pergamon, Oxford, pp. 1-64.

Salminen, R., Batista, M.J., Bidovec, M., Demetriades, A., De Vivo, B., De Vos, W., Duris, M., Gilucis, A., Gregorauskiene, V., Halamic, J., Heitzmann, P., Lima, A., Jordan, G., Klaver, G., Klein, P., Lis, J., Locutura, J., Marsina, K., Mazreku, A., O'Connor, P.J., Olsson, S.Å., Ottesen, R.-T., Petersell, V., Plant, J.A., Reeder, S., Salpeteur, I., Sandström, H., Siewers, U., Steenfelt, A., Tarvainen, T., 2005. Geochemical Atlas of Europe. Part 1: Background Information, Methodology and Maps. Geological Survey of Finland, Espoo, p. 526.

Schaltegger, U., Abrecht, J., rgen, Corfu, F., 2003. The Ordovician orogeny in the Alpine basement: constraints from geochronology and geochemistry in the Aar Massif (Central Alps). Swiss Bulletin of Mineralogy and Petrology 83, 183-239.

Schatz, A.-K., Buylaert, J.-P., Murray, A., Stevens, T., Scholten, T., 2012. Establishing a luminescence chronology for a palaeosol-loess profile at Tokaj (Hungary): A comparison of quartz OSL and polymineral IRSL signals. Quaternary Geochronology 10, 68-74.

Schatz, A.-K., Zech, M., Buggle, B., Gulyás, S., Hambach, U., Marković, S.B., Sümegi, P., Scholten, T., 2011. The late Quaternary loess record of Tokaj, Hungary: Reconstructing palaeoenvironment, vegetation and climate using stable C and N isotopes and biomarkers. Quaternary International 240, 52-61.

Schatz, A.K., Scholten, T., Kühn, P., 2014. Paleoclimate and weathering of the Tokaj (NE Hungary) loess-paleosol sequence: a comparison of geochemical weathering indices and paleoclimate parameters. Climate of the Past Discussions 10, 469-507.

Schnetger, B., 1992. Chemical-composition of loess from a local and worldwide view. Neues Jahrbuch für Mineralogie - Monatshefte, 29-47.

Sebe, K., Csillag, G., Ruszkiczay-Rüdiger, Z., Fodor, L., Thamó-Bozsó, E., Müller, P., Braucher, R., 2011. Wind erosion under cold climate: A Pleistocene periglacial mega-yardang system in Central Europe (Western Pannonian Basin, Hungary). Geomorphology 134, 470-482.

Seghedi, I., Downes, H., Szakács, A., Mason, P.R.D., Thirlwall, M.F., Roşu, E., Pécskay, Z., Márton, E., Panaiotu, C., 2004. Neogene–Quaternary magmatism and geodynamics in the Carpathian–Pannonian region: a synthesis. Lithos 72, 117-146.

Siebel, W., Shang, C.K., Reitter, E., Rohrmüller, J., Breiter, K., 2008. Two Distinctive Granite Suites in the SW Bohemian Massif and their Record of Emplacement: Constraints from Geochemistry and Zircon 207Pb/206Pb Chronology. Journal of Petrology 49, 1853-1872.

Smalley, I., O'Hara-Dhand, K., Wint, J., Machalett, B., Jary, Z., Jefferson, I., 2009. Rivers and loess: The significance of long river transportation in the complex event-sequence approach to loess deposit formation. Quaternary International 198, 7-18.

Smalley, I.J., Leach, J.A., 1978. The origin and distribution of the loess in the Danube basin and associated regions of East-Central Europe - A review. Sedimentary Geology 21, 1-26.

Smith, B.J., Wright, J.S., Whalley, W.B., 1991. Simulated aeolian abrasion of Pannonian sands and its implications for the origins of Hungarian loess. Earth Surface Processes and Landforms 16, 745-752.

Smith, J., Vance, D., Kemp, R.A., Archer, C., Toms, P., King, M., Zárate, M., 2003. Isotopic constraints on the source of Argentinian loess – with implications for atmospheric circulation and the provenance of Antarctic dust during recent glacial maxima. Earth and Planetary Science Letters 212, 181-196.

Smykatz-Kloss, B., 2003. Die Lößvorkommen des Pleiser Hügellandes bei Bonn und von Neustadt/Wied sowie der Picardie: Mineralogisch-geochemische und geomorphologische Charakterisierung, Verwitterungs-Beeinflussung und Herkunft der Lösse, Mathematisch-Naturwissenschaftlichen Fakultät. Rheinische Friedrich-Wilhelms-Universität Bonn, Bonn, Germany, p. 343.

Stuut, J.-B., Smalley, I., O'Hara-Dhand, K., 2009. Aeolian dust in Europe: African sources and European deposits. Quaternary International 198, 234-245.

Sümegi, P., Hertelendi, E., 1998. Reconstruction of microenvironmental changes in the Kopasz Hill loess area at Tokaj (Hungary) between 15 and 70 ka BP. Radiocarbon 40, 855-863.

Sümegi, P., Rudner, Z.E., 2001. In situ charcoal fragments as remains of natural wild fires in the upper Würm of the Carpathian Basin. Quaternary International 76–77, 165-176.

Sun, J., 2002. Provenance of loess material and formation of loess deposits on the Chinese Loess Plateau. Earth and Planetary Science Letters 203, 845-859.

Sun, J., 2005. Nd and Sr isotopic variations in Chinese eolian deposits during the past 8 Ma: Implications for provenance change. Earth and Planetary Science Letters 240, 454-466.

Svensson, A., Biscaye, P.E., Grousset, F.E., 2000. Characterization of late glacial continental dust in the Greenland Ice Core Project ice core. Journal of Geophysical Research: Atmospheres 105, 4637-4656.

Taylor, S.R., McLennan, S.M., 1985. The continental crust: its composition and evolution. Blackwell Scientific Publications, Oxford.

Taylor, S.R., McLennan, S.M., McCulloch, M.T., 1983. Geochemistry of loess, continental crustal composition and crustal model ages. Geochimica et Cosmochimica Acta 47, 1897-1905.

Thamó-Bozsó, E., Kovács, L.Ó., Magyari, Á., Marsi, I., 2014. Tracing the origin of loess in Hungary with the help of heavy mineral composition data. Quaternary International 319, 11-21.

Tricca, A., Stille, P., Steinmann, M., Kiefel, B., Samuel, J., Eikenberg, J., 1999. Rare earth elements and Sr and Nd isotopic compositions of dissolved and suspended loads from small river systems in the Vosges mountains (France), the river Rhine and groundwater. Chemical Geology 160, 139-158.

Újvári, G., Varga, A., Balogh-Brunstad, Z., 2008. Origin, weathering, and geochemical composition of loess in southwestern Hungary. Quaternary Research 69, 421-437.

Újvári, G., Varga, A., Ramos, F.C., Kovács, J., Németh, T., Stevens, T., 2012. Evaluating the use of clay mineralogy, Sr–Nd isotopes and zircon U–Pb ages in tracking dust provenance: An example from loess of the Carpathian Basin. Chemical Geology 304–305, 83-96.

Újvári, G., Varga, A., Raucsik, B., Kovács, J., 2014. The Paks loess-paleosol sequence: A record of chemical weathering and provenance for the last 800 ka in the mid-Carpathian Basin. Quaternary International 319, 22-37.

Varga, A., Szakmány, G., Árgyelán, T., Józsa, S., Raucsik, B., Máthé, Z., 2007. Complex examination of the Upper Paleozoic siliciclastic rocks from southern Transdanubia, SW Hungary - Mineralogical, petrographic, and geochemical study. Geological Society of America Special Papers 420, 221-240.

Varga, A., Újvári, G., Raucsik, B., 2011. Tectonic versus climatic control on the evolution of a loess–paleosol sequence at Beremend, Hungary: an integrated approach based on paleoecological, clay mineralogical, and geochemical data. Quaternary International 240, 71-86.

Varga, G., 2011. Similarities among the Plio–Pleistocene terrestrial aeolian dust deposits in the World and in Hungary. Quaternary International 234, 98-108.

Vďačný, M., Vozárová, A., Vozár, J., 2013. Geochemistry of the Permian sandstones from the Malužiná Formation in the Malé Karpaty Mts (Hronic Unit, Western Carpathians, Slovakia): implications for source-area weathering, provenance and tectonic setting. Geologica Carpathica 64, 23-38.

von Eynatten, H., 2003. Petrography and chemistry of sandstones from the Swiss Molasse Basin: an archive of the Oligocene to Miocene evolution of the Central Alps. Sedimentology 50, 703-724.

Zech, M., Rass, S., Buggle, B., Löscher, M., Zöller, L., 2012. Reconstruction of the late Quaternary paleoenvironments of the Nussloch loess paleosol sequence, Germany, using n-alkane biomarkers. Quaternary Research 78, 226-235.

Zhang, H., Lu, H., Jiang, S.-Y., Vandenberghe, J., Wang, S., Cosgrove, R., 2012. Provenance of loess deposits in the Eastern Qinling Mountains (central China) and their implications for the paleoenvironment. Quaternary Science Reviews 43, 94-102.

Zöller, L., Richter, D., Masuth, S., Wunner, L., Fischer, M., Antl-Weiser, W., 2013. Luminescence chronology of the Grub-Kranawetberg site, Austria. E&G Quaternary Science Journal 62, 127-135.